Title
PERTURBED ANGULAR CORRELATION MEASUREMENTS ON Ce140 AND Pr143

Author
Levy, Richard M.

Publication Date
1964-09-18

UCRL-11663

University of California

Ernest O. Lawrence Radiation Laboratory

PERTURBED ANGULAR CORRELATION MEASUREMENTS ON Ce^{140} AND Pr^{143}

Berkeley, California

DISCLAIMER

UCRL-11663

UNIVERSITY OF CALIFORNIA

Lawrence Radiation Laboratory
Berkeley, California

AEC Contract No. W-7405-eng-48

PERTURBED ANGULAR CORRELATION MEASUREMENTS ON Ce^{140} AND Pr^{143}

Richard M. Levy
(Ph.D. Thesis)

September 18, 1964

PERTURBED ANGULAR CORRELATION MEASUREMENTS ON Ce^{140} AND Pr^{143}

Contents

PERTURBED ANGULAR CORRELATION MEASUREMENTS ON Ce^{140} AND Pr^{143}

Richard M. Levy

Department of Chemistry and Lawrence Radiation Laboratory
University of California
Berkeley, California

September 18, 1964

ABSTRACT

The interaction strength between the nuclear magnetic moment and the effective magnetic field at the nucleus has been measured for the 2084 keV level in Ce^{140} and the 57 keV level in Pr^{143} by perturbed angular correlation of gamma radiation techniques.

For tetravalent Ce with a $4f^0$ configuration, the magnetic field at the nucleus is identical to the external field. This allows evaluation of the g-factor of the 2084 keV level as $g = 1.020 \pm 0.039$. The paramagnetic enhancement β due to one 4f electron for cerium in lanthanum metal gives $C = (114.3 \pm 16.1)^{\circ}$ K, where $\beta = 1 + (C/T)$.

The level structure of Pr^{143} has been confirmed as 7/2(0 keV), 5/2(57 keV), 3/2(350 keV) by nuclear alignment and angular correlation. The perturbed angular correlation gives for the 57 keV level, $g = 1.73 \pm 0.09$. Comparison with data on metallic sources establishes the oxidation state of praseodynium in solution as 4+ during the nuclear lifetime.

I. INTRODUCTION

A good deal of interest pervades the region of the lower rare earths. From a nuclear standpoint, the elucidation of the structures of spherical nuclei has been bolstered by the development of the quasi-particle theory of super-conductivity. While the exact prediction of nuclear energy level characteristics remains an elusive problem, the jump from purely empirical to semi-theoretical approaches emphasizes the importance of dependable and precise data.

Although measurements of excited state nuclear properties can be extremely difficult, and one to two such measurements have questionable influence on the overall theory, one must start with a single step to climb the highest mountain. We feel that this philosophy, in some sense, justifies the work described here.

From an atomic physics standpoint, the lower rare earths may provide the key to the exact form of the radial wave function of the 4f electrons. The uncertainty in this eigenfunction increases to a maximum for triply-ionized cerium with one 4f electron. This wave function is necessary for the tabulation of $\langle r^{-3} \rangle_{4f}$, the inverse mean cubed radius, a quantity which appears in all hyperfine interactions and is, thus, essential for the evaluation of nuclear and atomic magnetic moments.

Using the method of perturbed angular correlation of gamma radiation, we have measured nuclear excited state magnetic moments in Ce^{140} and Pr^{143}, and determined the internal field due to one 4f electron in Ce^{+3}. The measurements are discussed with regard to the existing theories, and correlated with other data.

II. THEORETICAL BACKGROUND

A. Introduction

For approximately twenty years the angular dependence of coincidence counting rates in gamma cascades has been utilized in the elucidation of nuclear energy level schemes. More recently, perturbations of these angular correlations have yielded information on magnetic dipole and electric quadrupole moments of excited nuclear states.

Hamilton first predicted an angular anisotropy of nuclear radiation in 1940.[1] Since that time many comprehensive review articles have summarized additional refinements and condensed the theory to a simple and practicable state.

The most elementary explanation for anisotropy in nuclear radiation is conservation of angular momentum. Thus, the initial angular momentum of the unstable nuclear state equals the vector sum of the angular momenta of the final state and of the emitted radiation. As vectors have direction as well as magnitude, a spatial dependence is defined. Or, mathematically, since any angular momentum eigenfunction can be expressed as a linear combination of spherical harmonics, the superposition of specific eigenstates defines a spatial dependence on the Euler angles, θ and ϕ .

For a randomly-oriented set of initial angular momentum eigenstates, isotropic radiation is given off. Nuclear alignment experiments achieve anisotropy by preferentially populating specific nuclear levels using large ratios of magnetic field to temperature. Angular correlation, on the other hand, looks at a non-random array of nuclear states by choosing only those nuclei in which the first radiative transition in a coincident cascade propagates into a specific detector in a given direction. The functional dependence of coincidence rate on angle can now be derived, as the nuclei which are observed "know" which is the the propagation direction, or the z-axis in the laboratory system.

B. Non-Perturbed Angular Correlation

The quantum mechanical derivation of the angular dependence of coincidence rate proceeds in a straight-forward way, starting with the interaction Hamiltonian, the gamma emission operator, between two states. For the case of a typical gamma cascade, $a(\gamma_1)b(\gamma_2)c$, the probability of the initial transition can be described by

$$W_{ab} \propto |H_{ab}|^2 = \langle a|H|b\rangle\langle a|H^*|b\rangle \quad , \tag{1}$$

where a and b encompass the quantum numbers which describe the states and H^* indicates the complex conjugate of the interaction Hamiltonian.[2] Thus, for the cascade, the total transition probability can be expressed,

$$W_{ac} = \sum_b |H_{ab}|^2 |H_{bc}|^2 \quad . \tag{2}$$

We may now write the matrix elements of the interaction Hamiltonian in the unique form:

$$H_{ab} = \sum_{m_a m_b} \langle I_a m_a|H|I_b m_b \Omega\rangle \quad , \tag{3}$$

where I and m are the nuclear spin and magnetic projection eigenvalues and $\Omega = \theta, \phi$ the observed angular parameters in the laboratory system.

As the interaction Hamiltonian acts on nuclear coordinate system parameters, a more appropriate form for Eq. (3) would be

$$H_{ab} = \sum_{L,M_1} \sum_{m_a m_b} \langle I_a m_a|H|I_b m_b L, M_1\rangle\langle L, M_1|\Omega\rangle, \tag{4}$$

with L_1 and M_1 the angular momentum carried off by the radiation and it projection upon the nuclear symmetry axis. The matrix for this transformation relates angular propagation to angular momentum and is just the spherical harmonic[3]

$$\langle L_1 M_1 | \Omega \rangle = Y^{L_1}_{M_1}(\Omega). \tag{5}$$

In the Biedenharn and Rose notation, the interaction Hamiltonian in the summation is expressed

$$\langle I_a m_a | T^{L_1}_{M_1} | I_b m_b \rangle \tag{6}$$

to emphasize the fact that this is a tensor operator which transforms as an angular momentum eigenfunction with the same eigenvalues. Because of this transformational property the Hamiltonian is proportional to all tensor operators of the same rank[4] and, using the Wigner-Eckart theorem, may be written as the product of spatially dependent vector coupling (Clebsch-Gordan) coefficients, and a physical constant, the reduced matrix element.[5]

$$H_{ab} = \sum_{L_1 M_1 m_a m_b} \langle L_1 I_b M_1 m_b | I_a m_a \rangle Y^{L_1}_{M_1}(\Omega) \langle I_a \| T^{L_1} \| I_b \rangle. \tag{7}$$

To further simplify the derivation, we must transform all involved quantization axes to a single laboratory system representation. This is accomplished by a rotation of the nuclear coordinate systems so that the symmetry axes are in the direction of the gamma ray propagation vector, or

$$Y^{L_1}_{\mu}(0) = \sum_{M_1} Y^{L_1}_{M_1}(\Omega) \mathcal{D}^{L_1}_{M_1,\mu}(-\Omega). \tag{8}$$

The matrix elements $D^{L_1}_{M_1\,\mu}(-\Omega)$ form a linear combination of spherical harmonics and are derivable from straightforward group theory.[6] The parameter μ, the projection of the angular momentum upon the laboratory system axis, can have only the values $\mu = \pm 1$ since a photon traveling in a given direction can carry only $\pm\hbar$ units of angular momentum in that direction. The Hamiltonian thus becomes

$$H_{ab} = \sum_{L_1 M_1 m_a m_b \mu} \langle L_1 I_b M_1 m_a | I_a m_a \rangle Y^{L_1}_{\mu}(0) \mathcal{D}^{L_1}_{\mu M_1}(-\Omega) \langle I_a \| T^{L_1} \| I_b \rangle . \quad (9)$$

To find $|H_{ab}|^2$ we use the fact that the product of two rotation matrix elements can be expressed as a linear combination of matrix elements from a third rotation operator

$$\mathcal{D}^{L_1}_{\mu M_1}(-\Omega)\,\mathcal{D}^{L_1'}_{\mu' M_1'}(-\Omega) = \sum_{k,c,d} \langle L_1 L_1' \mu \mu' | k, c \rangle \langle L_1 L_1' M_1 M_1' | k, d \rangle \mathcal{D}^{k}_{cd}(-\Omega) . \quad (10)$$

Additionally it can be shown that the summation over a product of three Clebsch-Gordan coefficients can be written as a product of a Clebsch-Gordan coefficient and a Racah coefficient.

$$\sum_{M_1 M_1' m_a} \langle L_1' I_b M_1' m_b | I_a m_a \rangle \langle L_1 I_b M_1 m_b | I_a m_a \rangle \langle L_1 L_1' M_1 M_1' | k, d \rangle$$
$$= (-1)^{I_b - m_b' - k_1} (2I_a + 1)^{1/2} \langle I_b I_b m_b - m_b' | k, d \rangle W(I_b I_a k, L_1'; L_1 I_b) \quad (11)$$

The functional form and tabulations of Racah coefficients is given in reference 7.

Substituting Eqs. (10) and (11) into the expression for $|H_{ab}|^2$, with the further simplifying assumption that the radiation is pure ($L_1 = L_1'$), we find

$$|H_{ab}|^2 = \sum_{k,c,d,\mu,\mu',m_b,m_b'} (-1)^{I_b+L_1}(2I_a+1)^{1/2}\langle I_b\|L_1\|I_a\rangle^2\langle I_bI_bm_b-m_b'|k,d\rangle \quad (12)$$
$$\times W(I_bI_ak_1L_1;L_1I_b)\langle L_1L_1\mu\mu'|kc\rangle Y_\mu^{L_1}(0)\,Y_{\mu'}^{L_1}(0)^*\mathcal{D}_{cd}^{k_1}(-\Omega).$$

Now as $\mu = \pm 1$, it can be shown[5]

$$\sum_{\mu\mu'}\langle L_1L_1\mu\mu'|kc\rangle Y_\mu^{L_1}(0)\,Y_{\mu'}^{L_1}(0)^* = \frac{2L+1}{8\pi}\langle L_1L_1,1-1|k0\rangle. \quad (13)$$

The simplifying feature $c = 0$, allows this index to be dropped from the summation, and with proper normalization reduces the rotation matrix to a spherical harmonic

$$\mathcal{D}_{od}^{k_1}(-\Omega) = Y_d^{k_1}(-\Omega), \quad (14)$$

so that

$$|H_{ab}|^2 = \sum_{k,d,m_b,m_b'}(-1)^{I_b+L_1}(2I_a+1)^{1/2}\frac{(2L_1+1)}{8\pi}\langle I_b\|L_1\|I_a\rangle^2\langle L_1L_1,1-1|k0\rangle$$
$$\times W(I_bI_ak_1L_1;L_1I_b)\langle I_bI_bm_b-m_b'|k,d\rangle Y_d^{k_1}(-\Omega). \quad (15)$$

Now forming the product $|H_{ab}|^2\ |H_{bc}|^2$, for no reorientation of the M_b states during the intermediate nuclear lifetime, we obtain a term

$$\sum_{m_am_b'}\langle I_bI_bm_b-m_b'|k_1d_1\rangle\langle I_bI_bm_b-m_b'|k_2d_2\rangle = \delta_{k_1k_2}\,\delta_{d_1d_2}. \quad (16)$$

This allows a further simplification

$$\sum_d Y_d^k(-\Omega_1) Y_d^k(\Omega_2) = P_k(\cos\theta) \quad , \tag{17}$$

where $\theta = \Omega_2 - \Omega_1$ and $P_k(\cos\theta)$ is a Legendre polynomial of degree k. The resultant equation for unperturbed angular correlation is thus

$$W(\theta) = \sum_k F_k F_k' P_k(\cos\theta) \tag{18}$$

where

$$F_k = (-1)^{I_b+L_1}(2I_a+1)^{1/2}(2L+1)\langle LL\,1-1|k0\rangle W(I_bI_akL;LI_b)\langle I_b\|L_1\|I_a\rangle^2 \tag{19}$$

The constants F_k and F_k' are functions of only angular momentum properties of a nuclear decay. Their values in this normalized form are conveniently tabulated by Ferentz and Rosenzweig.[8]

Frequently, one or both of the coincident transitions have admixtures of higher multipolarity radiation. As the Clebsch-Gordan and Racah coefficients carry only spatial information, the "physics" of the transition, the transision probability, must be contained in the reduced matrix element. We define the mixing ratio

$$\delta = \frac{\langle I_a\|T^{L'}\|I_b\rangle}{\langle I_a\|T^{L}\|I_b\rangle} \tag{20}$$

where $L' = L + 1$. The F_k for the mixed transition now takes the form

$$F_k = \frac{1}{1+\delta^2}F_k(I_aI_bLL) + \frac{\delta^2}{1+\delta^2}F_k(I_aI_bL'L') + \frac{2\delta}{1+\delta^2}F_k(I_aI_bLL'). \tag{21}$$

The first two terms account for pure L-pole and L'-pole transitions, and the final term the interference.

In cases where one or more transitions intervene between those of interest, a correction term must be inserted to account for possible reorientation of the intermediate nuclear states. The angular correlation is then expressed by

$$W(\theta) = \sum_k F_k' U_k F_k P_k(\cos\theta) \quad , \tag{22}$$

where U_k for each unobserved transition $I_1 \xrightarrow{L} I_2$ is given by[9]

$$U_k = (2I_1+1)^{1/2}(2I_2+1)^{1/2}(-1)^{I_1+I_2-L} W(I_1 I_1 I_2 I_2; kL) . \tag{23}$$

Several important conclusions emerge from the summation over orthogonalized Clebsch-Gordan coefficients and the triangle conditions of the Racah coefficients:

1. The index, k, is even and less than or equal to twice the minimum angular momentum encountered in the coincident cascade.[2]

2. For an intermediate stste spin of 1/2, there is no correlation.[10]

3. The functional dependence is symmetric around the intermediate state. For example, a 4(Q) 2(Q) 0 cascade would have the same angular correlation as 0 (Q) 2(Q) 4.

C. Perturbed Angular Correlation

1. Introduction

When the intermediate nuclear state in the cascade is substantially perturbed before emission of the second gamma ray, the perturbation will materialize experimentally in the angular correlation pattern. The criteria for this are sufficiently long nuclear lifetime, typically of the order of 10^{-5} - 10^{-11} seconds, and a strong interaction between nuclear electric or magnetic moments and fields at the nucleus.

The perturbation can cause both a rotation of the angular correlation and an attenuation of the anisotropy. Classically, an intermediate state nucleus precesses around the internal field with a frequency ω, dependent upon the interaction strength, for a time interval τ, the nuclear lifetime, giving a net rotation of its angular behavior of $\Delta\theta = \omega\tau$. Quantum-mechanically the perturbation corresponds to a diagonalization of eigenstates in the intermediate state. The attenuation of the anisotropy results from the uncertainty in τ over an ensemble of nuclei, imposing an unequal time of perturbation upon different nuclei.

For a static perturbation, the anisotropy can be attenuated no lower than a certain minimum (or "hard core") value.[11] The lower limit stems from the fact that nuclei in magnetic environments whose symmetry axes lie parallel to the axis of one of the cylindrical detectors exhibit no perturbation in the plane of the two detectors. In a polycrystalline, liquid, or gaseous sample such nuclei are statistically always present. For time-dependent perturbations, such as randomly fluctuating electric field gradients in a liquid, the anisotropy can be completely quenched. The time-dependent attenuation increases exponentially with a characteristic relaxation constant λ_k. The relative magnitude of λ_2 and λ_4, moreover, indicates whether the time-dependent perturbation is of electrostatic or magnetic nature.

2. Functional Dependence

a. General case

The perturbation results in an angular correlation function dependent upon time,

$$W(\theta,t) = \sum |H^{ab_1}|^2 |U^{b_1 b_2}(t)|^2 |H^{b_2 c}|^2 . \qquad (24)$$

U(t) is a unitary matrix which describes the time evolution of the intermediate state.

For a static perturbation K, the unitary operator satisfies the Schrödinger equation

$$\frac{\partial}{\partial t} U(t) = -\frac{i}{\hbar} K \cdot U(t) , \tag{25}$$

where both sides of the equation operate on an eigenstate $|m_b\rangle$. When $|m_b\rangle$, a nuclear coordinate system eigenstate, is an eigenfunction of K,

$$U|m_b\rangle = e^{-iE_b t/\hbar} |m_b\rangle . \tag{26}$$

Substituting in Eq. (24),

$$W(\theta,t) = \sum |H^{ab_1}|^2 e^{-i(E^{b_1} - E^{b_2})t/\hbar} |H^{b_2 c}|^2 . \tag{27}$$

In general, $|m_b\rangle$ may not be an eigenfunction of K. For example, in the presence of a hyperfine interaction coupling nuclear spin $\vec{I}$ with electronic angular momentum $\vec{J}$ to give an eigenvalue F, we must form a linear combination of nuclear states to diagonalize K. Denoting m as the generalized good quantum number, we have

$$|m\rangle = \sum_{m_b} \langle m|m_b\rangle |m_b\rangle . \tag{28}$$

The perturbation term in the Hamiltonian then becomes

$$|U(t)^{b_1 b_2}|^2 = \sum_{b_1 b_2 b_1' b_2'} \langle m^{b_1}|m\rangle \langle m^{b_1'}|m\rangle^* e^{-i(E_m - E_{m'})t/\hbar} \langle m'|m^{b_2}\rangle \langle m'|m^{b_2'}\rangle^* . \tag{29}$$

Remembering that for reorientation of the intermediate nuclear state, Eqs. (16) and (17) no longer hold, we have for the angular correlation function

$$W(\theta,t) = \sum_{k_1 k_2 d_1 d_2} \left\{ \sum_{m^{b_1} m^{b_2}} \langle I_b I_b m^{b_1} - m^{b_1'} | k_1 d_1 \rangle \langle I_b I_b m^{b_2} - m^{b_2'} | k_2 d_2 \rangle \right.$$

$$\left. \times \langle m^{b_1} | m \rangle \langle m^{b_1'} | m \rangle^* e^{-i(E_m - E_{m'})t/\hbar} \langle m' | m^{b_2} \rangle \langle m' | m^{b_2'} \rangle^* \right\} F^{k_1} F^{k_2'} Y_{d_1}^{k_1}(-\Omega_1) Y_{d_2}^{k_2}(\Omega_2) \quad (30)$$

The term in curly brackets, with suitable normalization, is referred to in the literature as $G_{k_1 k_2}^{d_1 d_2}(t)$. Eq. (30) is a completely general equation for the perturbed angular correlation function. Specific functional forms of $G_{k_1 k_2}^{d_1 d_2}$ for liquid and polycrystalline sources in the presence of electric and magnetic perturbations are tabulated by Abragam and Pound.[12] In addition, Alder, Matthias, et al. have developed a computer program which accounts for mixed perturbations.[13] Two examples of simple perturbations will be discussed here.

b. Axial internal field

In instances where an internal symmetry axis is defined by either a magnetic field or an axially symmetric electrostatic field, the projection eigenvalue m_b becomes a good quantum number considerable simplifying Eq. (30). The terms $\langle m_b | m \rangle$ become unity, and $m^{b1} = m^{b2}$, $m^{b1'} = m^{b2'}$. This implies $d_1 = d_2$. Now for polycrystalline or liquid sources the product of $Y_d^k(\Omega)$ matrix elements must be averaged over all Ω. This integral, through the orthogonality of spherical harmonics gives $k_1 = k_2$, so that

$$W(\theta,t) = \sum_k G_k(t) F_k F_k' P_k(\cos\theta) , \quad (31)$$

with

$$G_k(t) = \sum_{mm'} \langle I_b I_b m - m' | k d \rangle^2 e^{-i(E_m - E_{m'})t/\hbar} \quad (32)$$

A typical case of this sort occurs for a static electric interaction, where it can be shown,

$$E_m = \frac{eQ(\partial^2 V/\partial z^2)}{4I(2I-1)}\left[3m^2 - I(I+1)\right] \qquad (33)$$

where Q is the nuclear quadrupole moment and $(\partial^2 V/\partial Z^2)$ the axially symmetric electric field gradient.

c. Axial external field

When an externally applied field determines the symmetry axis, only a single rotation of the coordinate system is necessary to bring the z-axis into the direction of propagation. In the case investigated in this work, a magnetic field is applied perpendicular to the plane of the counters. The rotation of the nuclear z-axis to the propagation direction thus requires $\Omega = (\phi, \theta = \pi/2)$. The product of spherical harmonics in Eq. (30) gives

$$Y_d^k(-\phi_1, \pi/2)\, Y_d^k(\phi_2, \pi/2) = f(kd)\, e^{-id\theta} \qquad (34)$$

where $\theta = \phi_2 - \phi_1$ and $f(k,d)$ is a normalization term.

Now for interaction with a magnetic field, the nuclear states take on the eigenvalues

$$E_m = -\mu H(m/I) = -g\mu_N H m \qquad (35)$$

where μ is the nuclear magnetic moment, H the field at the nucleus, and $\mu_n = 5.05 \times 10^{-24}$ ergs/gauss, the nuclear magneton. From the magnetic selection rule $\Delta m = \pm 1$ we define the Larmor precession frequency

$$\omega_L = \frac{E_{m+1} - E_m}{\hbar} \qquad (36)$$

The exponential term in Eq. (32) can now be removed from the summation, as for Zeeman splitting the energy levels are equally spaced and $e^{-id\omega_L t}$ is independent of m. The Clebsch-Gordan coefficients drop out due to orthogonality conditions and we have

$$W(\theta,t) = \sum_k f(k,d)\, F_k F_k' \sum_{d=-k_{max}}^{+k_{max}} e^{id(\theta-\omega_L t)} \qquad (37)$$

From this it can be shown that

$$W(\theta,t) = 1 + \sum_{d=2}^{k_{max}} B_d \cos d(\theta-\omega_L t) \qquad (38)$$

where d takes on only even values and B_d encompasses F_k, F_k' and f(k,d). For $k_{max} = 4$ we have

$$B_2 = \frac{3/4\, F_2 F_2' + 5/16\, F_4 F_4'}{1 + 1/4\, F_2 F_2' + 9/16\, F_4 F_4'}$$

$$B_4 = \frac{35/64\, F_4 F_4'}{1 + 1/4\, F_2 F_2' + 9/16\, F_4 F_4'} \qquad (39)$$

d. Time dependence of perturbed angular correlation

From the general Eq. (30) it is apparent that the time dependence of the angular correlation in the presence of a static interaction is entirely contained in the exponential $e^{-i(E_m - E_{m'})t/\hbar}$. This term effectively produces a sinusoidal variation of anisotropy with time. It thus forms the basis for differential perturbed angular correlation measurements where the resolving time of the apparatus is sufficiently small to allow investigation of time independence.

For many decays it proves more convenient to study the total time integrated angular correlation. For a resolving time substantially

larger than the nuclear lifetime, the integrated time dependence can be approximated by

$$\frac{\int_0^\infty e^{-t/\tau} G_k(t)\,dt}{\int_0^\infty e^{-t/\tau}\,dt} \propto \frac{1}{\tau}\int_0^\infty e^{-t/\tau} e^{-i\Delta E t/\hbar}\,dt = \frac{1}{1+(\Delta E\tau/\hbar)^2} \qquad (40)$$

Here τ is the mean lifetime of the nuclear state, and the inclusion of the $e^{-t/\tau}$ term statistically averages the effect of the perturbation over a decaying ensemble of nuclei. The result is a constant attenuation term which depends upon $\Delta E/\hbar = \omega$, the frequency of the rotation caused by the perturbation. This effect can readily be seen in polycrystalline solids where randomly oriented electrostatic fields may partially smear out the anisotropy.

In this work we are concerned primarily with the effect of perpendicular magnetic fields upon angular correlations where $k_{max} = 2$. From Eq. (38) we have the integrated angular correlation

$$W(\theta) = \frac{1}{\tau}\int_0^\infty e^{-t/\tau} W(\theta,t) = \frac{1}{\tau}\int_0^\infty e^{-t/\tau} B_2 \cos 2(\theta - \omega_L t)$$

$$= \frac{B_2}{[1+(2\omega_L\tau)^2]^{1/2}} \cos 2(\theta - \Delta\theta). \qquad (41)$$

$$\Delta\theta = \tfrac{1}{2}\tan^{-1} 2\omega_L\tau .$$

For small rotations, where $\tan^{-1} 2\omega_L\tau \approx 2\omega_L\tau$, this equation describes the classical phenomenon of a nucleus precessing about an applied field at a frequency ω_L.

D. Applications of Perturbed Angular Correlation

1. Introduction

The form of Eqs. (40, 41) indicates that $\omega_L = \Delta E t/\hbar$ can be experimentally measured by the perturbed differential method through

the sinusoidal variation of anisotropy, or by the integral method through attenuation of anisotropy and, in the case of perpendicular magnetic fields, from the rotation of the angular correlation pattern. As ω_L depends upon a product of fields at the nucleus and excited state nuclear moments, perturbed angular correlation has important applications in both nuclear level systematics and solid state physics.

2. Nuclear Magnetic Moments

a. Introduction

While the preceding derivations hold for both electric and magnetic interactions, the majority of perturbed angular correlation measurements deal with magnetic phenomena. This in part stems from the difficulty in theoretically predicting electric field gradients and from the existence of detailed predictions for both magnetic moments and internal magnetic fields. Our attention will accordingly be focussed on magnetic interactions.

The theoretical prediction of nuclear magnetic moments is a problem not completely solved despite the great bulk of experimental values for both ground and excited states. An exact solution would require a precise knowledge of nuclear eigenfunctions. As these are not known, one must resort to successively more complicated approximations of nuclear models in order to approach the experimental data. A brief review of the effect of the more important approximations upon nuclear moments will be given here.

b. Single particle in a central potential

The first nuclear model to achieve considerable success in predicting magic numbers, transition probabilities, and nuclear moments was the single particle shell model proposed by Mayer and Jensen.[14] Protons are pictured as pairing off, as are neutrons, while any remaining odd particle moves in a central potential set up by the paired core. All angular momentum properties come from the unpaired nucleon.

One can therefore predict the gyromagnetic ratio g by adding vectorially the magnetic moments associated with the spin and orbital angular momenta of the particle or particles. This vector sum gives for the scalar quantity g_j

$$g_j = g_\ell \frac{j(j+1) + \ell(\ell+1) - s(s+1)}{2j(j+1)} + g_s \frac{j(j+1) + s(s+1) - \ell(\ell+1)}{2j(j+1)}$$

$$= g_\ell \pm \frac{1}{2\ell+1}(g_s - g_\ell) \qquad (42)$$

where the total single-particle angular momentum satisfies the vector sum $j = \ell \pm s$.

From measurements on free protons and neutrons, we have

$g_s = +5.586$	for protons	$g_s = -3.826$	for neutrons
$g_\ell = +1.00$		$g_\ell = 0.00$	

With the approximation that the free proton and neutron g values remain unchanged in heavy nuclei, the expected g_j values for spin and orbital moments parallel and antiparallel, the Schmidt limits, can be calculated.[15] These values, shown in Table I, constitute the best single rough estimate of experimental values. The grouping of g_j values for unpaired particles from the same nuclear shell attests to the validity of the theory, although perturbations must be proposed to account for the deviations inward from the Schmidt values.

If more than one unpaired particle exists, formulae similar to Eq. (42) vectorially couple the angular momenta to give the resultant g_j. One interesting consequence of this equation is that unpaired nucleons with identical j couple to give the same g_j as the single nucleon.

Table I. Schmidt limit g_j values for single particle states.

		$\ell = 0$	1	2	3	4	5
Protons	$\ell + s$	+5.59	+2.52	+1.92	+1.66	+1.51	+1.419
	$\ell - s$		-0.530	+0.83	+0.345	+0.492	+0.581
Neutrons	$\ell + s$	-3.82	-1.27	-0.76	-0.546	-0.424	-0.348
	$\ell - s$		+1.276	+0.77	+0.548	+0.426	+0.386

c. Collective model

Despite the success of the single-particle model, many nuclear phenomena remained unexplained, namely anomalously high transition probabilities for certain low lying states and unexpectedly large quadrupole moments. These effects appear predominantly in areas far from closed shells and can be attributed to a permanently deformed nucleus with collective as well as single particle degrees of freedom.

The first quantum mechanical treatment of collective motion was presented in 1952 by Bohr[16] and extended the following year by Bohr and Mottelson.[17] The method involves the coupling of intrinsic single particle motion with angular momentum $\vec{J}$ to rotational angular momentum $\vec{R}$. Empirical evidence supports the contention that for nuclei sufficiently far from a closed-shell configuration the coupling is "strong"; that is the precession frequencies of the two angular momenta are sufficiently different that the rotational motion follows the single particle motion adiabatically. Quantum-mechanically states, the Hamiltonian is separable into an intrinsic and a collective part, and the wave function is an antisymmetrized product of intrinsic and collective eigenfunctions. This coupling scheme is indicated in Fig. 1.

A further refinement of the scheme was offered by Nilsson, who proposed that the single particle moves not in a spherical central potential, but in a deformed harmonic oscillator potential.[18] Thus the intrinsic angular momentum j is no longer a good quantum number at large deformations. However, l_z, s_z, and j_z, the projections upon the nuclear symmetry axis, now become constants of the motion, and with the oscillator quantum number N, provide a new complete representation for the nuclear states.

The nuclear magnetic moment may be simply described as a vector sum of the intrinsic and collective components.

$$g_I \vec{I} = g_l \vec{l} + g_s \vec{s} + g_r \vec{R} = g_j \vec{j} + g_r \vec{R} \,. \qquad (43)$$

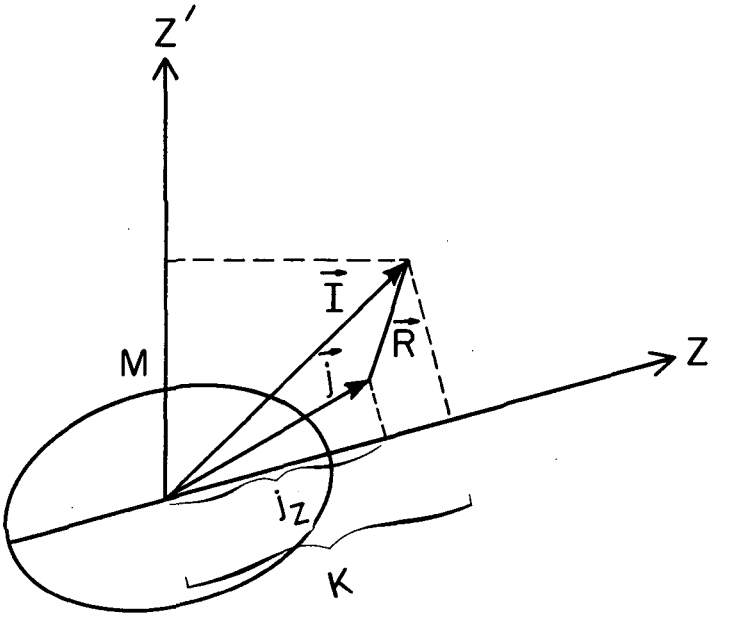

MU-34769

Fig. 1. Coupling scheme for strong interaction between collective and intrinsic angular momenta.

Performing the necessary rotations from the nuclear to the laboratory system, it can be shown that for $K > 1$,

$$\mu = \langle \vec{\mu} \rangle_{M=I} = g_r I + \frac{j_z K}{I+1} (g_j - g_r) . \tag{44}$$

Equating j_z with K for an axially symmetric nucleus, one obtains

$$g_I = g_r + \frac{K^2}{I(I+1)} (g_K - g_r) . \tag{45}$$

For an even-even nucleus $K = 0$ in the ground state and the nuclear g-factor is just g_r. The value of g_r is conventionally estimated as Z/A for a rigid rotator, althrough experimental values fall somewhat below this. The probable reason for the discrepancy is the pairing force, which will be discussed below.

d. Pairing force and quasi particles

One feature of nuclear systematics not amenable to the above treatments is the existence of surprisingly large energy gaps to the first excited state for even-even nuclei in the region of mass number 150-190. The inclusion of a residual force, a short-range pairing force between two like nucleons, has produced semi-quantitative agreement between theory and experiment.

To formally describe the pairing interaction, we add to the customary Hamiltonian the residual interaction,

$$\mathcal{H} = \mathcal{H}_0 + V$$

$$V = \langle j m \; j -m | V_{pair} | j' m' \; j' -m' \rangle . \tag{46}$$

Now in order to account for the fact that V is diagonalized in only a two-particle paired system, we transform from single particle eigenfunctions to a function in which two particles are paired to give $J = 0$.

A mathematically convenient eigenfunction is the one proposed by Bardeen, Cooper, and Schrieffer[19] to describe large energy gaps and superconductivity in solids, or[20]

$$\Psi = \prod_{\alpha} \left[\mu_{\alpha} + \nu_{\alpha} c_{\alpha}^{+} c_{\bar{\alpha}}^{+} \right] |0\rangle . \qquad (47)$$

Here $|0\rangle$ is the single particle vacuum operated on by the creation operator C_{α}^{+} and its complex conjugate $C_{\bar{\alpha}}^{+}$ to give a pair which occupies a given level with probability V_{α}^{2} or leaves it vacant with probability u_{α}^{2}.

This eigenfunction is analogous to a diffuse Fermi surface in solids. That is, in regions away from closed shells, where the level density is relatively high, each level will have a finite probability of occupation and of vacancy, or of containing a particle or a hole. Thus, the quasi-particle defined by this eigenfunction, has both particle and hole characteristics and is sometimes considered as a coupling between a particle and a hole.[21]

Operating on the quasi-particle eigenfunction with the total Hamiltonian produces a depression from the energies of the unfilled single particle shells, resulting in the characteristic energy gap to the first excited state. The details of this formulation are quite sensitive to the density of unfilled levels in the single particle scheme and consequently to the proton and neutron configurations.

As unfilled shells contribute almost exclusively to collective deformation properties of the nucleus, Nilsson and Prior find a significant dependence between quasi-particle gap energies and moments of inertia and rotational g-factors g_r.[21] These authors accordingly predict the latter two quantities on the basis of rigorous quasi-particle expectations and find quite good agreement with experiment. In particular, the g_r values fall, with the experimental values, consistently below the estimate $g_r = Z/A$.

Kisslinger and Sorensen first investigated the same problem in a region of small deformation, that of single closed shell nuclei.[23]

These nuclei have the advantageous feature that interactions between neutrons and protons can be neglected, and the excited state quasi-particle behavior evolves solely from the unfilled shell. The calculated predictions for transition probabilities are found to be in good agreement with experiment, justifying the quasi-particle designation in this region. In a later work these authors have extended the quasi-particle treatment to a wider range of the periodic table.[84]

Because the g-factors of a particle and a hole in the same shell are identical, the g-factor for an excited state composed of a broken particle pair is no different from that for a single particle pair from the same nuclear shells. Thus, the simple vector coupling treatment of particles from Nilsson levels remains valid for quasi-particle magnetic moments.

e. Summary

A number of models have been proposed to account for the deviation of single particle magnetic moments from the Schmidt limits, although no single picture has given a completely satisfactory fit. Two of the later formulations will be mentioned here for completeness.

Noya, Arima, and Horie have proposed a δ-force which enables configuration mixing of ground and higher excited states.[24] This force is justified as being compatible with the absence of high nuclear spin levels. For a small admixture of excited states, the wave function becomes

$$\psi = \left(|0\rangle + \sum_n \alpha_n |n\rangle\right) \Big/ \left(1 + \sum_n |\alpha_n|^2\right) \qquad (48)$$

where the excited states $|n\rangle$ are mixed into the ground state $|0\rangle$ with probability $|\alpha_n\rangle^2$. This gives an expectation value for the operator F

$$\langle F\rangle \cong \langle 0|F|0\rangle + 2\sum_n \alpha_n \langle 0|F|n\rangle \,. \qquad (49)$$

It becomes apparent from Eq. (49) that a one percent admixture of an excited state ($|\alpha_n|^2 = .01$) results in a twenty percent admixture to the operator F. Thus, extremely small admixtures can perhaps partially explain the observed deviations from the Schmidt limits.

A comparable approach has been suggested by Bodenstedt and Rogers where excited configurations of the core are admixed instead of single particle states.[21] As the magnetic moment operator is a tensor of rank one and the ground state has angular momentum zero (in an even-even nucleus), the states admixed by this operator must be of rank one. This simplified core polarization model reproduces with reasonable accuracy the experimental single particle magnetic moments.

It is unfortunate that experimental precision generally gives inconclusive quantitative choice between different models and different magnetic moment corrections due to residual forces. The primary goal of magnetic moment measurements has been the elucidation of energy level schemes using simple Schmidt limits. A compilation of these measurements has been prepared by Bodenstedt.[25] These attest significantly to the value and broad scope of the method.

3. Internal Fields

a. Introduction

From the perturbed angular correlation function, it is apparent that nuclear magnetic moments can be determined only when the magnetic field at the nucleus is known. The converse of this statement is also true and has stimulated a broad study of internal fields complementary to Mössbauer, nuclear magnetic and electron spin resonance, and low temperature nuclear polarization data.

The following discussion of internal fields will deal with only rare earth ions and atoms. This region, characterized by an electron configuration $4f^n$, $5d^0$, $6s^2$ upon a xenon core, is the focal point of the experimental work discussed below. The relative depth of the unfilled 4f shell within the electron cloud insures effective immunity from outside chemical disturbances. Thus, any external fields or crystal

fields can be dealt with as perturbations to the electron configuration, and in the limit of pure Russell-Saunders coupling, the quantum numbers S, L, J, and M, label the states. Throughout the derivation, we will assume Russell-Saunders behavior.

b. Generalized treatment

We wish to find the expectation value of the internal field— H_{int} due to unpaired 4f electrons, or

$$\langle H_{int} \rangle = \sum_i \langle \alpha_i | H_i | \alpha_i \rangle e^{-E_{\alpha_i}/kT} \Big/ \sum_{\alpha_i} e^{-E_{\alpha_i}/kT} \tag{50}$$

where $|\alpha_i\rangle$ represents an electronic state with energy E_{α_i}. Our procedure will be to explain α quantum mechanically using first-order perturbation theory and to substitute for H_i the classical internal field set up by a rotating electron.

To determine $|\alpha\rangle$ one must take into account the fact that the unfilled 4f shell will have a permanent magnetic moment. This will interact with the external field to give an additional term in the Hamiltonian,

$$\mathcal{H}' = -\vec{\mu}_z \vec{H}_{ext}$$

$$E' = -\mu_B H_{ext} \langle SLJM | \mu_z | SLJM \rangle = -\mu_B H_{ext} M \langle J \| \Lambda \| J \rangle \tag{51}$$

where $\langle J \| \Lambda \| J \rangle$ is the g-factor of the electronic shell, or

$$\langle J \| \Lambda \| J \rangle = g_j = 1 + (g_s - 1) \frac{J(J+1) + S(S+1) - L(L+1)}{2J(J+1)} \tag{52}$$

Additionally, the magnetic moment operator will mix the ground state with excited states as long as the conditions $\Delta L = \Delta S = \Delta M = 0$, $\Delta J = 0, \pm 1$ are satisfied. Thus, the pertinent wave function $|\alpha\rangle$ in the presence of a perturbing external field has a zero-order component which is a product of the isotropic Hamiltonian eigenfunction and the contribution due to the magnetic moment operator; and a first order admixture due to states with $\Delta J = \pm 1$.

$$|\alpha\rangle = |SLJM\rangle + \mu_B H_{ext} \left\{ \frac{\langle J+1 \| \Lambda \| J \rangle \left[(J+1)^2 - M^2\right]^{1/2}}{E_J - E_{J+1}} |SL\ J+1\ M\rangle \right.$$

$$\left. + \frac{\langle J \| \Lambda \| J-1 \rangle \left(J^2 - M^2\right)^{1/2}}{E_J - E_{J-1}} |SL\ J-1\ M\rangle \right\} . \qquad (53)$$

A detailed derivation of Eq. (53) is worked out by Gunther and Lindgren.[26]

Now inserting the eigenfunction $|\alpha\rangle$ into Eq. (50) we find

$$\frac{H_{int}}{\mu_B H_{ext}} = \sum_{J=|L-S|}^{L+S} \sum_{M} \frac{M \langle J \| \Lambda \| J \rangle \langle LSJM | H_i | LSJM \rangle e^{-E_J/kT}}{\sum_{J=|L-S|}^{L+S} (2J+1)\, e^{-E_J/kT}}$$

$$+ \sum_{J=|L-S|}^{L+S} \sum_{M} \frac{\langle J' \| \Lambda \| J \rangle \left(J'^2 - M^2\right)^{1/2} \langle LSJ'M | H_i | LSJM \rangle \left(e^{-E_J/kT} - e^{-E_{J'}/kT}\right)}{(E_J - E_{J'}) \sum_{J=|L-S|}^{L+S} (2J+1)\, e^{-E_J/kT}} \qquad (54)$$

where $J' = J + 1$ and the other quantities have the usual significance.

Neglecting a Fermi contact term, the internal field matrix element can be computed starting with the classical expression,

$$H_i = \sum_k \frac{e}{c} \frac{\vec{v}_k \times \vec{r}_k}{r_k^3} - \frac{s_k}{r_k^3} - \frac{3(r_k \cdot s_k) r_k}{r_k^5} \qquad (55)$$

where the first term on the right expresses the field due to the orbital motion of the electrons with velocity V_k and distance r_k from the

nucleus; and the second and third terms evolve from the dipole-dipole interaction between nuclear and electronic spins.

Using the Wigner-Eckart theorem and the principle of operator equivalence, Elliot and Stevens have derived the simplified form,

$$\langle LSJM|H_i|LSJM\rangle = 2\mu_B \langle r^{-3}\rangle \langle J\|N\|J\rangle M$$

$$\langle LSJM|H_i|LSJ{-}1\,M\rangle = 2\mu_B \langle r^{-3}\rangle \langle J\|N\|J-1\rangle (J^2-M^2)^{1/2} \qquad (56)$$

and have tabulated the values for the reduced matrix elements.[27] Substituting these values in Eq. (54) one can calculate from a completely general expression the internal field due to unpaired 4f electrons.

c. Simplified treatment

In the specific rare earth ions investigated here, as in most rare earths, the electronic fine structure splitting is so large that a pure, zero order ground state configuration very closely approximates the true situation. Thus, in the general equation, the summation over J values and the admixture of $J \pm 1$ can be disregarded.

An equally valid and more intuitive approach is to consider the unpaired spin density as polarized by the external field, so that an effective field at the nucleus occurs with

$$H_{int} = \beta H_{ext} \qquad (57)$$

In the presence of an axial hyperfine interaction, the constant β arises from two terms in the spin Hamiltonian

$$\mathcal{H} = g_N \mu_N H_{ext} I_z + A \bar{J}_z I_z \qquad (58)$$

where $\bar{J}_z$ is the average projection of electronic angular momentum calculated over the thermal range, A is the hyperfine coupling constant,

and $g_n \mu_n I_z$ the maximum projection of the nuclear magnetic moment. Substituting the Van Vleck expression for temperature dependent paramagnetic susceptivility, into Eq. (57),[28] one finds

$$H_{int} = H_{ext}\left(1 + \frac{A(g_{eff})^2 \mu_B}{g_{\parallel} g_n \mu_N 3kT}\right) \tag{59}$$

where g_{eff} is the effective number of Bohr magnetons, $g_J[J(J+1)]^{1/2}$ in the overall paramagnetic susceptivility, and $g_{\parallel}$ is the axial susceptibility.[29]

The hyperfine term in A is just the attraction of the nuclear magnetic moment to the internal field due to the electrons. This field is given by Eq. (55). The term can therefore be expressed

$$\mathcal{H}_{hfs} = A\bar{J}_z I_z = \frac{2\mu_B \mu_N}{I} \langle r^{-3} \rangle N \cdot I \tag{60}$$

where in a manifold of constant J with a maximum magnetic projection M

$$N \equiv \langle JM | N | JM \rangle = J \langle J \| N \| J \rangle . \tag{61}$$

Substituting into Eq. (59) the analytical expression for A and the fact that $g_{\parallel}\mu_B \bar{J}_z$ is equivalent to $\langle J\|\Lambda\|J\rangle \mu_B J$ in an isotropic medium,[29] the paramagnetic correction factor becomes

$$\beta = 1 + \frac{2\mu_B^2}{3kT} \langle r^{-3} \rangle \frac{\langle J \| N \| J \rangle}{\langle J \| \Lambda \| J \rangle} (g_{eff})^2 . \tag{62}$$

The quantities g_{eff} and $\langle r^{-3} \rangle$ add some uncertainty to the calculation of β and will be discussed below.

d. Corrections

(1) g_{eff}. The calculation of g_{eff} depends upon a precise knowledge of the Lande g-factor. This is slightly complicated by the spin-orbit coupling term in the Hamiltonian which produces small deviations from pure Russell-Saunders coupling by mixing states of the same J but different L and S values.

The spin-orbit coupling takes the form,

$$\mathcal{H}' = \sum_i \xi(r_i)\vec{l}_i \cdot \vec{s}_i \qquad (63)$$

which, by the Wigner-Eckart theorem is proportional to $\vec{L} \cdot \vec{S}$. The angular portion of the mixing matrix elements can thus be represented by vector coupling coefficients.

As the correction to the Lande-g-factor takes the form of a second order perturbation, the precise energies of excited J states are required. Thus, the radial dependence appears both in the radial integrals used to evaluate the zero order eigenfunctions and the spin-orbit coupling constant, $\xi(r_i)$. Good experimental data for both these quantities exist for the triply ionized rare earths and empirical formulae have been derived.[30] For neutral atoms, enough experimental evidence is available to allow a reasonable estimate of an empirical formula by induction.[31]

The resultant theoretical values of g_{eff} and the old Van Vleck values for the ground state of the rare earth ions are compared in Table II.

(2) $\langle r^{-3} \rangle$. The second and more important variable in the determination of the paramagnetic correction constant is $\langle r^{-3} \rangle$, the reciprocal cube of the mean 4f electron radius. Several divergent theoretical predictions exist for this quantity.

Bleaney in 1955 proposed evaluation of $\langle r^{-3} \rangle$ from hydrogenic radial wave functions modified by electronic screening of the nuclear charge.[32] The wave function gives a fine structire constant

Table II. Summary of quantities relevant to internal fields in triply-ionized rare earths.

Element (+3)	$_{58}$Ce	$_{59}$Pr	$_{60}$Nd	$_{61}$Pm	$_{62}$Sm	$_{63}$Eu	$_{64}$Gd
g_J $J(J+1)$	2.54	3.58	3.62	2.68	0.84	0	7.94
g_{eff}	2.54	3.60	3.64	2.81	.87	0	7.92
$\langle 1/r^3 \rangle$ a_0^{-3} (Lind.)	3.66	4.26	4.86	5.46	6.07	6.70	7.35
$\langle 1/r^3 \rangle$ a_0^{-3} (F.W.)	4.72	5.37	6.03		7.36		8.84
$(A_{4f} + A_{core})/A_{4f}$		1.020	1.024	1.034	1.048		
T_c ($^\circ$ K)	-50°	-21°				-3°	310°
$\langle 1/r^3 \rangle$ a_0^{-3} (Bleaney)	4.44	5.06	5.64	6.18	6.72	7.28	7.89

Element (+3)	$_{65}$Tb	$_{66}$Dy	$_{67}$Ho	$_{68}$Er	$_{69}$Tm	$_{70}$Yb
g_J $J(J+1)$	9.72	10.6	10.6	9.58	7.56	4.54
g_{eff}	9.70	10.5	10.42	9.50	7.52	4.53
$\langle 1/r^3 \rangle$ a_0^{-3} (Lind.)	8.03	8.74	9.50	10.32	11.20	12.18
$\langle 1/r^3 \rangle$ a_0^{-3} (F.W.)		10.34		12.01		13.83
$(A_{4f} + A_{core})/A_{4f}$	0.932	0.970	0.979	0.984	0.988	0.990
T_c ($^\circ$ K)	237°	154°	87°	47°	20°	-5°
$\langle 1/r^3 \rangle$ a_0^{-3} (Bleaney)	8.53	9.20	9.91	10.60	11.61	12.50

$$\xi(r_i) = \frac{2(Z-\sigma)^4 \mu_B^2}{n^3 l(l+1/2)(l+1) a_0^3} \qquad (64)$$

where σ is the screening constant and varies from 34.6 to 35.9 for the rare earths, a_0 is the first Bohr radius, n and l are electronic quantum numbers, and Z is the nuclear charge. Now, since the fine structure constant $\xi(r_i)$ is proportional to $(1/r)\, dV/dr$ and since V in a hydrogen-like atom varies as $1/r$, a simple relationship exists between $\langle r^{-3} \rangle$ and $\xi(r_i)$. From experimental splittings, therefore, Bleaney derived the empirical formula,[32]

$$\langle r^{-3} \rangle = 0.89 (Z-47)^{3/2} \text{ Å}^{-3}. \qquad (65)$$

Ridley later performed Hartree self-consistent-field (SCF) calculations for Pr^{+3} and Tm^{+3}.[33] These gave good agreement with the hydrogenic spin-orbit splitting constant, but quite poor agreement on Slater integrals and $\langle r^{-3} \rangle$.

Cabezas and Lindgren subsequently refined the approach by using a modified hydrogenic radial eigenfunction,

$$R(r) = N r^4 e^{-ar} \cosh \kappa (ar - 4) \qquad (66)$$

with N a normalization term and $\underline{a}$ and κ empirical constants.[34] The constant κ was varied to give the best fit with the Ridley SCF radial wave function, which is substantially wider (more diffuse) than the hydrogenic orbital. Although the constant $\underline{a}$ could be similarly evaluated, it was thought wiser to determine this from the fine structure constant.

Soon after, Judd and Lindgren gave values of $\langle r^{-3} \rangle$ for rare earth atoms and ions using a constant value of $\kappa = 0.42$ in the radial function.[30] Lindgren slightly improved this procedure by allowing κ to vary from 0.420 to 0.396 in order to best fit the known and interpolated SCF funtions.[35]

More recent work has been done by Freeman and Watson using Hartree-Fock eigenfunctions.[36] However, these results may be inconsistent in that exchange terms were included in the calculation of the wave functions but neglected in the calculation of the fine structure constant. The latter may be in error by as much as 30%.

The Lindgren and Freeman and Watson values for $\langle r^{-3} \rangle$ in triply ionized rare earths are summarized in rows 4 and 5 of Table II.

Several experimental results for absolute values of nuclear magnetic moments in rare earths have been cited by Bleaney.[31] Combining these with hyperfine interaction data and Judd-Lindgren atom-ion radius ratios, and correcting for core polarization, Bleaney deduced $\langle r^{-3} \rangle$ for Nd, Er, Tm, and Yb. Interpolation through the experimental points gives a preliminary estimate of $\langle r^{-3} \rangle$ over the rare earth series. Bleaney's interpolated values for the ions are given in column 8, Table II. Fig. 2 illustrates that the interpolated curve starts quite near the Freeman-Watson values for the lower rare earths, but decreases toward the Lindgren results at the upper end of the series.

(3) Core polarization. A further alteration in the paramagnetic correction term, β, is due to the spin polarization of electrons in closed shells. In the atoms this is negligible, but in the rare earth ions the electronic charge would be expected to exert a slight polarization upon the core electron spin density. An unpaired s-electron spin contribution would impose a particularly strong field at the nucleus through the Fermi contact term. A $p_{1/2}$ electron may also contribute a smaller amount.

To estimate this effect one may compare atomic and ionic hyperfine interactions in Eu and Eu^{+2} both of which exhibit an electronic $4f^7\ 8s_{7/2}$ configuration. Two measurements of nuclear and electronic moments and hyperfine interaction constants in atoms and ions make this study feasible. Sandars and Woodgate[38] with a triple resonance atomic beam ($\Delta M_J = 0$, $\Delta M_I = \pm 1$), determine these quantities for Eu^{151} and Eu^{153}. Baker and Williams deduce the same quantities for Eu^{+2} in a CaF_2 lattice by e.p.r. and endor measurements.[39]

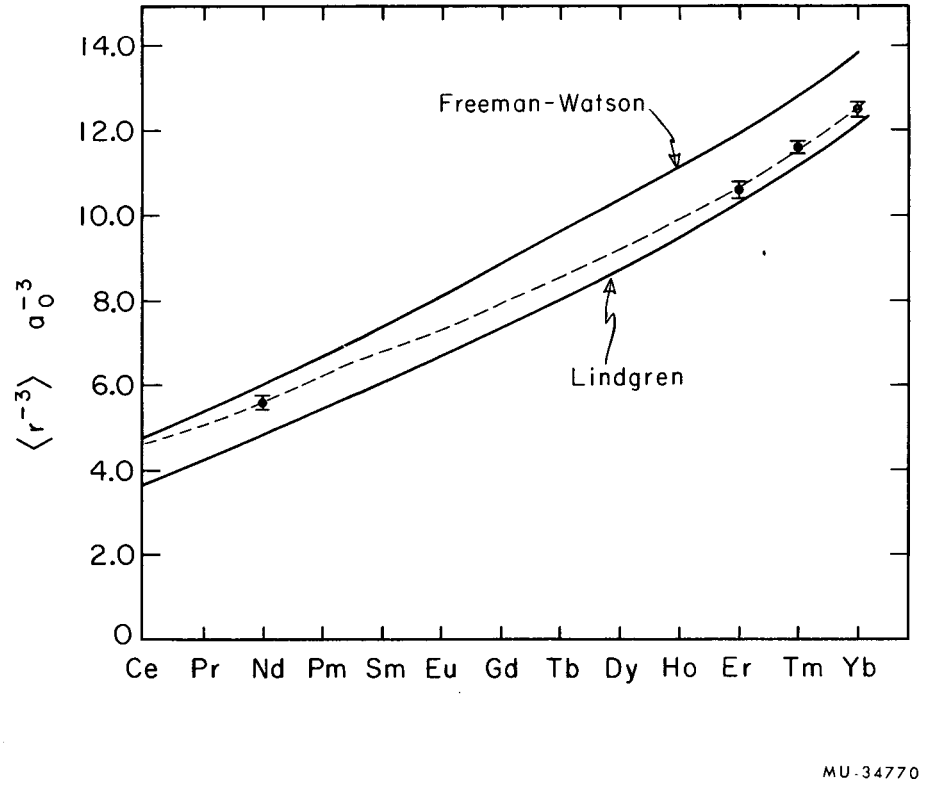

Fig. 2. Variation of $\langle r^{-3} \rangle$ in the rare earth series. The dashed line represents Bleaney's interpolated values.

Both determinations yield a finite hyperfine interaction term and an anomaly between the ratio of nuclear magnetic moments and hyperfine interaction constants for Eu^{151} and Eu^{153}. The finite hyperfine term indicates, in part, a slight breakdown of Russell-Saunders coupling. The anomaly in ratios is explained by Bohr and Weisskopf as due to the effect of minutely different nuclear charge distributions upon the unpaired s or $p_{1/2}$ spin density within the nucleus.[40] Thus, there are clearly internal fields due to both unfilled f shells and the cores.

From the data Bleaney deduced an empirical expression for the hyperfine interaction constant due to only the core,[31]

$$A_{core} = -(63 \pm 10)(g_j - 1)\, g_I \quad Mc/sec. \tag{67}$$

Utilizing this correction upon experimental hyperfine interaction results, Bleaney calculated ratios of $\langle r^{-3} \rangle$ for atoms and ions. These give qualitative agreement with the Judd-Lindgren theoretical results.

To incorporate the core correction into β, one may substitute an effective $\langle r^{-3} \rangle$ due to all the electrons,

$$\langle r^{-3} \rangle_{eff} = \langle r^{-3} \rangle_{4f} \left(\frac{A_{4f} + A_{core}}{A_{4f}} \right) \tag{68}$$

where A is the hyperfine interaction constant. These correction terms, where experimental evidence is available, have been calculated by Bleaney and are indicated in row 6, Table II.

(4) Cooperative effects in metals. An important consideration for the paramagnetic correction in metals is the existence of a Weiss field which contributes to the paramagnetic susceptibility and thus to the internal field.

Classically the paramagnetic susceptibility is just the total magnetization $M = N\mu \langle \cos \theta \rangle$ divided by the composite field $H_{tot.} = H_{ext} + H_c$, where μ is the atomic magnetic moment, N the number of atoms, $\langle \cos \theta \rangle$ the expectation value of the inclination of μ from H_{ext},

and H_c the Weiss field. At high temperatures where $\mu H \ll kT$, $\langle \cos \theta \rangle$ is approximated by $\mu H_{tot.}/3kT$. Thus the resultant susceptibility is[41]

$$\frac{M}{H_{ext}+H_c} = \frac{N\mu^2}{3kT} \equiv \frac{C}{T} \quad . \tag{69}$$

Making use of the fact that the Weiss field is a cooperative effect and proportional to the magnetization, $H_c = \lambda M$, we find the susceptibility to the external field

$$\chi = \frac{M}{H_{ext}} = \frac{C}{T-T_c} \tag{70}$$

where $T_c = \lambda C$ is the paramagnetic Curie temperature. This form must now be substituted into Eq. (62) to tabulate β for the rare earth metals.

The paramagnetic Curie temperature has been determined experimentally from susceptibility measurements for most of the rare earth metals.[42] These values are given in row 7, Table II.

e. Summary

It is apparent that the paramagnetic correction entails a good deal of uncertainty. It does at the same time, however, present an experimental handle for investigating these uncertainties when the nuclear magnetic moment is known.

In the application of the paramagnetic correction to perturbed angular correlation, we find the additional complication of possible electronic reorientation during the lifetime of the nuclear state. As the entire formalism of paramagnetic corrections rests upon the assumption of a rapid attainment of equilibrium by the electrons, some mention should be made of theoretical and experimental data on this phenomenon.

Two independent mechanisms may cause perturbations. In K-capture or internal conversion, a hole is created in an inner shell.

For the rare earths, this hole moves through inner shells mainly by radiative processes and through outer shells by emission of Auger electrons. The latter creates more holes which likewise move outward from the nucleus. The time duration of this has been estimated as 10^{-14} - 10^{-15} sec.[11] The line-width of the x-rays alone indicates a lifetime of of 1-2 $\times$ 10^{-16} sec.[26] This mechanism, therefore, probably has no effect upon angular correlation.

The excitation of the outer shell, from the accumulation of holes described above, or from the sudden change in Z through the emission of a β^- particle, decays in a metal by pick-up of readily available electrons from the conduction band, or in solution by random collisions with surrounding atoms. In the metal, equilibrium is attained rapidly. For the case in solution, Abragam and Pound define a correlation time, or electronic relaxation time, which contributes a time-dependent perturbation to the angular correlation by disturbing nuclear orientations.[12] For a very short relaxation time, the nucleus cannot follow the rapid electronic motion, and sees an average field (described by the paramagnetic correction). Typically small time-dependent perturbations in the rare earths, show a relaxation time of the order of 10^{-12} - 10^{-14} sec at room temperature in solution.[43]

Thus, throughout this work, where time-dependent perturbations in solution are negligible, we will assume that the electronic shells take up the configuration of the daughter element in nuclear decay in a time short compared to the nuclear lifetime; and that electronic relaxation is fast enough to permit thermal averaging.

A summary of expected values at room temperature for Lindgren, Freeman and Watson, and Bleaney values of $\langle r^{-3} \rangle$ is presented in Table III.

Table III. Values of the paramagnetic correction term β for different evaluations of $\langle 1/r^3 \rangle$.

Element (+3)	Bleaney (interpolated)	Lindgren	Freeman-Watson
$_{58}Ce$	1.42	1.34	1.43
$_{59}Pr$	2.00	1.84	2.06
$_{60}Nd$	2.25	2.08	2.06
$_{61}Pm$	1.92	1.81	
$_{62}Sm$	1.16	1.14	1.18
$_{63}Eu$	0.52	0.56	
$_{64}Gd$	1.23	1.21	1.26
$_{65}Tb$	3.57	3.42	
$_{66}Dy$	6.02	5.77	6.60
$_{67}Ho$	7.24	6.98	
$_{68}Er$	6.82	6.67	7.60
$_{69}Tm$	5.08	4.94	
$_{70}Yb$	2.58	2.54	2.75

III. APPARATUS

A. Introduction

The angular correlation function points out the possibility for measuring the Larmor frequency by two different experimental methods: the differential method, in which the resolving time of the apparatus is small compared to the mean life of the intermediate state; and the integral method in which it is quite large. The applicability of either method depends to a great extend upon the specific isotope to be investigated.

In the integral method, the entire angular dependence pattern is determined with and without a magnetic field perpendicular to the plane of the counters. The perturbed correlation is attenuated and rotated through an angle $\Delta\theta$. Minimizing the error by solving

$$\frac{1}{\omega_L\tau}\,\frac{d(\omega_L\tau)}{d(\Delta\theta)} = 0 \qquad (1)$$

one finds the optimum rotation is $\Delta\theta = 22.5^\circ$ corresponding to $\omega_L\tau = 0.5$. Even if this condition can be met, an experimental accuracy of 1% in $\Delta\theta$ leads to an error of 8% in $\omega_L\tau$. For a typical unperturbed anisotropy of 15%, this requires a total of 400,000 coincidences. A further inadequacy of the integral method stems from the presence of electric field gradient perturbations and background anisotropies. The former can cause attenuation of the correlation pattern beyond that from Larmor precession. An axially symmetrical electric field gradient, for example, rotates magnetic substates clockwise and counter-clockwise with equal probability.[2] Background anisotropy, from Compton edges and overlapping peaks, usually will not be rotated by a magnetic field, and unless corrected for, will give an unsymmetric correlation pattern. In addition, for very large $\omega_L\tau$, the anisotropy is smeared out enough to make this method useless.

In spite of the difficulties, however, the integral method has been used extensively, especially where $\omega_L \tau$ is quite small.

When $\omega_L \tau \geq \pi/4$, that is when one precession of the nucleus occurs within four nuclear lifetimes, the differential method becomes valuable. This method has been conceived and developed since 1961, and has already been used to measure at least nine excited-state moments.

Experimentally this involves a measurement of coincidence rate, in a magnetic field, as a function of time. For a pure $P_2(\cos\theta)$ distribution, one observes superimposed on the intermediate state decay curve, a sine wave of frequency $2\omega_L$ and amplitude equal to the anisotropy. The effect can be doubled by performing a field up-field down experiment with the counters at 45° or 135° to one another. In this case division by the decay curve gives the normalized function

$$R = 2\frac{W(\theta,t)_+ - W(\theta,t)_-}{W(\theta,t)_+ + W(\theta,t)_-} = 2A_2 \sin 2\omega_L t \qquad (2)$$

where the plus and minus subscripts denote the direction of the magnetic field.

In practice, Eq. (2) must be integrated over the resolving time of the apparatus. Hrynkiewicz has shown that this correction lowers the amplitude and changes the phase, but does not affect the frequency.[44]

The great advantage of the differential method lies in the possibility of measuring large $\omega_L \tau$ values by fitting a sine curve over many cycles. Background corrections are usually unnecessary, and sufficient statistics can be collected in a fraction of the time required for the integral method.

The experimental apparatus for both the integral and differential methods has been constructed. Two distinct experimental arrangements have been employed: an earlier model using vacuum-tube electronics and a later transistorized version.

The recent upswing in the use of transistorized electronics and the availability of 12 V and 24 V power supplies at this laboratory have prompted this change. The advantages of transistor circuitry-insensitivity to thermal gradients, gain stability, low power requirements, and compact size—justify the effort in constructing the apparatus.

The preliminary designs for much of the transistor circuitry have been modelled after those of the Bodenstedt angular correlation group at the University of Hamburg. Semi-empirical methods employed here have optimized the circuitry for the particular experimental requirements. Coupling schemes for the circuits with the best pulse shape and time resolution characteristics will be given in the text.

While this circuitry has proved more dependable and given better data, the time spent on the older system and the use of some data from it, require also a brief description of the vacuum tube electronics.

B. Integral Method

1. Introduction

The system used for integral angular correlation is the "fast-slow" coincidence circuit. This consists of an energy dependent phase, which selects the desired transitions in the decay scheme, and a time sensitive portion, which accurately defines the resolving time. The two distinct divisions are coordinated to give the total experimental coincidence spectrum. Figure 3 illustrates a block diagram.

2. Detectors

The detectors are positioned on the periphery of a circular aluminum table, facing toward the exact center where the sample is mounted. Specially made aluminum mountings allow the angular position of the counters and their distance from the source to be adjusted.

Cylindrical NaI(Tl) scintillation crystals are used in all experiments. At first two in. and three in. Harshaw crystals integrally mounted on ten-stage photomultiplier tubes (Dumont 6292) were used. These had energy resolutions (full width at half maximum) of better than 9%.

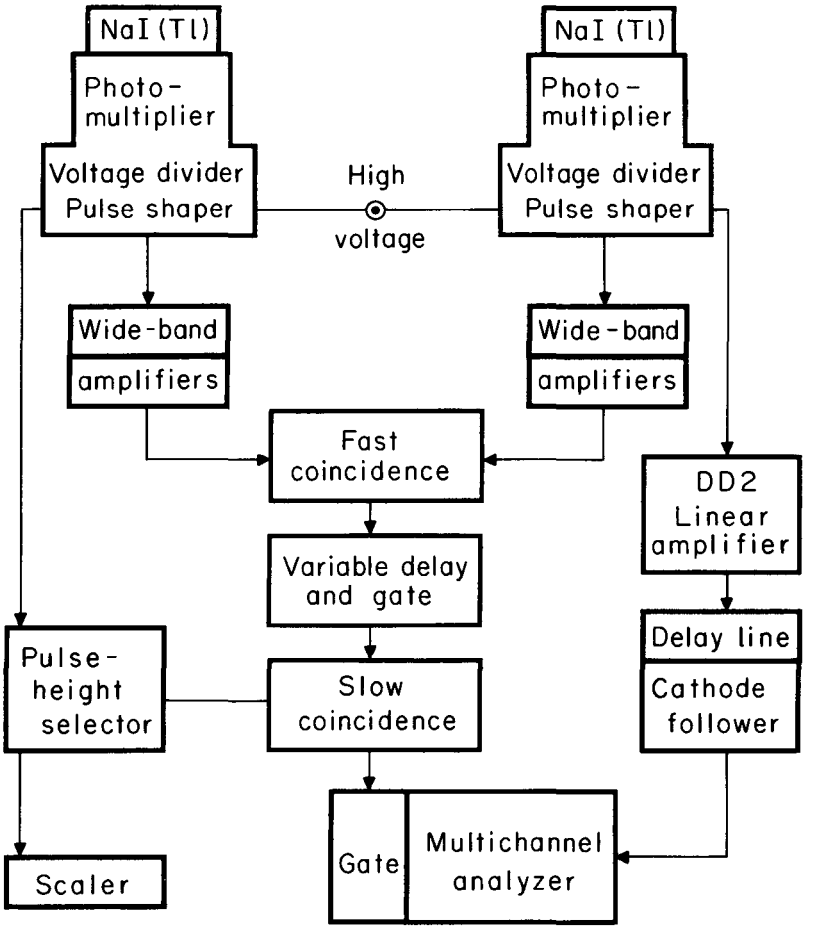

Fig. 3. Block diagram of fast-slow coincidence system.

In later experiments, strong magnetic fields necessitated the use of 12 in. light pipes between the crystal and the photomultiplier. For high energy transitions lucite light guides have proven satisfactory. For low energy radiation, where NaI(Tl) crystal time resolution characteristics are already unfavorable, quartz light pipes have been necessary in order to avoid further time uncertainties. Relatively bubble-free quartz, purchased from the Harshaw Co. of Cleveland, O., has been shaped into 12 in. cylinders of 1-1/2 in. diameter and carefully polished at this laboratory. These contribute negligible time uncertainty.

The crystals and light pipes are optically sealed onto RCA 6810A or Amperex 56AVP tubes using Dow-Corning C-2-0057 silicone grease compound and black electrical tape. The tubes are further magnetically shielded with a mu-metal cylinder and two cold-rolled iron pipes concentrically placed. With this shielding, the gain shift of the photomultipliers in the maximum magnetic field attainable in this system amounts to less than 0.5%.

Operational high voltages on the tubes range around 1.6-1.9 kV for the 6810A tubes and 2.2-2.6 kV for the 56AVP tubes.

3. Fast Coincidence Components

a. Vacuum tube version

The fast, time-sensitive pulses are taken off the fourteenth dynode, routed through a standard pre-amplifier available at this laboratory, and fed into Hewlett Packard wide band amplifiers. The latter have time uncertainties measured at less than 0.5 nsec. The intervening 125 Ω cable is kept as short as possible (< 10 ft) and plugged directly into the photomultiplier tube base with no unnecessary connectors or joints. This effectively eliminates spurious bursts of pulses.

Two wide band amplifiers at maximum gain are generally enough to increase the fast pulse beyond the 4 V threshold of the coincidence unit. Delays into the fast coincidence unit are matched using suitable lengths of 200 Ω cable (RG 63/U) which introduce one nsec delay per foot of cable.

The coincidence selection is performed by a two pentode 6BN6 circuit. To reduce slight threshold and baseline shifts, a ground copper shield has been inserted between the pentodes, and all leads are carefully shielded from one another. Time resolution is achieved by clipping the pulses with a variable length 125 Ω cable. For all experiments performed using this apparatus, a resolving time of $2\tau_0 \cong 18$ nsec has given sufficiently high coincidence rate and true-to-chance ratio.

b. Transistorized version

Although the transistor circuitry was designed primarily for differential angular correlation, it has been readily adaptable to the integral method by simply using the time-to-height converter as a fast coincidence unit. The input requirements of the latter, a square 6 V negative pulse, therefore dictate the pulse criteria of the fast output pre-amplifier.

This pre-amplifier essentially performs two functions: the low-level limiting of the fourteenth dynode output pulse to approximately equalize the rise time of the high and low energy pulses; and the amplification of the limited pulse. The circuit for this is laid out on a circular card which, along with the voltage divider and slow-output pre-amplifier, fits into a cylindrical aluminum can directly behind the photomultiplier tube.

The circuit diagrams for the voltage divider used with the 56AVP tube and the fast output limiter are given in Figs. 4 and 5.

The time-to-height converter will be described below.

4. Energy Selection Components

a. Vacuum-tube version

The energy sensitive pulse from one detector is taken off the tenth dynode of the photomultiplier tube. After being inverted and suitably shaped, it passes through five feet of 52 Ω (RG 58/U) cable into the single channel analyzer of a Victoreen DD2 linear amplifier. Pulse height and the width of the gate are set by examining the self coincidence spectrum on the display of a pulse height analyzer. Counting

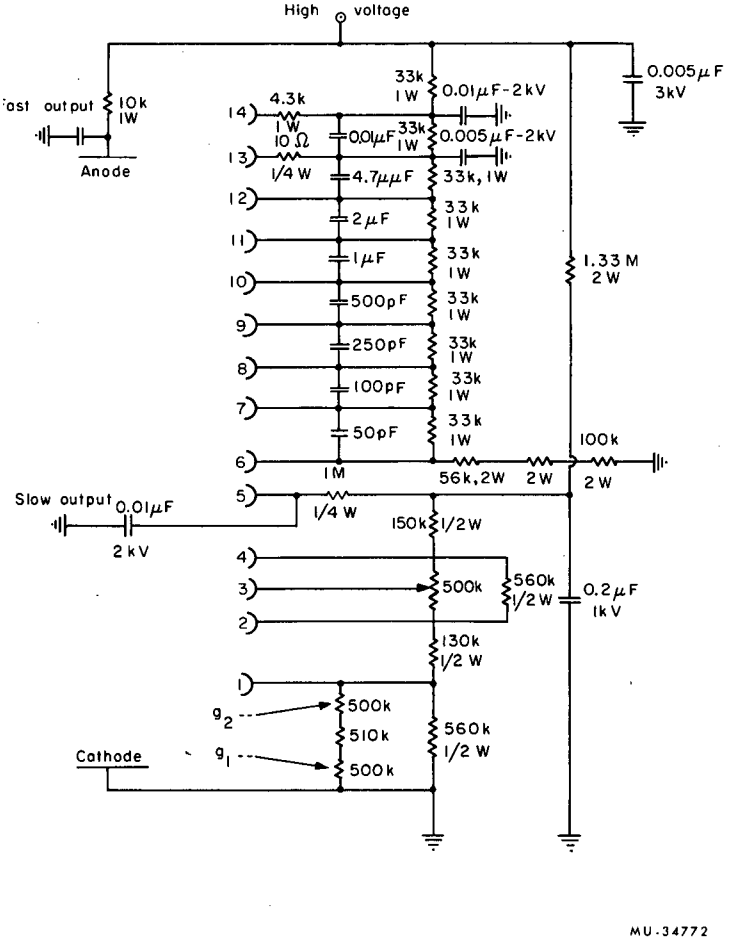

Fig. 4. Coupling scheme of voltage divider used with 56AVP tubes.

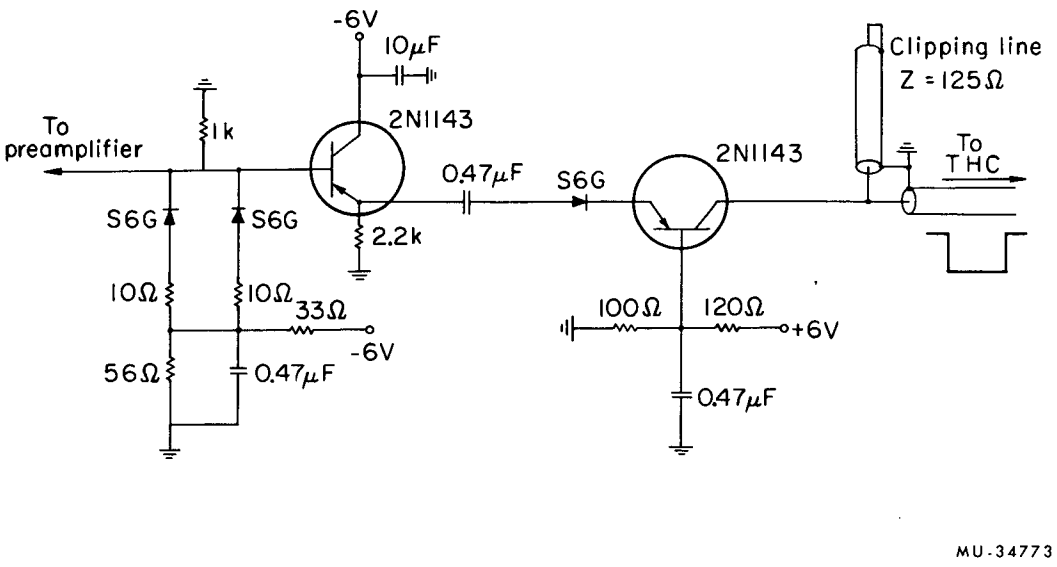

Fig. 5. Circuit diagram of fast pulse pre-amplifier ("limiter").

rate is monitored by a three cycle decade scaler in order to insure suitable geometry corrections for the moveable counter.

The single channel analyzer gates and the standard 20 V fast coincidence unit output pulses are fed into a transistorized slow coincidence unit. A variable delay and gate matches the fast coincidence output to the 15. μsec delay of the pulse height selector. Gate widths are adjusted to be approximately equal.

From the non-moveable counter, a slow output pulse is routed through a separate DD2 linear amplifier and into a 100-channel (Penco) or 400-Channel (RIDL) pulse height analyzer triggered by the slow coincidence output. Because of the delay introduced by the single channel analyzer, 1.2 μsec delay is inserted in the display pulse using 14 ft of 2000 Ω (RG 176/U) cable. The resultant pulse is driven by a cathode follower through 15 ft of 52 Ω cable and into the pulse height analyzer.

The coincidence rate is determined by integrating the number of counts contained under the desired peak in the spectrum. The performance of the apparatus is periodically checked by investigating the known Ni^{60} angular correlation. The decay scheme and experimental angular correlation spectrum is shown in Fig. 6. Our corrected value of $A_2 = 0.097 \pm 0.010$, $A_4 = 0.000 \pm 0.01$ agrees within experimental error with other experimenters.

b. Transistorized version

In the transistorized apparatus amplification of slow pulses and the matching of the fast coincidence pulses with the energy sensitive pulses are performed by a Cosmic multiple coincidence unit, model 801. This unit accomplishes the energy selection, and in its most sensitive setting can give a coincidence resolving time of about 40 nsec. Variable delays of up to 700 nsec can be switched in, and as many as four different coincidence conditions may be met simultaneously.

The circuitry of the amplifier associated with this unit, a Cosmic double-delay-line clipped linear amplifier, model 901, requires an input pulse of rise time less than 0.5 μsec and a decay time of approximately

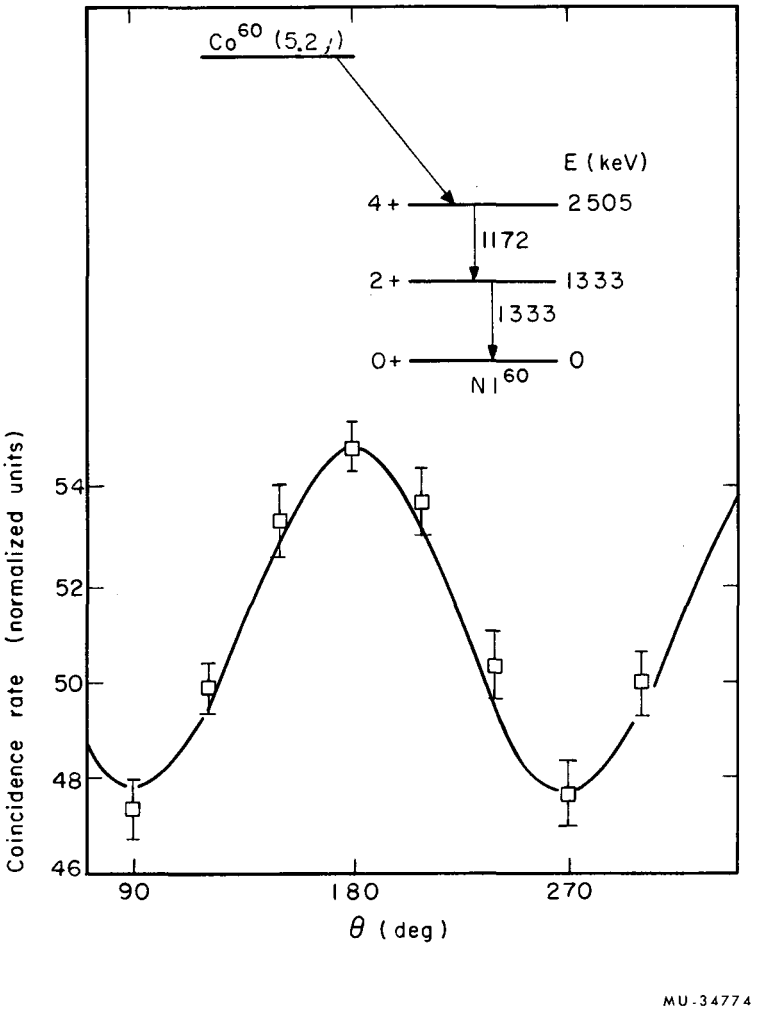

Fig. 6. Ni^{60} calibration angular correlation and decay scheme.

100 μsec. To satisfy this condition, we achieve best results taking the slow pulse from the fifth dynode of a 56AVP tube and amplifying with the coupling scheme shown in Fig. 7, a standard LRL (11X 26708-1) pre-amplifier.

C. Differential Method

The differential method involves converting the time delay between two pulses to a voltage and displaying it on a pulse height analyzer. A time-to-height converter with inherent resolution of 0.5 nsec has been designed and built by Donald Wieber at this laboratory,[45] and has proved adequate for angular correlation experiments using the vacuum electronics.

The "fast" circuitry is essentially the same as in the integral method, with the time-to-height converter substituting for the fast coincidence unit. At this point the output pulses from the wide-band amplifiers pass through discriminators and shapers and into the time-to-height converter. The pulse from the first transition in the gamma cascade, or the "start" pulse, triggers a constant current onto a fixed integrating capacitor. After time t the "stop" pulse opens the capacitor circuit. The charge build-up on the capacitor represents a voltage, $V = (I/C)t$, directly proportional to the time delay. This is then amplified and passed into a RIDL 400-channel analyzer. Figure 8 shows a diagram of the system.

At the extremely high singles rates necessary for good coincidence statistics (> 500,000 cpm), base line shift in this time-to-height converter causes appreciable time jitter. The input has therefore been modified to include a fast coincidence circuit on the start side. The original start pulse is delayed 80 nsec to guarantee that it will be the one to trigger the fast coincidence output and accordingly the "start" circuit of the time-to-height converter. A block diagram of the modified system is shown in Fig. 9.

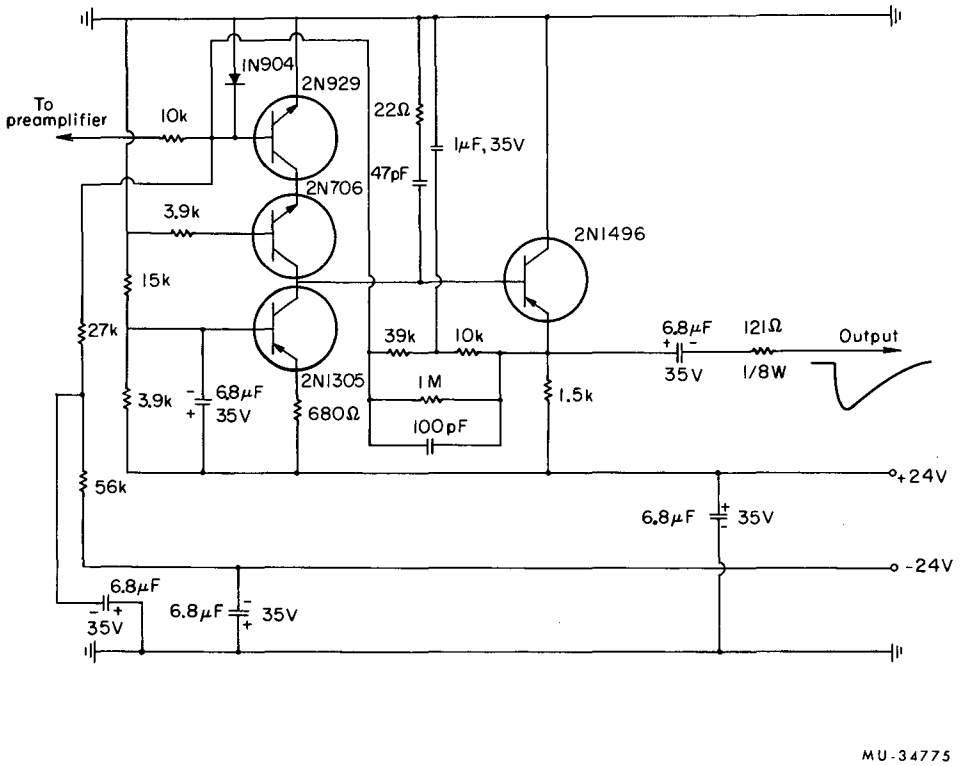

Fig. 7. Circuit diagram of slow pulse pre-amplifier.

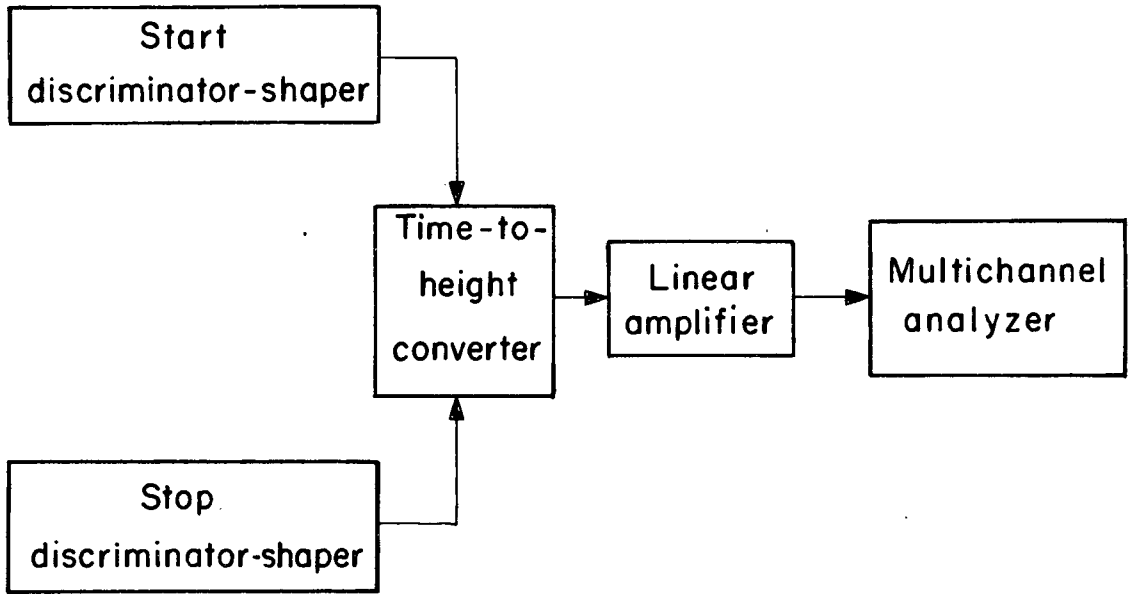

Fig. 8. Components of the Wieber ramp-type time-to-height converter.

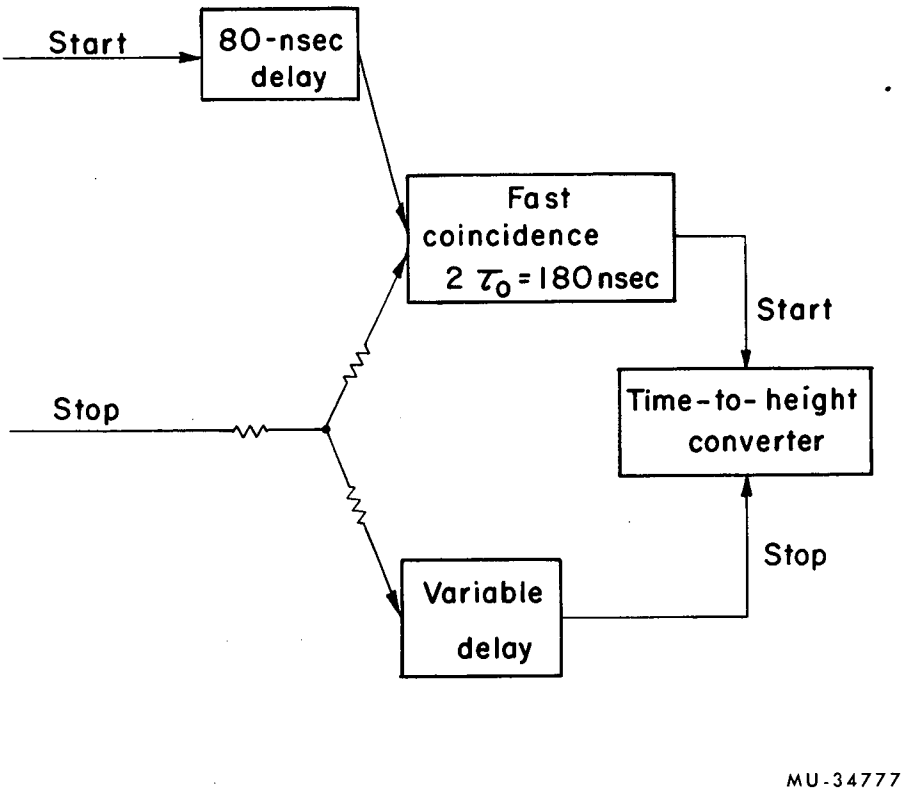

Fig. 9. Modification of Wieber converter for high counting rates.

All delays are inserted with variable delay boxes and 125 Ω (10 in./1 nsec) cable. Prompt stop pulses are delayed at least 4 nsec from start pulses to insure a properly shaped decay curve.

Both 6810A and 56AVP photomultipliers give a resolution of about 3.8 nsec for the Na^{22} positron annihilation radiation, the limiting factor in the resolution being the scintillation crystal and the 12 in. light guides.

On the energy-sensitive side of the system, the only difference from the integral method is that now both start and stop pulses are single channel analyzed and passed through a transistorized coincidence unit. The output of the latter triggers the pulse height analyzer.

The apparatus is calibrated by delaying the stop pulses in Na^{22} with various lengths of time-calibrated 125 Ω cable. The linearity remains well within experimental error at delays as great as 48 nsec. A double check on the performance of the apparatus has been made by differentially measuring the known g-factor of the 482 keV level in Ta^{181}. Applying a magnetic field of 30,000 ± 300 G, and observing the time-dependent anisotropy of the 133 keV-482 keV coincident cascade, we obtain a value of g = 1.15 ± 0.20, within experimental error of previously determined values.

The time-to-height converter associated with the transistorized pre-amplifiers operates on the overlap principle. The 6 V negative square pulses from the limiter are clipped to the desired length by a 125 Ω cable shorted to ground at one end. These pulses are then added algebraically, and a sensitively biased transistor passes current only during the period of overlap. An integrating capacitor then discharges a pulse of height proportional to the width of the overlap. This pulse is amplified and fed directly into a multi-channel analyzer gated by energy sensitive coincidences.

Necessary delays in the input pulses are supplied by 125 Ω cables. If the second transition in the cascade is delayed with respect to the first, the spectrum on the pulse height analyzer will exhibit time delay increasing from high energy to low energy.

The only advantage of this time-to-height converter over the Wieber model is that higher counting rates are possible. Resolution and dependability are about the same. The circuit diagram is shown in Fig. 10.

D. Magnet

The magnet used in all experiments is a water-cooled 2/3 ohm iron-core "C" magnet, designed at this laboratory, and built by Pacific Electric Motor Co. (and dubbed "Caesar"). Elipsoidal pole pieces (7% cobalt, 93% iron) with an air gap of 3/4 in. give a maximum magnetic field of 30.0 ± 0.3 kG. An additional set of pole tips with flat faces 1/2 in. in diameter and an air gap of 1/2 in. allows a maximum field of 42.0 ± 0.2 kG.

A hole parallel to the magnetic field through the exact center of the solenoid and the upper pole tip permits insertion of dewars for low temperature experiments. The hole measures 3/4 in. diameter in the pole piece and 2 in. to the top of the magnet. A slight indentation in the lower pole piece gives a smaller field gradient along the axis. This gradient, at maximum field, is approximately 1.5 kG from the magnet axis to the edge of the hole (3/8 in.), with a minimum along the axis.

For improved magnetic shielding of the photomultipliers, a solid iron block 4 in. thick has been secured to the open side of the "C" magnet. This attenuates the stray field by a factor of about 20 at the photomultiplier tube faces.

A photograph of the apparatus, with low temperature dewars in place, is included.

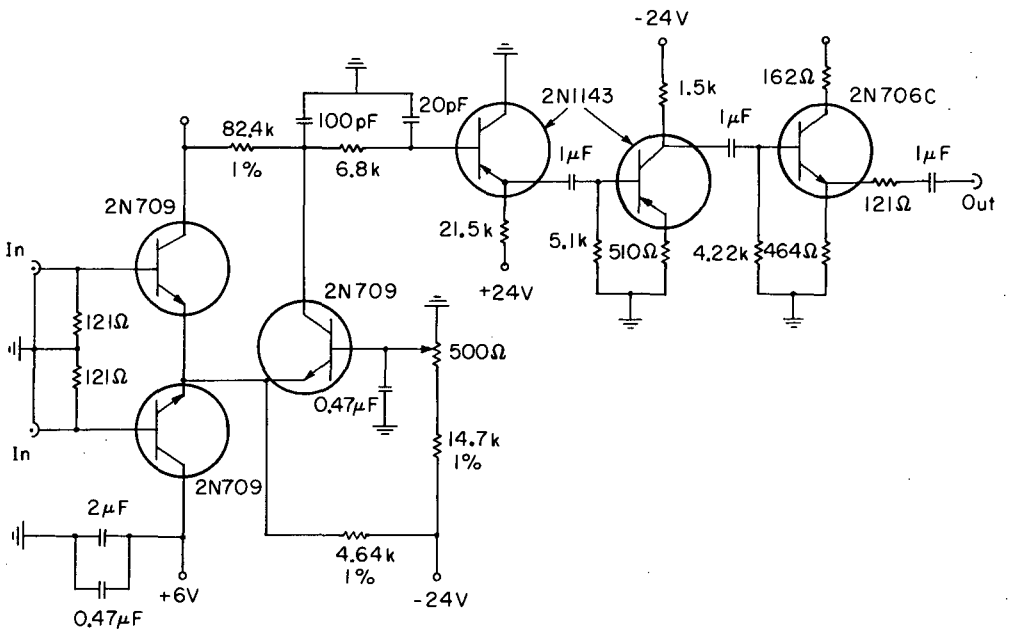

Fig. 10. Circuit diagram of overlap time-to-height converter.

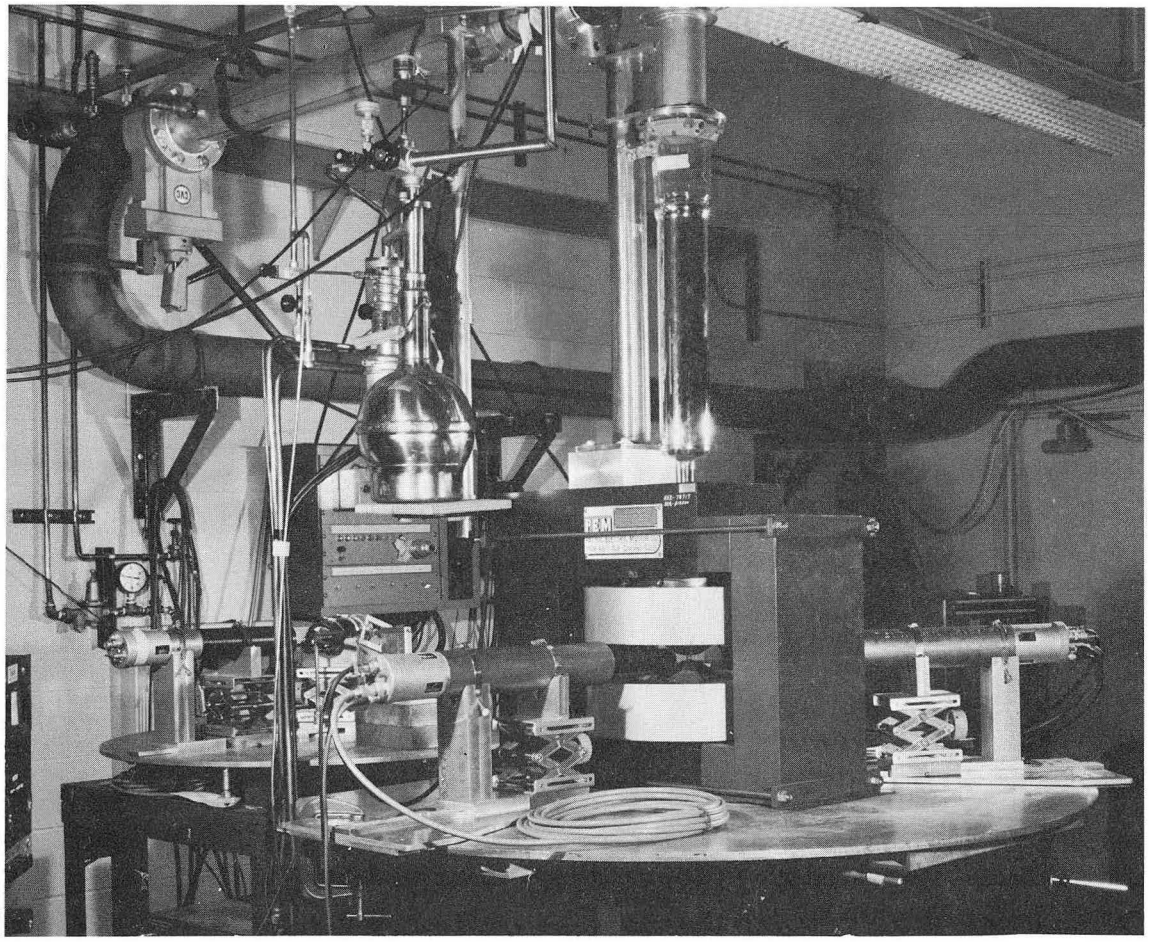

ZN-4492

Fig. 10a. Photograph of angular correlation apparatus.

IV. EXPERIMENTAL PROCEDURES

A. Optimization of Coincidence Rate

In any coincidence experiment, a compromise must be reached between a desirably fast accumulation of data and a small ratio of chance, or accidental, coincidences to true events. Optimization is customarily achieved by an empirical variation of source strength and resolving time of the apparatus.

To appreciate the importance of these qualities, consider the simplified decay $a(\gamma_1)\, b(\gamma_2)\, c$, where all nuclear disintegrations follow the same cascading route. In an approximately isotropic case, the true coincidence rate will be the rate of disintegrations N, times the efficiency of the counters for the gamma energies of interest ϵ, times the fractional solid angle Ω.

$$\text{true coincidence rate} = N\epsilon_1\epsilon_2\Omega_1\Omega_2 . \qquad (1)$$

For purely random coincidences, the counting rate is approximated by the product of the average fraction of the time during which the gate is open due to γ_1, and the experimental counting rate of γ_2, or

$$\text{random coincidence rate} = \left[N\epsilon_1\Omega_1\tau_0\right]\epsilon_2\Omega_2 N \qquad (2)$$

where τ_0 is the resolving time.

The true-to-chance ratio, therefore, is proportional to $1/N\tau_0$, and independent of counter efficiencies and geometry.

When many competing transitions exist in a nuclear decay, the value of N becomes effectively larger, and a weaker source must be used. For this reason, each isotope investigated by coincidence methods has a characteristic optimum strength. A very rough rule-of-thumb employed in this work states that for a resolving time of the order of 20 nsec and a total sample decay of the order of 1 MeV, a sample strength of 15 mR/1 in. gives a true-to-chance ratio of about 10:1.

B. Corrections to Data

1. Peak Shifts

In the integral method, the total coincidence spectrum is displayed on a suitably gated pulse height analyzer. Peak shifts of up to one channel or about 0.5 keV have been observed and corrected for.

Since, for a given time resolution, higher peak position would give a wider peak, the correction factor used is

$$1 + \left(\frac{\Delta E}{E}\right)\left(\frac{C_{Adj}}{C_p}\right) \qquad (3)$$

where $\Delta E/E$ is the fractional energy shift and C_{adj}/C_p the ratio of average number of counts in channels adjacent to the peak and channels in the peak.

2. Solid Angle

Solid angle corrections are made following the treatment of Rose, such that a correction term Q_k^2 is inserted in the angular correlation function:[46]

$$W(\theta) = \sum_k A_k Q_k^2 P_k(\cos\theta). \qquad (4)$$

Q_k^2 is a function of geometrical solid angles and absorption coefficients. In a typical case of 2 in. diameter scintillators at a distance of 7 cm from a Ni^{60} source, $Q_2^2 = 0.905$. Tables of solid angle corrections as a function of crystal thickness, distance from source, and gamma energies have been tabulated by Yates.[47]

3. Singles Rate

A constant monitoring of the singles rate in the moveable counter allows correction for both decay of short-lived samples and geometrical differences in counter placement. In all integral experiments, results are expressed as coincidences/singles.

4. Background

Probably the largest single correction in the integral method results from background. Incorrect treatment of background can lead to mistaken anisotropies and drastically wrong angles of rotation of a correlation pattern.

Since the anisotropy of the background can give misleading results for rotation measurements, its sign and magnitude must be carefully analyzed by studying the three or more channels on either side of the peak. Weighing the background in accordance with peak-to-background ratio, one may subtract a correction term for each point in the experimental angular correlation curve.

To minimize the effect of background, only those peak channels above half maximum are counted in the true coincidence rate. Purely chance events in the peak may be estimated by observing coincidence rates at very large delays.

In the differential method, background can be estimated from the flat portion of the decay curve at large delays. Its effect is a damping of the apparent anisotropy. Subtraction of the flat background from the experimental curve gives the true decay curve.

5. Prompt Coincidences and Resolution

In all experiments performed using the differential time-to-height conversion, the finite resolving time of the apparatus attenuates and smears out fine structure, and more important, distorts the very early portions of the decay curve. The cause of the distortion is the fact that an ideal decay curve, with no counts before time zero on the time delay scale must be integrated over a resolution which includes both positive and negative time uncertainties. At small delays, therefore, unsymmetric corrections for resolution give sharp distortion.

To give quantitative basis to this effect, we can fairly closely approximate the resolution of the apparatus for a typical case by an exponential curve symmetric with respect to both negative and positive delay. Integrating the ideal curve over the resolution, we find for the experimentally expected result:

$$N(t)_{exp} \propto N_0 \int_0^t e^{-\lambda t'} e^{-\lambda_0 (t-t')} dt' \qquad \text{for } t' < t$$

$$N(t)_{exp} \propto N_0 \int_t^\infty e^{-\lambda t'} e^{-\lambda_0 (t'-t)} dt' \qquad \text{for } t' > t \,. \qquad (5)$$

In both equations $e^{-\lambda t'}$ is the true decay curve for infinitely good resolution, with λ_0 the decay constant of the intermediate state, and λ_0 is the decay constant representing the prompt resolution curve. Performing the integrations and adding the terms, we find

$$N(t)_{exp} \propto C_1 e^{-\lambda t} - C_2 e^{-\lambda_0 t} \,, \qquad (6)$$

where C_1 and C_2 are both positive constants. From this it is apparent that for good resolution (large λ_0) the decay curve approaches the true time dependence, $C_1 e^{-\lambda t}$, and that at lower delays, the second term depresses the observed decay by a relatively larger amount.

The sinusoidal variation of perturbed angular correlation is amenable to similar treatment, as

$$R(t) \propto \int_0^t A \sin \omega t' \, e^{-\lambda_0 (t-t')} dt' \qquad \text{for } t' < t$$

$$R(t) \propto \int_t^\infty A \sin \omega t' \, e^{-\lambda_0 (t'-t)} dt' \qquad \text{for } t' > t \,, \qquad (7)$$

where $R(t)$ is the experimentally observed dependence of the normalized difference in field up and field down measurements, and $A \sin \omega t$ is the sine wave expected for angular correlations with no terms higher than $P_2 (\cos \theta)$.

Performing the integration we find:

$$R(t) \propto \frac{\lambda_e}{\omega} \sin \omega t + e^{-\lambda_0 t} \cong \frac{T}{T_0} \sin \omega t + e^{-t/T} \qquad (8)$$

where T and τ_0 are the period of nuclear precession and the full width at half maximum of the prompt decay curve respectively. Thus the effect of the finite resolution is to give an anomalously high amplitude at lower time delays (in addition to overall attenuation of the anisotropy). The effect of the distortion for $T/\tau_0 = 1,2,$ and ∞ is shown in Fig. 11.

Typically, in these experiments τ_0 is of the order of 4-6 nsec and $T/\tau_0 \approx 4$, so that the distortion is appreciable only at very small time delays. Thus, ignoring the points taken over the first 2-3 nsec enables a satisfactory fit of experimental data with a constant-amplitude sine wave.

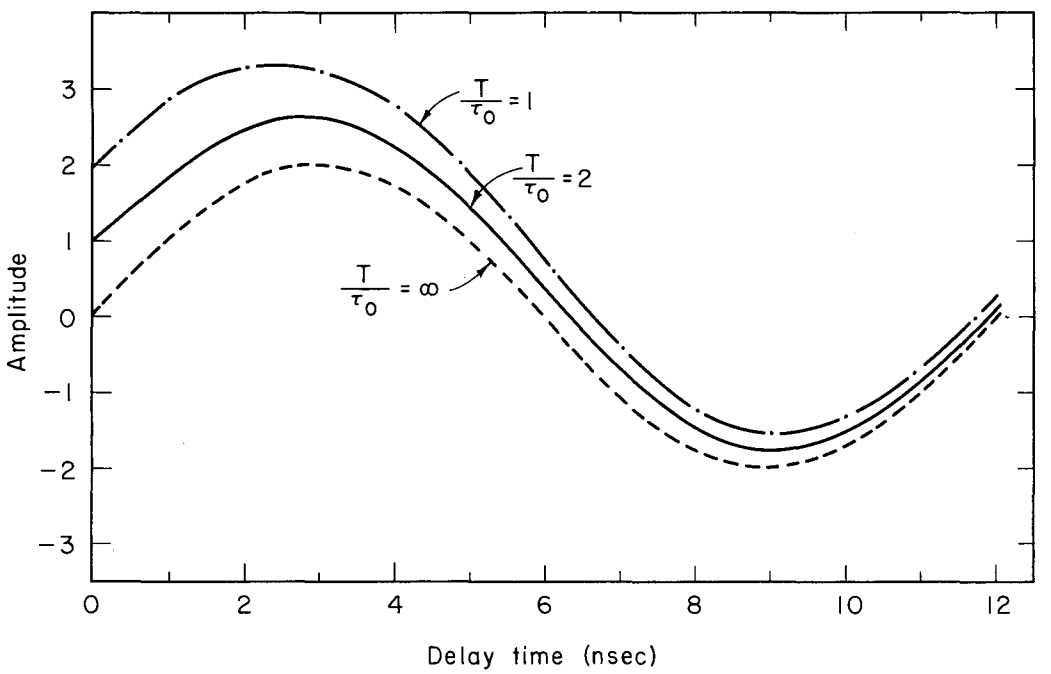

Fig. 11. Distortion in R(t) at low delays due to exponential prompt resolution of time-to-height converter.

V. Ce^{140}

A. Introduction

The first requisite for performing a perturbed angular correlation measurement is a suitably long lifetime for the intermediate nuclear state in a cascade. It is doubly fortunate that such a lifetime exists for the 2084 keV level of Ce^{140}, a nucleus with significant properties both in nuclear decay systematics and internal field considerations.

Ce^{140} occurs in a region of small nuclear deformation with a closed shell of 82 neutrons and a partially filled shell of 58 protons. Although the general systematics of this region have been reported in detail, only recently, with the adoption of the quasi-particle formalism, has quantitative theoretical treatment become possible.

Scharff-Goldhaber and Weneser showed in 1955 that in even-even nuclei with neutron number $36 \leq N \leq 88$, the ratio of energies of the second and first excited states is about 2:1.[48] As these energies usually appear too low to be considered single particle excitations, and as rotational levels would give a ratio of about 10:3, the excitations were attributed to vibrational phonons.

This conclusion is substantiated empirically by the spin assignments of 2+ for the first excited states, and 0+, 2+, or 4+, for the two-phonon level. In addition, E2 transitions from the first 2+ state occur from ten to fifty times faster than the single particle estimate, cross-over decays are rare, and M1 admixtures appear only negligibly for $2+ \longrightarrow 2+$ transitions. All these characteristics fit the quadrupole vibrational model.[49]

Later work with residual forces in the nucleus gave a slightly different description and readied the way for quasi-particle mathematics. Lutsenko showed in 1963 that two nucleons with $j \geq 1$ will couple to $I = 0+, 2+, 4+, \ldots(2j+1)$.[50] In the limit of a short range pairing force, $I = 0+$ occurs most favorably, correspondingly lowering the ground state with respect to the degenerate $[2+, 4+, \ldots(2j+1)]$

level. This accounts for the large energy gap in spherical nuclei. As the deviation from spherical symmetry increases, a long-range quadrupole force becomes important. This force acts primarily on the 2+ level, which it lowers into the energy gap. It can be seen qualitatively that the energy of the 2+ excited state decreases with deformation in this region to the point at N = 88 where pure rotational bands appear.

Kisslinger and Sorensen adopted quasi-particle eigenfunctions to diagonalize the short-range pairing Hamiltonian and included the long-range force as a perturbation.[23] The resultant mathematics allow a quantitative prediction of the energy of the primarily collective 2+ first excited state and, from the single particle eigenfunctions, the first few quasi-particle levels.

The decay scheme of Ce^{140} may illustrate many of the characteristics mentioned here. In view of the present importance of accurate energy designations in this region, and the availability of high resolution lithium-drifted germanium counters Ge(Li) at this laboratory, a preliminary study of the decay scheme has been made. The peaks observed in this work are compared in Table IV with the work of earlier experimenters using electron spectroscopy and pair spectrometry techniques. A tentative decay scheme, based in part upon relative intensities and coincidence work, is proposed in Fig. 12. The spin assignments are deduced from previous unperturbed angular correlation work.

Several features deserve mention:

(1) The level at 1597 keV is the 2+ collective vibration predicted by Kisslinger and Sorensen. Its lifetime has been measured as $(1.10 \pm 0.15) \times 10^{-13}$ sec, about 16 times shorter than the single particle estimate.[51]

(2) The 0+ level at 1902 keV decays through an E0 mechanism. Conversion electrons for the transition to ground have been observed.[52]

(3) The state at 2084 keV has energy of the order of single particle excitations, and in the Kisslinger and Sorensen notation is a two quasi-particle state. Its decay to the 2+ state shows a nuclear mean life of $(4.97 \pm 0.09) \times 10^{-9}$ sec, a retardation by a factor of 17 from the single particle estimate.[53]

Table IV. Peaks observed in Ce^{140} in this experiment (Ge(Li)) and by previous work. Energies are in keV. Errors in the Ge(Li) experiment are ± 1.0 keV.

Ge(Li)	Ref. 54	Ref. 55	Ref. 52	Ref. 56	Ref. 57	Ref. 58	Ref. 59	Ref. 60	Ref. 61
109	110.4	110							
131	130.7	130							
172	173.0								
	241.4	240							
268	265.4	270							
329	328.6	328				323			328
432.8	431.3					434			435
487	486.4	485				491			
573									
						643			635
751	751.8					748			753
815	815.8	815				815			818
868			868			868			874
924	926					923			927
1496									
1596	1597	1600			1600	1597		1598	
	1904		1902			1909		1900	
2350			2350			2343		2373	2355
2522			2525	2550	2500	2515	2530	2535	2530
			2910	2900	3000	2890	2915	2890	2900
							3110	3100	3100
								3250	
							3380		

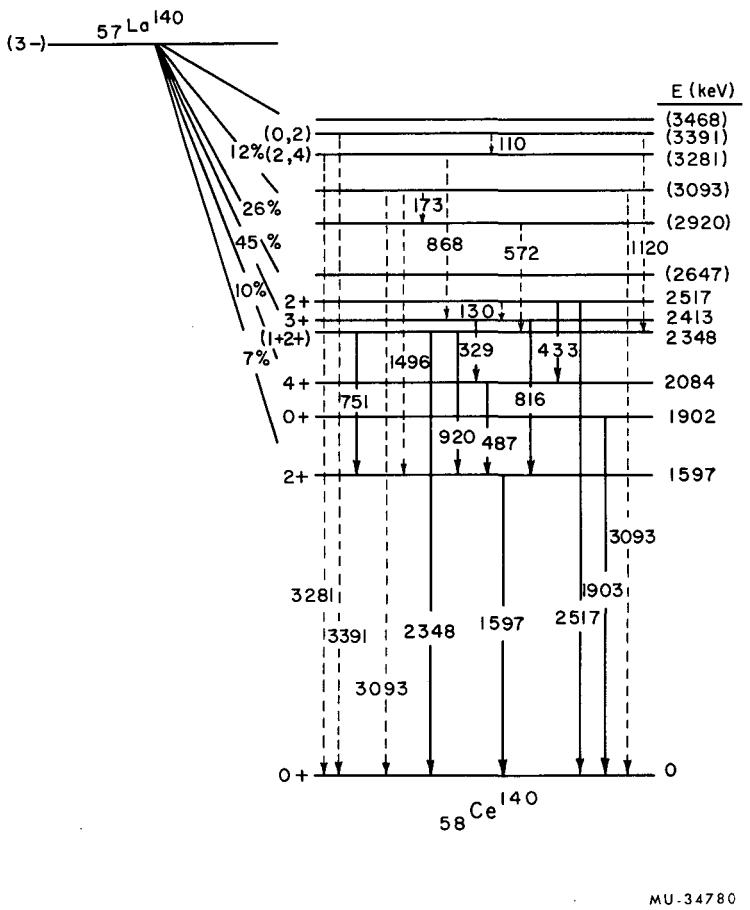

Fig. 12. Proposed decay scheme of La^{140}. Parentheses and dashed lines indicate features which are strongly indicated but have not been conclusively proved. β-decay branching amplitudes are taken from Simons.[61]

(4) The states around 3300 keV appear at approximately twice the energy of the 2+ first excited state, and may be two-phonon quadrupole-vibration levels. We have looked carefully for the high energy transitions with a 3 in. × 3 in. NaI(Tl) crystal detector and found strong indication of two of the peaks. The high energy spectrum is shown in Fig. 12a. We have measured the magnetic moment of the 2084 keV level by observation of the perturbation of a perpendicular magnetic field upon the 329 keV-487 keV angular correlation. Internal field ambiguities are fortunately negated by the fact that Ce^{+4} is stable and not paramagnetic. Thus, the effective field equals the applied field.

Further information has come from this work in performing the same measurement upon Ce^{+3} in lanthanum metal. The enhancement of the internal field allows the evaluation of the paramagnetic correction β. As indicated above, the uncertainty in the theoretical basis for predicting β is greatest for the lower rare earths. This is, therefore, a particularly important case.

B. Experimental Procedure and Results

1. Sample Preparation

Throughout this work sample preparation has been handled in an unchanging fashion.

About 20 mg of powdered La_2O_3 is sealed in a quartz capsule 1 in. long and 4 mm in diameter, and irradiated for 6-10 h in a flux of 1×10^{12} neutrons/cm^2/sec at the Livermore pool type reactor. The capsule, containing an activity of about 1R/in. of La^{140} is opened in a dry box, and the powder dissolved in 3N HNO_3 by gentle heating. Samples for counting are made up by drawing two or three drops of solution into a spitzer and flame sealing the ends of the spitzer. The sample is shaken into the closed tip to approximate as closely as possible a point source.

In preparing metallic lanthanum samples, care must be taken to prevent surface oxidation. The metal is stored under toluene which has been dried through contact with elemental sodium. Prior to irradiation, a 5-10 chunk is shaved off with a razor blade and sealed under argon in

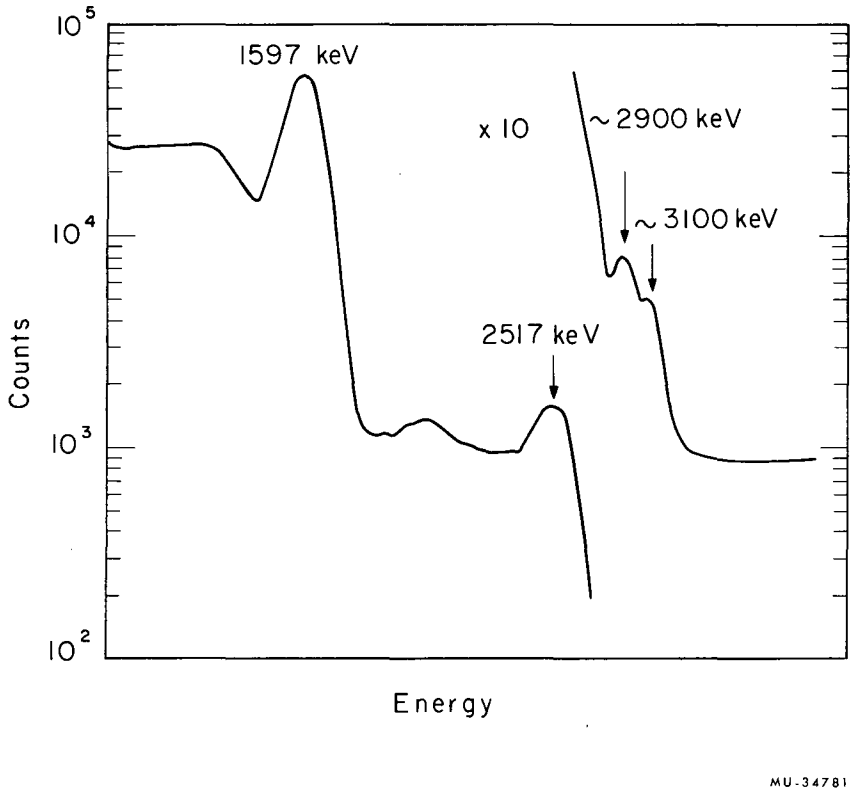

Fig. 12a. High energy spectrum of La^{140} (3 in. × 3 in. NaI(Tl) detector).

a quartz capsule. Irradiation times are typically less than 10 min at 1×10^{12} neutrons/cm^2/sec. The source for counting is sealed under argon in a glass spitzer.

2. Integral Angular Correlation Measurements

a. Determination of anisotropy

Integral measurements were performed using the vacuum tube apparatus with a resolving time of 18 nsec. The 487 keV radiation was gated in the moveable counter and the properly triggered coincidence spectrum displayed on a pulse height analyzer. The position of the gate and the desired peak channels is shown in Fig. 13.

The experimental anisotropy of about 6% between the 90° and 180° counts gives an uncorrected angular correlation function,

$$W(\theta) = 1 - (0.047 \pm 0.003) P_2(\cos\theta) , \qquad (1)$$

the P_4 coefficient being negligible.

An analysis of the three channels on either side of the 329 keV peak shows an approximate anisotropy as large as in the peak and of opposite sign. As background comprises about 25% of the total counts under the peak, the correction multiplies the experimental anisotropy by a factor of $(4/3)^2$. Including the solid angle correction $Q_2^2 = (0.94)^2$, we find

$$A_2 = -0.095 \pm 0.030 . \qquad (2)$$

b. Magnetic moment measurement

Perturbed integral measurements have been carried out in fields of 10.425 ± 0.075 kG and 27.970 ± 0.200 kG, with magnetic field calibrations being performed regularly. Preliminary counts on the liquid source were taken with the detectors at successive 40 deg intervals to one another, for both magnetic field directions. Normalization for singles

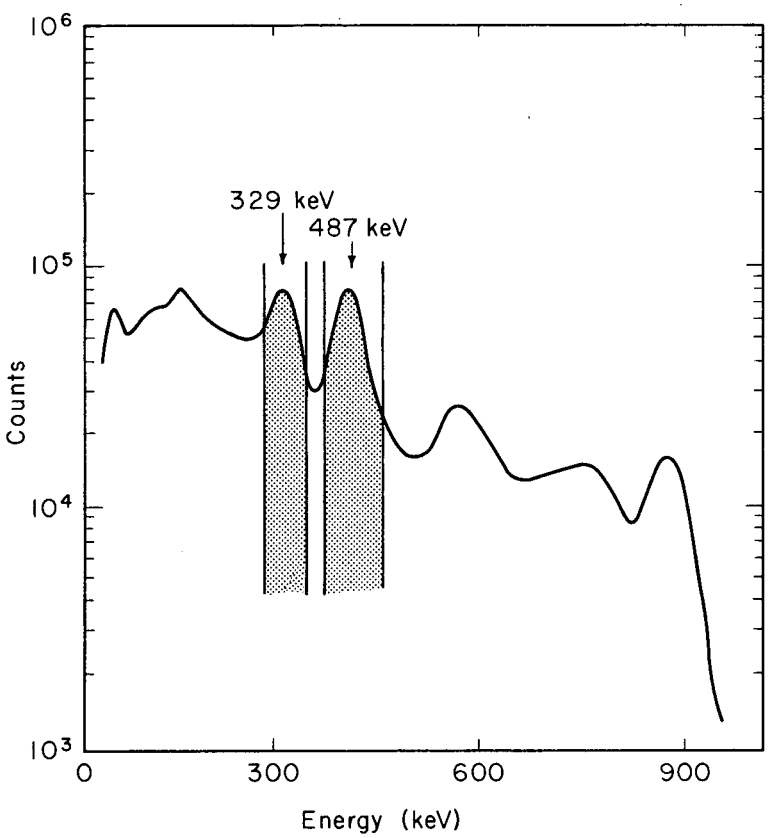

Fig. 13. Singles spectrum of La^{140} (1 in. × 1-1/2 in. NaI(Tl) detector). Shaded portion indicates gate settings for angular correlation.

and comparison with the unperturbed angular correlation now gives a qualitative estimate of the rotation. From the field direction the sign of the magnetic moment can be deduced as positive, and we find the value $g \cong 1$. These results for magnetic field up and down are shown in Fig. 14. It should be noticed that larger rotations give a smaller anisotropy.

Because an unrotated anisotropic background distorts these curves from a perfect Legendre polynomial shape, they cannot be directly used for an exact g-factor evaluation. Instead we utilize additive functional dependences of the perturbed and unperturbed anisotropies. The total correlation function becomes

$$W_{exp}(\theta) = W_{true}(\theta) + W_{bkg}(\theta) . \qquad (3)$$

Assuming that the background comprises 25% of the peak for the unperturbed case and has an equal magnitude and the opposite sign of anisotropy, we have for the integrated function

$$W_{exp}(\theta,H) = \frac{B_2}{[1+(2\omega\tau)^2]^{1/2}} \cos 2(\theta-\Delta\theta) - \frac{B_2}{4}(\cos 2\theta) \qquad (4)$$

where $\Delta\theta = (1/2)\tan^{-1}(2\omega_L\tau)$.

Coincidence rates for the two angles on the maximum slope portion of the curve rotated by a field of 10.425 kG have been measured with good statistical accuracy, giving

$$W(115°, H) = 154701$$
$$W(210°, H) = 156046 .$$

Now, eliminating the term B_2 by forming the ratio

$$\frac{W(210°) - W(115°)}{W(210°) + W(115°)} ,$$

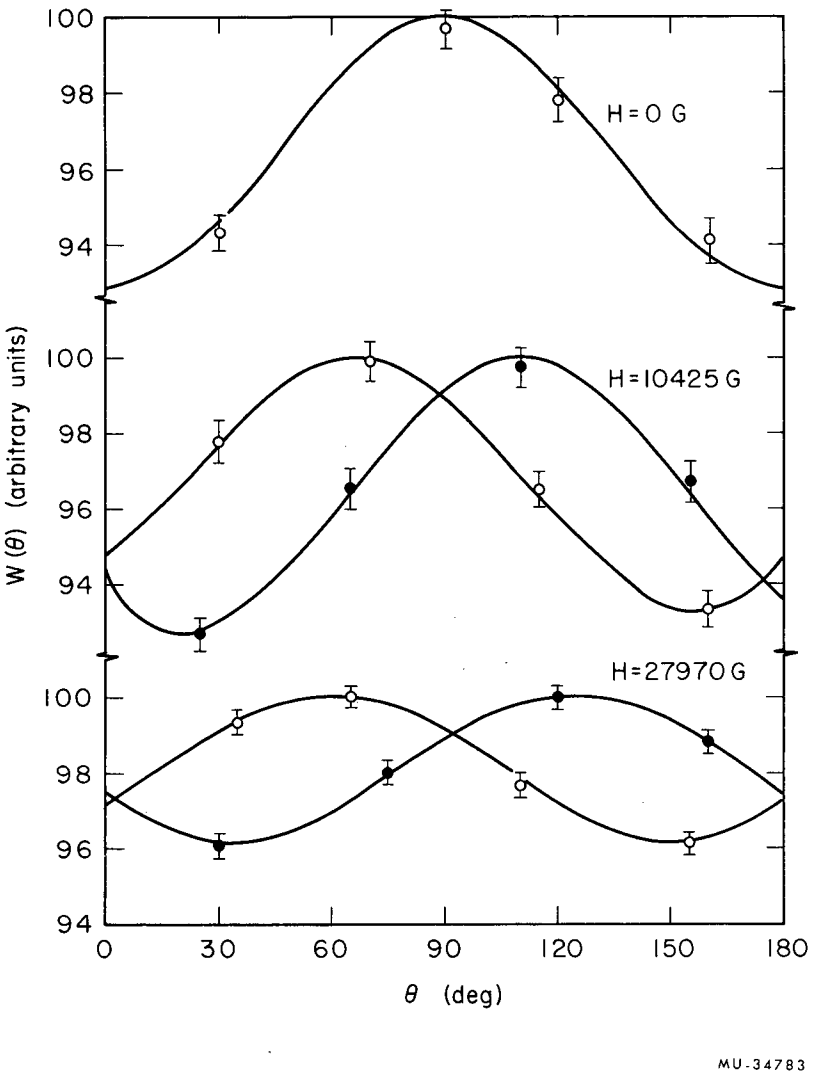

Fig. 14. Unperturbed and perturbed angular correlation results for the 329 keV—487 keV coincidence in Ce^{140}.

the evaluation of $2\omega_L\tau$ becomes a problem of straightforward algebra. In this case, $\omega\tau = 0.245$, giving $g = 0.99$. The assignment of an error depends predominantly on the uncertainty in the background correction and is of the order of 10%. It is interesting to note that the neglect of the anisotropic background would give a g-factor of approximately twice the proper magnitude.

3. Differential Angular Correlation Measurements

a. Calibration

In view of the uncertainty inherent in the integral method, detailed measurements on Ce^{140} have been performed using the differential angular correlation apparatus. Linearity checks were periodically performed using the Na^{22} 511 keV-511 keV annihilation radiation coincidence with varying delays. Typical time calibration settings suitable for frequencies of rotation observed in this experiment range around 0.70-0.90 nsec/channel on the pulse height analyzer.

The prompt resolution curve, obtained using the La^{140} cascade gate settings on Na^{22}, is fairly symmetric, with a full width at half maximum of $2\tau_0 = 4.8$ nsec. The half-life of the 2084 keV state in Ce^{140} has been measured and gives a limiting slope corresponding to a lifetime of 3.52 ± 0.10 nsec, in excellent agreement with other determinations.[53,62] The prompt resolution curve and lifetime data are illustrated in Fig. 15.

In this particular run, γ_1, in the cascade has been delayed relative to γ_2. For all determinations, complementary data has been obtained with large delays in γ_2 to provide a check on the performance of the time-to-height converter.

In addition, a careful study of the variation of anisotropy with time has been carried out by comparing the time dependence of coincidences at 90° and 180°. Counts are taken alternately over short intervals of time (20 min) to eliminate effects of drifting gates or varying true-to-chance ratios. The behavior of Ce^{+4} solution and of Ce^{+3} in lanthanum metal indicate no fine structure or attenuation of anisotropy with time. A representative run is shown in Fig. 16. For purposes of this experiment we may accordingly assume that time-dependent and static quadrupole perturbations are negligible, or $A_2(t) = \text{constant}$.

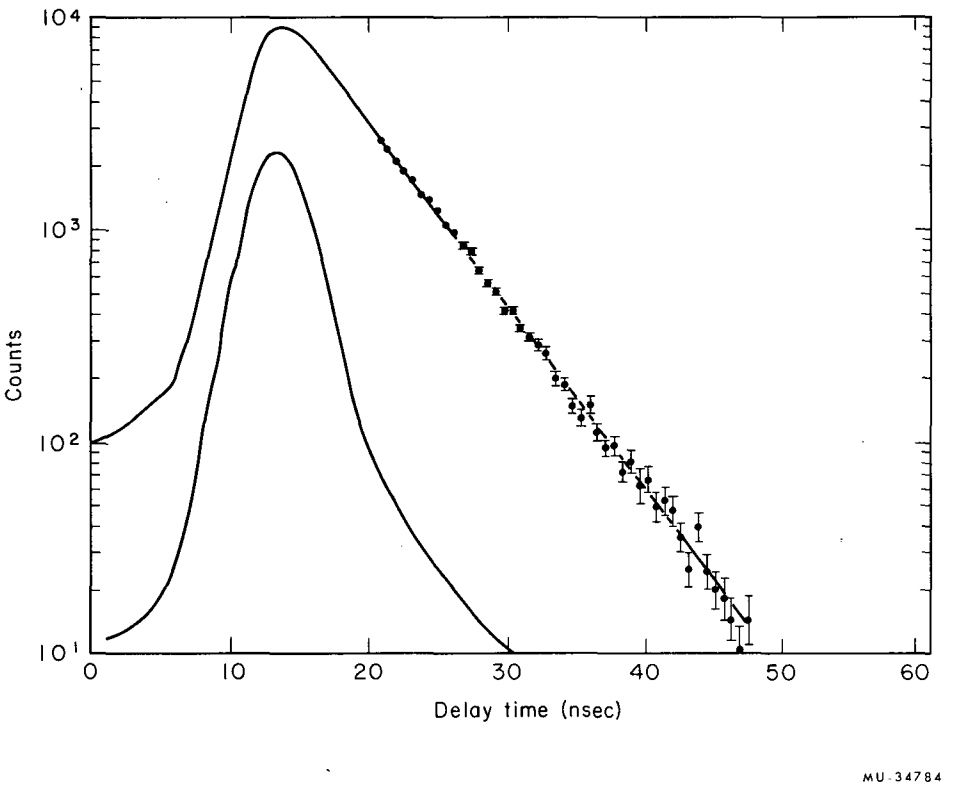

Fig. 15. Prompt resolution curve and decay curve for the 329 keV—487 keV cascade in Ce^{140}.

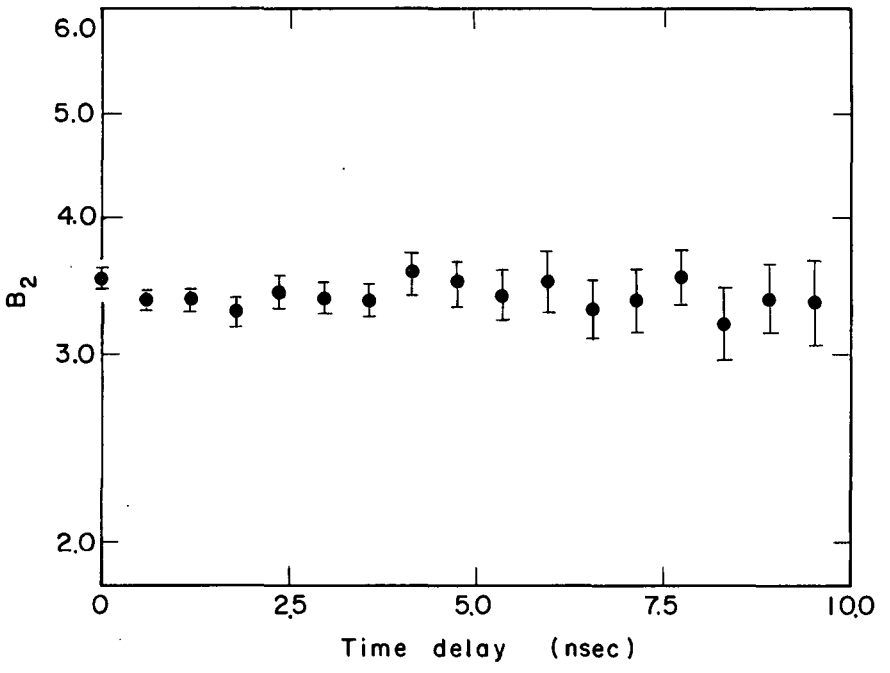

Fig. 16. Variation of anisotropy with time delay in the 329 keV—487 keV angular correlation in Ce^{140}.

b. Magnetic moment measurements

Three separate magnetic moment determinations have been performed. Runs with magnetic field up and field down were alternated over 70-80 hours on liquid samples periodically adjusted to give a sample strength of 30 mR/2 in. A total of about 350,000 coincidences has been collected. Magnetic field and time calibration measurements were taken at the beginning and at the end of each run.

After subtracting the flat background from the decay curve, the sinusoidal variation was determined from the ratio $R = (W+ - W-)/(W+ + W-)$, with + and - denoting field directions. A resultant curve for field strength 42.1 kG is shown in Fig. 17. The first three channels have been disregarded due to the distortion caused by the prompt resolution curve. The three curves determined in this way have been fitted by a least squares method to pure sine waves. The resultant frequencies and $g\beta$ values are summarized in the first three columns of Table V.

The weighted average for the g-factor of the 2084 keV level is thus

$$g = 1.020 \pm 0.039 \quad . \qquad (5)$$

c. Paramagnetic corrections

Measurements similar to those above have been performed on samples made by neutron bombardment of lanthanum metal. The radiating atoms are thus cerium impurities in lanthanum metal. The magnetic field in this case is enhanced by a contribution from the paramagnetic cerium 4f electron, and the rotational frequency, compared to that of Ce^{+4} in solution, gives the paramagnetic correction.

Point sources of lanthanum metal are used. Two successful runs have been made at both room temperature and 77° K. The latter temperature is attained by suspending a large dewar flask through the axial hole in the magnet, so that its tip reaches the exact center of the magnet pole gap. The metal sample, sealed under helium in a small capillary tube, is placed in the dewar and cooled with liquid nitrogen.

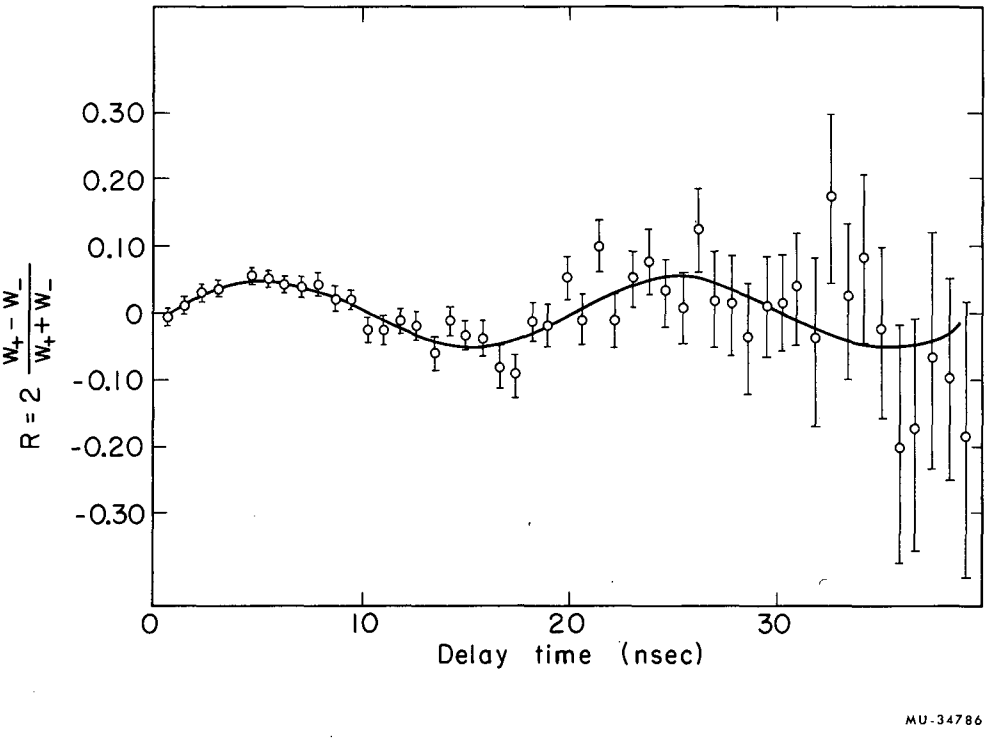

Fig. 17. Differential rotation of the 2084 keV level in Ce^{140} in an external magnetic field of 42.1 kG.

Table V. Summary of perturbed differential angular correlation results in Ce^{140}.

Source	Field (kG)	Temp. ^oK	Time calibration nsec/channel	Amplitude	ν_L $\frac{\text{cycles}}{\text{channel}}$	$g\beta$	β
La^{+3} sol'n.	29.7 ± 0.4	298	0.79 ± 0.02	7.23 ± 0.89	0.0399 ± 0.0032	1.115 ± 0.095	1.00
La^{+3} sol'n.	29.7 ± 0.4	298	0.79 ± 0.02	8.02 ± 0.73	0.0356 ± 0.0021	0.994 ± 0.059	1.00
La^{+3} sol'n.	42.1 ± 0.1	298	0.63 ± 0.03	4.99 ± 0.49	0.0404 ± 0.0017	0.998 ± 0.042	1.00
La metal	30.0 ± 0.2	298	0.94 ± 0.02	4.77 ± 0.80	0.0570 ± 0.0050	1.325 ± 0.133	1.30
La metal	33.95 ± 0.10	298	0.79 ± 0.02	6.67 ± 0.60	0.0562 ± 0.0030	1.376 ± 0.075	1.35
La metal	30.0 ± 0.2	77.4	0.94 ± 0.02	3.33 ± 0.40	0.0890 ± 0.0150	2.069 ± 0.372	2.03
La metal	29.8 ± 0.2	77.4	0.63 ± 0.03	3.91 ± 1.22	0.0724 ± 0.0066	2.528 ± 0.230	2.48

Two resultant curves for room temperature and liquid nitrogen temperature are shown in Fig. 18. The curves are normalized in time calibration and external field strength to illustrate the effect of temperature. Each curve represents a total of about 700,000 coincidences taken over about 80-100 hours. A summary of the four metal runs is given in Table V.

The weighted average of the results for the room temperature measurements give $g\beta = 1.359 \pm 0.068$. Dividing by the g value obtained from the measurements on Ce^{+4}, we obtain $\beta = 1.33 \pm 0.08$. In the same way, the weighted determinations at 77° K give $\beta = 2.33 \pm 0.20$.

C. Discussion of Results

1. Preliminary Material

In angular correlation work, there is a dangerous tendency to ascribe precise quantitative significance to experimental measurements of anisotropies and of attenuation factors (G_k). The presence of so many variables in this work—background anisotropies, solid angle corrections, unresolved photopeaks, scattering from nearby objects, electronic gain drifts, sample impurities, etc.—make an exact analysis of integral angular correlation data extremely tenuous. For this reason, the approach in parts of this discussion will be one of "indications" rather than flat conclusions.

At least five measurements of A_2 have previously been reported,[63-67] ranging in value from -0.092 to -0.197, while A_4 in all cases is close to zero. A weighted average of these results gives $A_2 = -0.097 \pm 0.003$. Our measurement of $A_2 = -0.095 \pm 0.030$ shows good agreement.

The proposed cascade which fits this data is 3+ (D,Q)4 + (D)2+. Several justifications for this assignment can be suggested.

(1) Previous angular correlation work on the 816 keV-1597 keV, 487 keV-1597 keV, and 329 keV-1597 keV cascades give anisotropies consistent with this spin assignment.[64] This evidence is not wholly conclusive, as Bishop et al. have measured the 816 keV-1597 keV coincidence spectrum and found no quadrupole component in the first transition.[63]

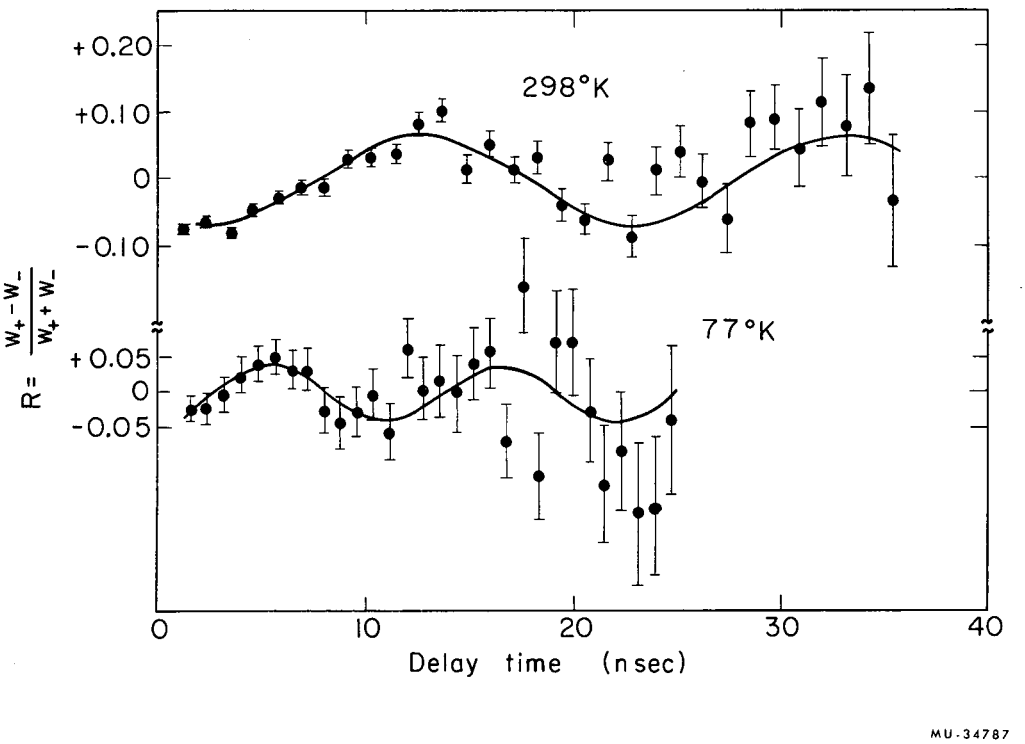

Fig. 18. Differential measurements of R(t) for Ce^{140} in lanthanum metal. The curves are normalized in time calibration and applied field to show the effect of temperature upon the paramagnetic correction.

(2) Since the spin of the mother isotope La^{140} has been confirmed as 3-,[68] and the β branch to the 2413 keV level accounts for 45% of the total β decays with a log-ft = 7.7, one would expect from β systematics that this level has a spin of 2+, 3+, 4+, 2-, 3-, or 4-. The angular correlation data admits a quadrupole radiation component of up to 0.5%. (A pure dipole transition would give $A_2 = -0.14$.) As an E1-M2 mixed transition is much less likely than M1-E2, negative parity is improbable.

(3) Quasi-particle theory predicts that the energy levels in this region evolve from broken pairs in the $d_{5/2}$ and $g_{7/2}$ single particle subshells. These protons would have positive parity. Moreover, Rho has predicted a quasi-particle level very near this energy and composed by $(d_{5/2}\ g_{7/2})_3$.

2. Magnetic Moment Measurement

Three magnetic moment measurements besides ours have been performed upon the 2084 keV level of Ce^{140}. These are summarized in Table VI.

A possible interpretation of the determined g-factor may be inferred from the work of Kisslinger and Sorenson on single closed shell nuclei. Assuming a quasi-particle eigenfunction and inserting a long-range quadrupole force to explain the recurring 2+ first excited state in SCS nuclei, these authors predict the composition of experimental levels on the basis of single particle shells. A diagram of shell energy behavior is shown in Fig. 19.[23] It can be seen that the few existing experimental levels at these energies cluster reasonably close to the shell model predictions.

A perhaps more utilitarian form of the quasi-particle interaction has been comprehensively treated by Rho.[70] Unlike the Kisslinger and Sorensen scheme, Rho's model employs a single set of forces to explain both the collective-like 2+ first excited state and the higher, quasi-particle states. It has the additional complication, however, that the pairing force matrix elements are now not constant but are computed from a gaussian force.

Table VI. Resume of experimental data on the 2084 keV 4+ level in Ce^{140}.

Reference	Method	g	Comments
(69)	Diff. + Int.	1.11 ± 0.04	Performed on several sample media
(66)	Diff.	1.15 ± 0.08	Follow rotation through < 1 cycle
(67)	Diff.	0.95 ± 0.1	Fit using $G_2 = 0.90$
This work	Diff. + Int.	1.02 ± 0.04	

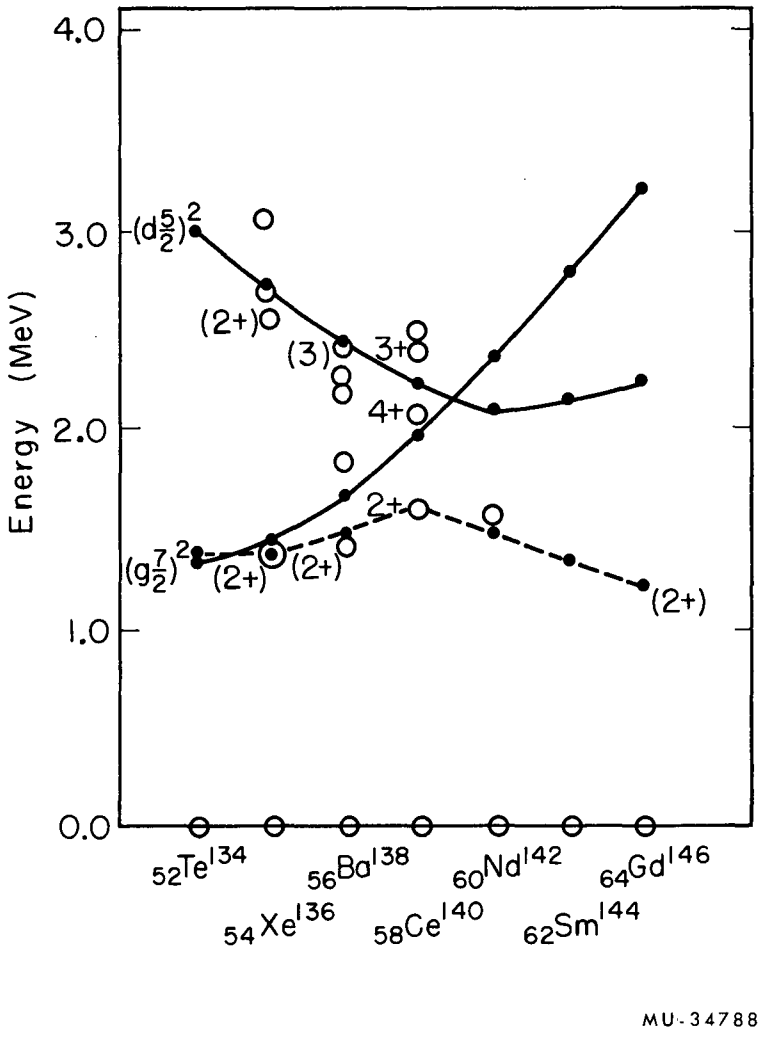

Fig. 19. Kisslinger and Sorensen quasi-particle levels for single closed shell nuclei. Hollow circles represent experimental points.

Varying force parameters to obtain the best fit with experimental levels, Rho predicts the level scheme shown in Fig. 20 for Ce^{140}, and achieves a good fit with experiment. This procedure allows exact wave functions to be tabulated. For the 2084 keV level, Rho finds

$$\psi_{4+}^{2084} \cong 0.30 \left| (d_{5/2})^2 \right\rangle_{4+} + 0.91 \left| (g_{7/2})^2 \right\rangle_{4+} - 0.26 \left| (d_{5/2} g_{7/2}) \right\rangle_{4+} \quad (6)$$

Due to the proximity of the $(d_{5/2})^2$ and $(g_{7/2})^2$ energies in Ce^{140} in both the Kisslinger and Sorensen and Rho derivations, it is probably most appropriate to consider excited state properties, particularly magnetic moments, as arising from admixed single particle states.

As has been stated before, quasi-particle levels exhibit the same magnetic moments as the single particles composing them. Estimates of magnetic moments accordingly stem from vector coupling of expected single particle moments, which can be deduced from experimentally determined values for odd protons in the region $Z \cong 57$-61. The Schmidt limits and the experimental values of g-factors are compared in Table VII.

Only one of the experimental values is for an excited nuclear state, the 91 keV 5/2+ state in Pm^{147}. This was determined by perturbed angular correlation and originally reported as $g = 1.42$.[73] The paramagnetic correction used in evaluating this term was $\beta = 2.16$, mid-way between the hydrogenic predictions for Pm^{+3} and its parent Nd^{+3}. Correcting this to $\beta = 1.90$, slightly below the Bleaney interpolated estimate for Pm^{+3}, we obtain $g = 1.61$. Although this involves the assumption of the rapid reduction of the Pm^{+4}, the overwhelming majority of angular correlation experiments indicate that this is much more likely than a compromise paramagnetic enhancement.

Using the experimental estimates of g and the Rho wave function for the 2084 keV state gives $g = 0.90$, slightly lower than our value. Whereas this wave function predicts an 82% predominance of $(g_{7/2})^2$ configuration, our result indicates a maximum probability for this state of 73%. The conclusion that can be drawn from our data, therefore, is that

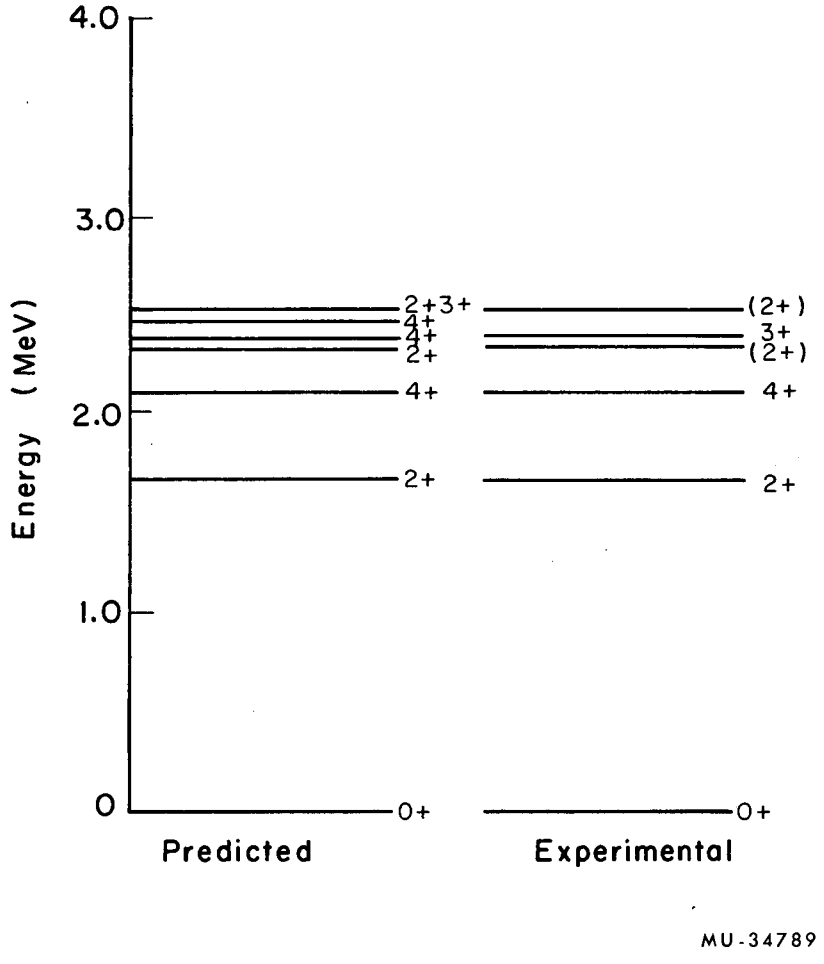

Fig. 20. Level scheme predicted by Rho for Ce^{140}. Experimental levels are shown for comparison.

Table VII. Experimental and Schmidt g-values for odd protons where $57 \leq Z \leq 61$. The last row gives the coupled value for $I = 4+$.

Spin	Isotope	E(keV)	Method	Value	Experimental estimate	Schmidt value
$7/2^+$	$_{57}La^{139}$	0	NMR[15]	0.794	0.78	0.49
	$_{61}Pm^{147}$	0	ESR[71]	0.771		
$5/2^+$	$_{59}Pr^{141}$	0	ESR[72]	1.70	1.65	1.92
	$_{61}Pm^{147}$	91	PAC[73]	1.61		
$(a_{5/2}\ g_{7/2})_4$					1.14	.96

while the 2084 keV level may have a strong contribution from $(g_{7/2})^2$, the configurations $(d_{5/2})^2$ and $(d_{5/2}\ g_{7/2})$ appear with comparable amplitudes and cannot be neglected.

The justification for using empirical rather than Schmidt limit values in calculating the theoretical g-factor comes in part from the calculated Schmidt limit value of g = 0.66, well outside of experimental error. The inference one draws is that the force, or mixing, which quenches the intrinsic magnetic moments below the Schmidt values is of a different nature than the straightforward configuration interactions discussed by Rho. This is compatible with the treatment of Kisslinger and Sorensen in calculating magnetic moments from quasi-particle plus δ-force models.[84]

3. Internal Fields

a. In solution

There is little doubt that the assumption of a paramagnetic correction of unity in aqueous solution is a valid one. The triply-ionized lanthanum decays to Ce^{+4}, an ion stabilized by the spherically symmetric $4f^0$ configuration. In dilute HNO_3, the Ce^{-3} - Ce^{+4} pair has an oxidation potential

$$Ce^{+3} \longrightarrow Ce^{+4} + e^- \qquad \mathcal{E} = -1.61\ V. \qquad (74)$$

The reduction of Ce^{+4} by water is thermodynamically expected. This reaction has been found, however, to proceed slowly at room temperature, with a half life of the order of hours.[75] Thus, one would not expect appreciable reduction in the first thirty or forty nsec.

Further verification has been provided by Körner who found that even in a reducing solution of Fe^{+2}, the reaction did not proceed rapidly enough to paramagnetically perturb the Ce^{140} angular correlation.[69]

b. In the metal

While much data exists on the internal fields in paramagnetic rare earth salts, very little is known of this property in metals. The problem of evaluating the field in the metal and of deducing $\langle r^{-3} \rangle$, therefore, involves a number of assumptions. In this treatment, although an exact value for $\langle r^{-3} \rangle$ can be derived, necessarily large errors will have to be attached to account for crystal field approximations.

Two crystal structures of lanthanum metal are stable, although the predominant form at the temperatures of this experiment is the lanthanum (A3') structure, a close-packed modification in which layers are stacked ABACABAC.[76] In pure hexagonal close packing, the layer alternation is ABAB, while in cubic close packing ABCABC prevails. It consequently can be seen that lanthanum metal layers see alternately a crystal field of cubic and of hexagonal symmetry.

One can show, moreover, that cubic close packing results in a face-centered cubic space lattice with close-packed layers corresponding to the 111 plane of the unit cube. An elongation of the unit cube along the body diagonal converts the symmetry seen by each site from cubic to trigonal. Elliot and Stevens have demonstrated that trigonal symmetry (C_{3h}) and the symmetry associated with hexagonal close packing (D_{3h}) impose exactly the same crystal field (Stark) splittings upon the rare earth 4f shell.[77] Thus, a perturbation of the cubic cell gives sites of hexagonal symmetry.

Following the lead of Bleaney, who found that hexagonal splitting is much smaller than cubic splitting in praseodymium metal (A3'),[78] we will consider the lanthanum structure as pure cubic with a small trigonal distortion in alternate layers. The predominant Stark splitting will therefore be of cubic symmetry, and at the relatively high temperatures of these experiments, the small hexagonal perturbations can be disregarded. The best justification for this approach comes from the differential experimental results on lanthanum metal which indicate no attenuation of anisotropy due to differing magnetic fields, and exhibit a discrete rotation frequency.

The actual Stark splitting in cerium, as in most rare earths, is simplified by the fact that the inner 4f shell is well shielded by outer filled orbitals, and the splitting is not large enough to mix orbital angular momentum quantum states. Typical Stark splittings in rare earth salts are of the order of 300 cm^{-1}.[79] In Ce^{+3}, the unperturbed ground state has a ^2F configuration, with the J = 5/2 ground level lying approximately 2000 cm^{-1} below J = 7/2.[42] At room temperature and lower, the upper level is negligibly populated and may be disregarded.

An angular momentum J = 5/2 can be shown by group theoretical arguments to be split in cubic symmetry into two levels, a degenerate quartet and doublet. We must, therefore, evaluate the internal field due to this splitting. As was seen in an earlier section, the internal field is just the expectation value of the operator H_{int} with eigenfunctions α. In this simple case, where j is single valued, the internal field becomes

$$\langle H_{int} \rangle = -2\mu_B \langle r^{-3} \rangle \langle J \| N \| J \rangle \langle J_z \rangle . \tag{7}$$

$\langle J_Z \rangle$ is the expectation value over the thermal range, or

$$\langle J_z \rangle = \sum M e^{-E_M/kT} \Big/ \sum e^{-E_M/kT} , \tag{8}$$

It has been shown, moreover, that for a J = 5/2 state in a field of cubic symmetry $\langle J_Z \rangle$ is reduced from the value for a free ion in an external magnetic field by a factor $f(x) < 1$ where[80]

$$f(x) = \frac{\frac{5}{21} + \frac{26}{21} e^{-x} + \frac{32}{21} x \left(1 - e^{-x}\right)}{1 + 2e^{-x}} \tag{9}$$

$$x = \Delta E / kT .$$

Here ΔE is the splitting between the doublet and quartet, and is positive for the doublet lowest.

As the bulk magnetic susceptibility of a metal is also proportional to $\langle J_z \rangle$, measurements of this sort can give some clue to the sign and magnitude of ΔE. White and co-workers, for example, find an anomaly in the susceptibility of Ce^{+3} in the cubic lattice $LaAl_2$,[80] which indicates an energy gap corresponding to about 200° K. Determinations by other workers on pure cerium metal give a splitting of 200-250° K.[81] The positive sign of ΔE and the limiting value of $f(x)$ as $x \longrightarrow \infty$ agree with the designation of the doublet as the ground state.

It is a somewhat hazardous business to extrapolate from these two qualitative measurements to the expected ΔE for cerium in lanthanum metal. A slightly smaller value of ΔE, at least, can be expected due to the larger lattice spacing in lanthanum compared to cerium. A low value of ΔE is also internally consistent with the experimental data for the two temperatures in the differential measurements. As a crude estimate we choose, therefore, an energy gap corresponding to 160° K.

Inserting this value into the crystal field correction factor, we find

$$\begin{aligned} f(x) &= 0.83 \quad \text{at } 77.4\ ^\circ K \\ f(x) &= 0.985 \quad \text{at } 300\ ^\circ K\ . \end{aligned} \tag{10}$$

Dividing the paramagnetic corrections by $f(x)$ and taking the weighted average for $C = \beta T$, we have

$$\begin{aligned} C &= (114.3 \pm 16.1)\ ^\circ K \\ \langle r^{-3} \rangle &= (3.94 \pm 0.56)\ \text{a.u.} \end{aligned} \tag{11}$$

Although both the Bleaney and the Lindgren predicted values for $\langle r^{-3} \rangle$ are covered by this value, the Freeman-Watson prediction is outside of experimental error. The relatively low experimental value indicates that Bleaney's interpolated curve rises perhaps too sharply in this region.

The conclusiveness of this result depends quite sensitively upon the estimate $\Delta E = 160^{\circ}$ K. Figure 21 shows a plot of the value of $\langle r^{-3} \rangle$ as a function of ΔE for our experimental data. For a ΔE in the region of 160° K, an error of 1 deg gives a difference of 0.005 a.u. This error increases rapidly with increasing ΔE. It is probably safe to assign an upper limit of $\pm 40^{\circ}$ K in ΔE, giving an uncertainty of 0.20 a.u. in $\langle r^{-3} \rangle$. This uncertainty is small compared to the statistical error.

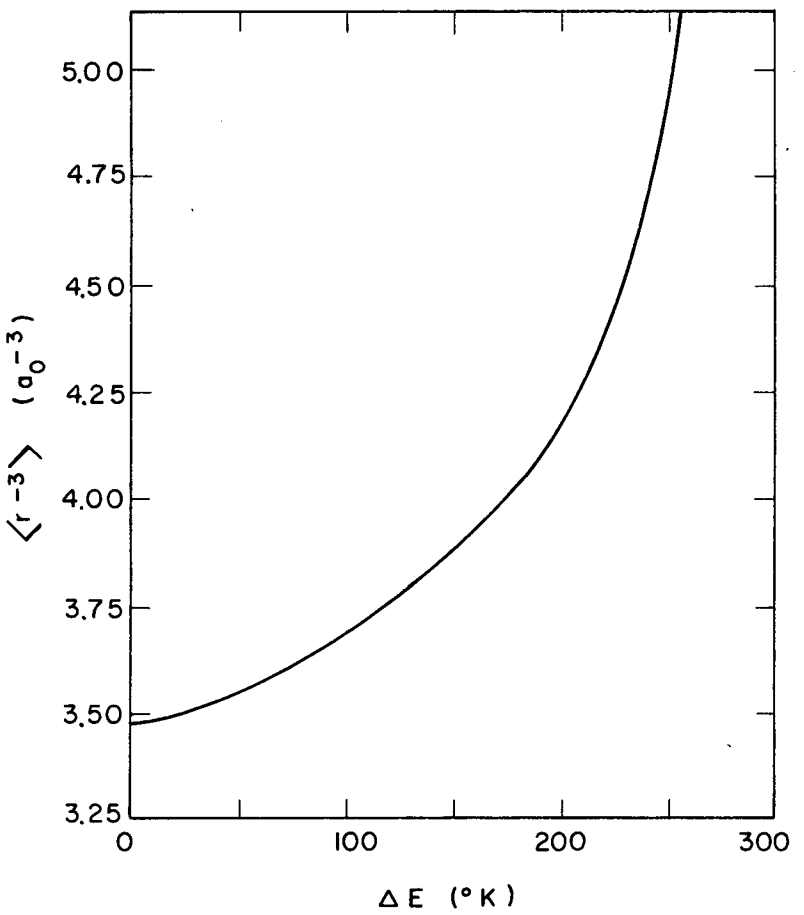

Fig. 21. Corrected values of $\langle r^{-3} \rangle$ as a function of crystal field splittings in lanthanum metal.

VI. Pr^{143}

A. Introduction

Throughout the preceding discussion of Ce^{140}, it has perhaps become apparent that no single unified theory has yet presented an all-inclusive characterization of spherical nuclei. In aesthetic terms, it would be extremely pleasing if such a theory could be worked out a priori. In a pragmatic scientific sense, however, the procedure has been one of varying parameters and perturbing simple models to fit the increasing supply of experimental data.

With this in mind, we have measured, by perturbed angular correlation, the magnetic moment of the 57 keV level in Pr^{143}, and comparing angular correlation and nuclear alignment data, have deduced the spins and parities of the 57 keV and 351 keV states.

Pr^{143} is an odd-even nucleus with 59 protons and 84 neutrons, two over the major closed shell. The lower excited states may be considered single quasi-particle states, their energies and transition probabilities being amenable to the treatment of Kisslinger and Sorensen.[23] The spins and parities of these levels take on the values of the single particle shells in this region, which are, in order of ascending energy: $g_{7/2}$, $d_{5/2}$, $d_{3/2}$, $h_{11/2}$. Although there is no large energy gap as in even-even nuclei due to the fact that a pair need not be broken, vibrational phonons, or states of a collective nature, are expected between energies of 400 keV and 1000 keV.[48]

A tentative decay scheme has been worked out utilizing high resolution Ge(Li) spectroscopy and coincidence counting with both Ge(Li) and NaI(Tl) detectors. The results are shown in Fig. 22. The experimental gamma energies are compared with previous work in Table VIII.

Several features applicable to this work deserve mention. These can best be discussed from a nuclear systematics approach. A resumé of the properties of the few known odd proton nuclei in this region is given in Table IX.

The spin sequences give some insight into the trends in this region. The crude empirical behavior, which fortunately bears out quasi-particle

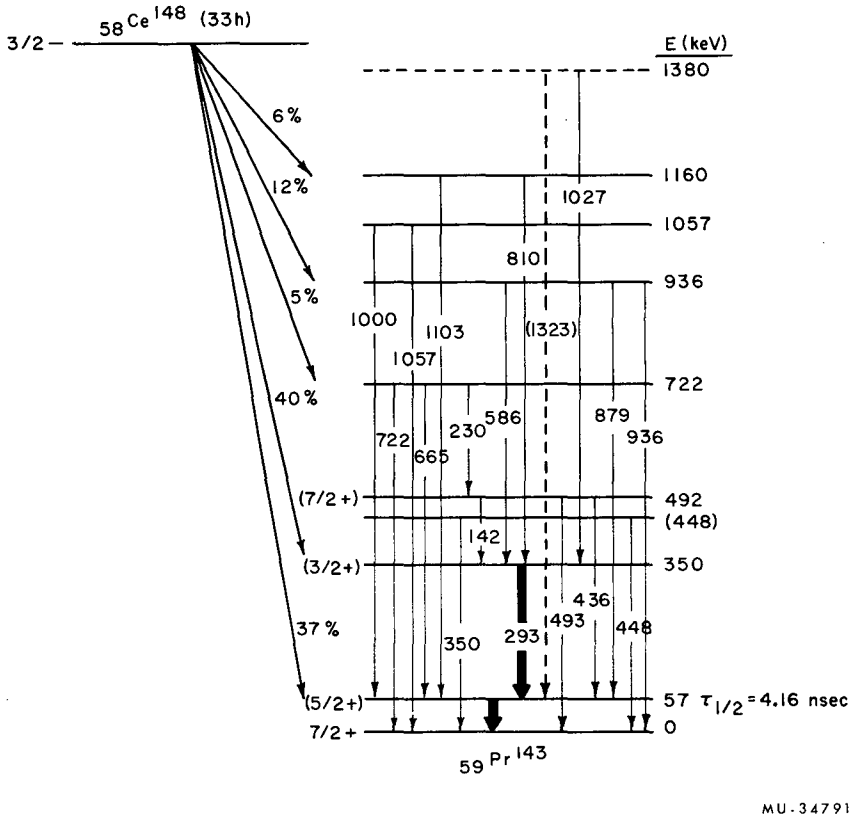

Fig. 22. Decay scheme of Pr^{143}.

Table VIII. Energies of gamma transitions in Pr^{143}.

Reference 82	Reference 83	This work
57.4	56	57.4
232	230	231.6
		279.6
294	293	293.0
351	341	350.6
		436.0
493	488	491.8
565	565	586.4
668	665	664.3
722	718	721.6
		809
861	870	880.7
		937.5
		1004
		1061
1100	1087	1103
		1325

Table IX. Summary of properties of spherical, odd-proton rare-earth nuclei.

Isotope	Level (keV)	Spin	$T_{1/2}$(nsec)	g-factor[85]
$^{137}_{57}La_{80}$	0	(7/2)		
	10	(5/2)	8.9	
$^{139}_{57}La_{82}$	0	7/2		0.79
	165	5/2	1.5	
$^{141}_{59}PR_{82}$	0	5/2		1.70
	142	7/2	1.8	
$^{143}_{59}Pr_{84}$	0	7/2		0.78
	57	(5/2)	4.2	
	351	(3/2)		
$^{147}_{61}Pm_{86}$	0	7/2		0.77
	91	5/2	2.5	1.61
	412	(3/2)		

predictions, indicates that the addition of neutrons depresses the $g_{7/2}$ below the $d_{5/2}$ shell, while addition of protons does the opposite.

In the case of Pr^{143}, the ground state spin has been measured by atomic beam methods to be I = 7/2+.[86] On comparison with Pm^{147}, which differs only by the addition of an alpha particle, one is tempted to predict spins 5/2+ and 3/2+ for the excited states of Pr^{143}.

This prediction is further strengthened by the combination of β branching intensities as measured by Martin,[82] and the recently determined spin of 3/2- for 33 h Ce^{143}.[87] More will be said of this below.

B. Experimental Procedure and Results

1. Experimental conditions

As in Ce^{140}, angular correlations have been performed on both liquid and solid sources of Ce^{143}. The former are produced by bombarding 87% enriched Ce^{142} in CeO_2 in a flux of 8×10^{13} thermal neutrons/cm^2/sec at the Vallecitos reactor for 16-24 hours. The powder is dissolved by gentle heating in a solution of 3N HNO_3 and a few drops of 20% H_2O_2. The solution is boiled to dryness and taken up in distilled water. A small aliquot is sucked into a capillary tube which is subsequently sealed. Usable sample strengths range around 30-45 mR/2 in. This gives a counting rate of about 10^5 cpm in the 294 keV peak using a 2-in. diameter detector at 7 cm distance, and a coincidence true-to-chance ratio of 10:1.

Solid sources are prepared by 6-10 hour bombardments at a flux of 1×10^{13} neutrons/cm^2/sec upon 5-10 mg chunks of cerium metal sealed in quartz under argon. Active samples register about 30-50 mR/in.

The detector with the optimum high gain, low noise characteristics gates on the 57 keV gamma transition. Operational high voltages are kept at a maximum (2250-2500 V). A 1/2-in. thick NaI(Tl) crystal and a 7 mil Pb absorber backed by 2 mil Cu foil (to absorb Pn x-rays) give the best resolution characteristics. A typical spectrum thus obtained is reproduced in Fig. 23.

The high energy detector gives good results for the 294 keV transition with a 1-1/2-in. × 1-1/2 in. NaI(Tl) crystal and a 20 mil Cd absorber.

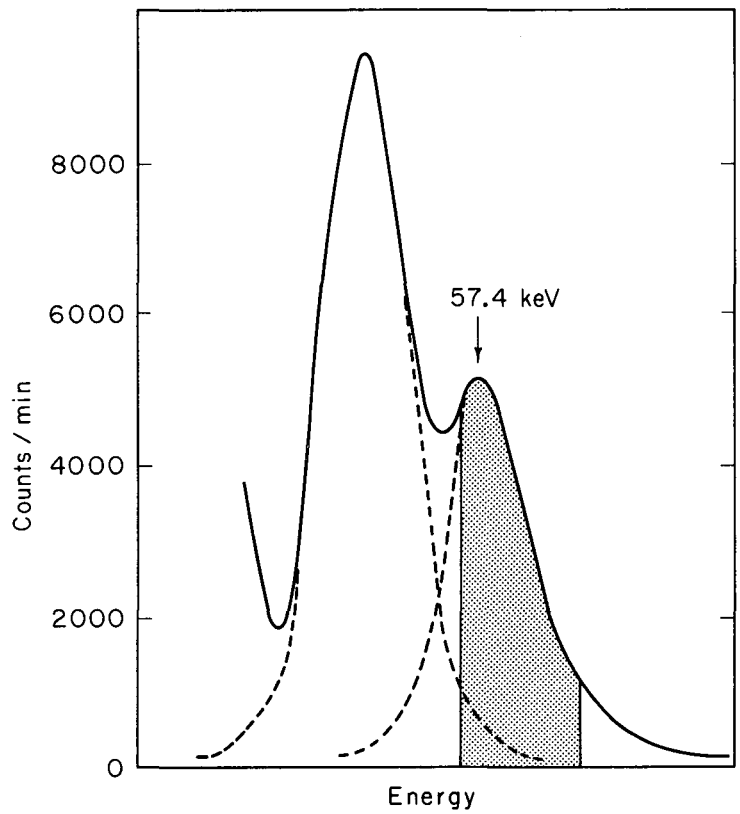

Fig. 23. Low energy portion of Pr^{143} spectrum, taken with 1-1/2 in. × 1-1/2 in. NaI(Tl) crystal and 7 mil Pb absorber. Shaded portion indicates gate used in angular correlation measurements.

The spectrum observed by this detector, as gated by the 57 keV transition is shown by the solid line in Fig. 24.

2. Anisotropy measurements

The unperturbed angular correlation for the 294 keV-57 keV cascade has been measured by gating on the 57 keV gamma ray in the moveable counter and measuring the number of counts under the 294 keV peak. Counts of 20-30 minute duration have been taken at each of three angles, $\theta = 90^\circ$, 180°, 135°, over a total period of about 40 hours. The total number of coincidences collected is

$$W(180^\circ) = 29475$$
$$W(135^\circ) = 27285$$
$$W(90^\circ) = 25015$$

Background is isotropic and contributes less than 3% of the total counts. The uncorrected angular correlation is shown in Fig. 25. Adjusting this value to account for solid angle [$Q_2Q'_2 = (0.9345)(0.9483)$], we find

$$W(\theta) = 1 + (0.133 \pm 0.007)P_2(\cos\theta) + 0.000 \pm 0.006\, P_4(\cos\theta). \quad (1)$$

This result agrees with previous experimenters who found $A_2 = 0.132 \pm 0.019$[83] and $A_2 = 0.132 \pm 0.010$.[88]

3. Integral g-factor measurements

Measurements of the g-factor have been performed upon Ce^{143} solutions using the perturbed integral method. To eliminate the effect of geometrical uncertainties inherent in an experiment where counters are rotated, a magnetic field up-field down angular correlation with counters permanently set at 135° to one another proved desirable. In order to optimize the external field magnitude, it is instructive to consider the counting rate difference ΔW as a function of $2\omega_L\tau$. We find for a pure P_2 anisotropy

$$W(\theta, H) = \frac{B_2}{\left[1 + (2\omega\tau)^2\right]^{1/2}} \cos 2(\theta - \Delta\theta). \quad (2)$$

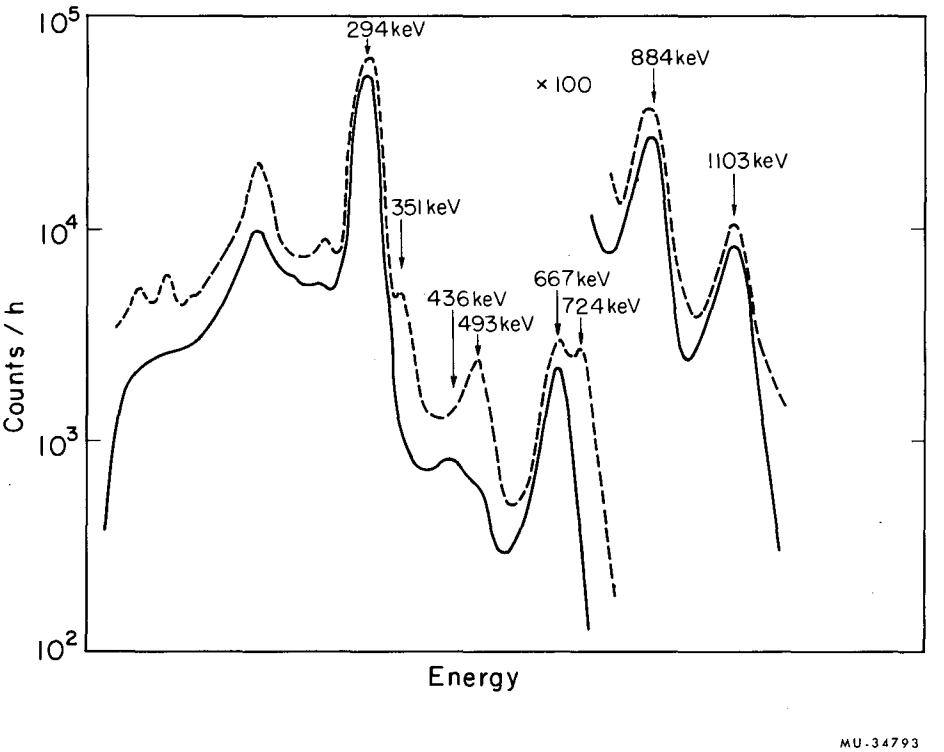

Fig. 24. Pr^{143} singles spectrum (dashed line) and spectrum in coincidence with 57 keV transition. Spectra were taken with 1-1/2 in. × 1 in. NaI(Tl) crystal with 20 mil Cd absorber.

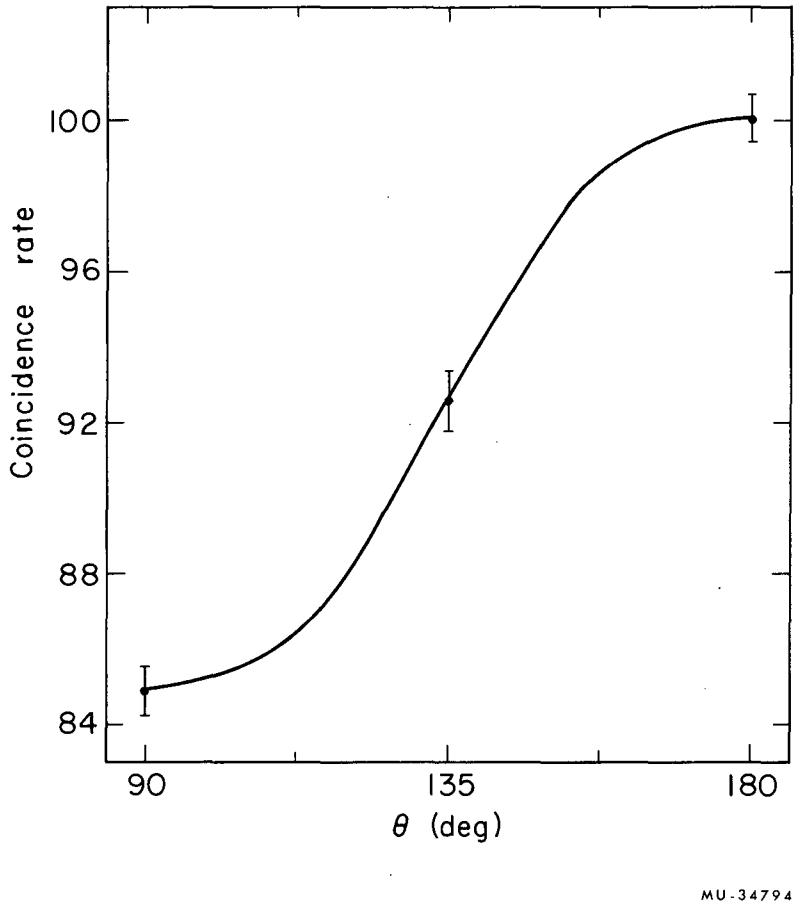

Fig. 25. Unperturbed angular correlation of 294 keV—57 keV cascade in Pr^{143}.

For the field up-field down difference this gives

$$\Delta W = \frac{B_2}{[1 + (2\omega\tau)^2]^{1/2}} \left[\cos 2(\theta - \Delta\theta) - \cos 2(\theta + \Delta\theta)\right]. \qquad (3)$$

Substituting the necessary trigonometric identities, we find

$$\chi = \frac{1 \pm (1 - a^2)^{1/2}}{a} \qquad (4)$$

where $x = 2\omega_L\gamma$ and $a = \Delta W/B_2$. A plot of this functional dependence is shown in Fig. 26. It is obvious from error considerations that a small $2\omega_L\gamma$, and consequently a small magnetic field, is desirable.

Using permanent magnetis, we have applied fields of 2.2 kG and 3.84 kG and obtained $\Delta W/B_2$ values of about 0.5-0.75. Runs have been made at both fields on two different source solutions: Ce^{+4} in an oxidizing solution of 1N BrO_3^- and 10 N HNO_3, and Ce^{+3} in a reducing medium of 3 N H_2O_2. Successive 20 minute counts have been taken for each field direction over a period of 6-8 h for each result quoted. The experimental data are summarized in Table XII.

The value $g\beta$, the product of the g-factor and the paramagnetic correction can be calculated directly from the functional relationship of $2\omega_L\tau$ and $\Delta W/B_2$. We find for a reducing solution (Ce^{+3}) the average

$$g\beta = 2.48 \pm 0.97 \qquad (5)$$

and for the oxidizing medium (Ce^{+4})

$$g\beta = 2.65 \pm 0.65 \qquad (6)$$

4. Differential measurements

a. Half life

Time calibration and general procedure have been the same for Pr^{143} as for Ce^{140}, with the exception that only the overlap time-to-height converter and transistorized system have been used.

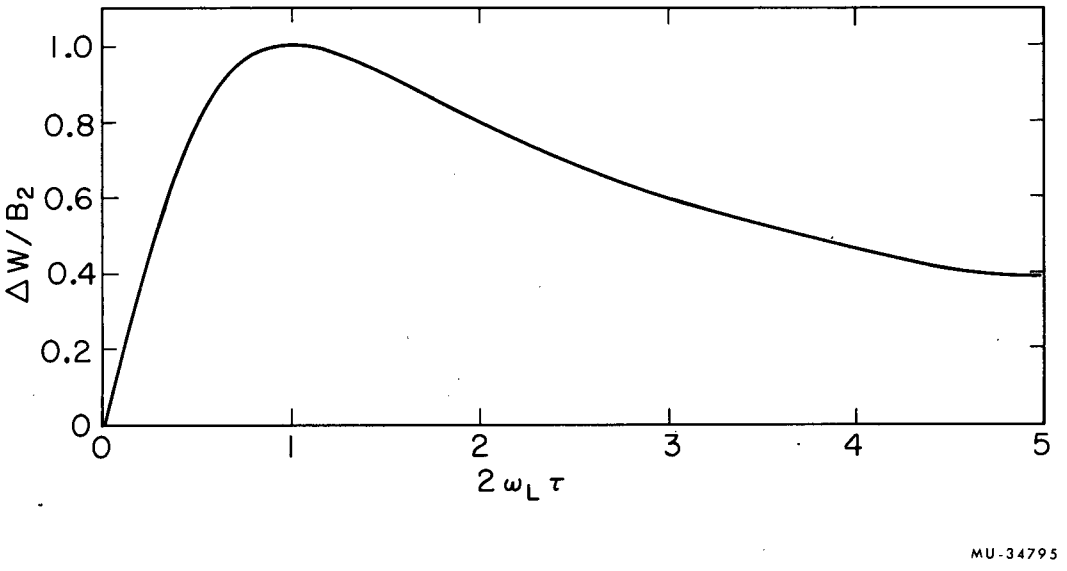

Fig. 26. Functional dependence of precession frequency upon field dependent integral coincidence rate.

Table X. Summary of integral angular correlation data on 294 keV-57 keV cascade in Pr^{143}. The plus and minus indicate the direction of the field (H).

Source	H(kG)	W_+	W_-	Percent change	$g\beta$
$Ce^{+3}+HNO_3+H_2O_2$	2.2	9970	9584	4.0±1.9	1.97±1.30
$Ce^{+3}+HNO_3+H_2O_2$	2.2	12478	11796	5.6±1.7	2.88±1.90
$Ce^{+3}+HNO_3+H_2O_2$	3.84	10102	9484	6.3±1.8	2.60±1.75
$Ce^{+3}+HNO_3+BrO_3^-$	2.2	15094	14391	4.8±1.5	2.58±1.13
$Ce^{+3}+HNO_3+BrO_3^-$	2.2	20244	19345	4.5±1.4	3.64±1.36
$Ce^{+3}+HNO_3+BrO_3^-$	3.84	15715	14895	5.4±1.5	1.74±0.82

The prompt resoltuion curve for the 294 keV-57 keV coincidence has a resolution of $2\tau_o = 6.0$ nsec, and is wider on the 57 keV side due to poorer time characteristics for low energy pulses. Runs have been made with relative delay in both γ_1 and γ_2 to check for unsymmetrical behavior of the electronics, but no appreciable difference in shape could be detected.

The lifetime measurement of the 57 keV state of Pr^{143} is shown along with the prompt resolution in Fig. 27. The limiting slope, away from the small delay portion distorted by resolution, gives a half-life of

$$\tau_{1/2} = 4.23 \pm 0.15 \text{ nsec} \quad . \tag{7}$$

This agrees satisfactorily with the measurement of Graham (4.17 ± 0.09 nsec)[89] and Bózek (4.20 ± 0.07 nsec).[88]

b. Perturbed angular correlation—liquid source

Four independent determinations of $g\beta$ have been performed by the differential method upon Pr^{143} in aqueous solution. Fields of 16.1 kG, 19.1 kG, and 23.45 kG have been used and relative delay has been inserted in both γ_1 and γ_2. From 1-1/2 to 2 complete cycles have been observed and amplitudes approaching the unperturbed anisotropy have been achieved for very low fields.

The R(t) curves for three separate fields are shown together in Fig. 28. It can be seen that the higher the frequency, the larger is the distortion at small delays. The three curves agree remarkably well in $g\beta$ determination, giving values within 2% of one another. The results are summarized in Table XI. The average value for $g\beta$ from all the curves is

$$g\beta = 2.58 \pm 0.13 \quad . \tag{8}$$

Complementary to this measurement a determination of $A_2(t)$ has been made by observing the differential spectrum at 180° and 90°. The results indicate no appreciable attenuation of the anisotropy over 25 nsec.

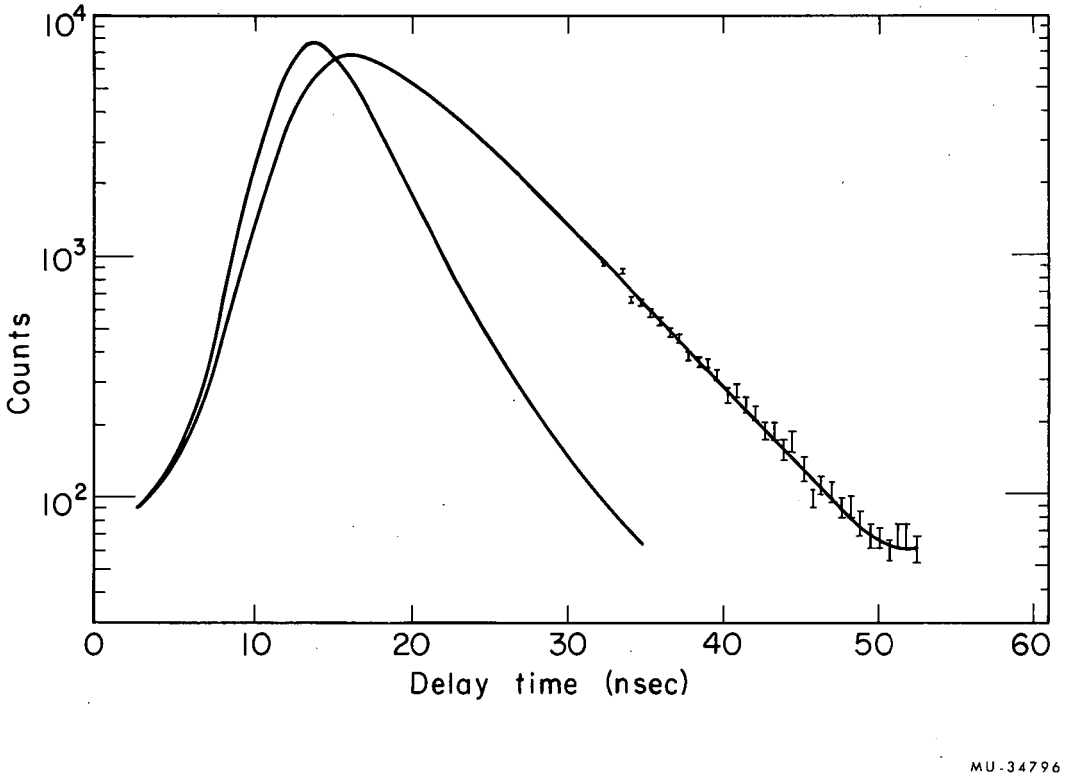

Fig. 27. Prompt resolution curve and decay curve for 294 keV—57 keV cascade in Pr^{143}.

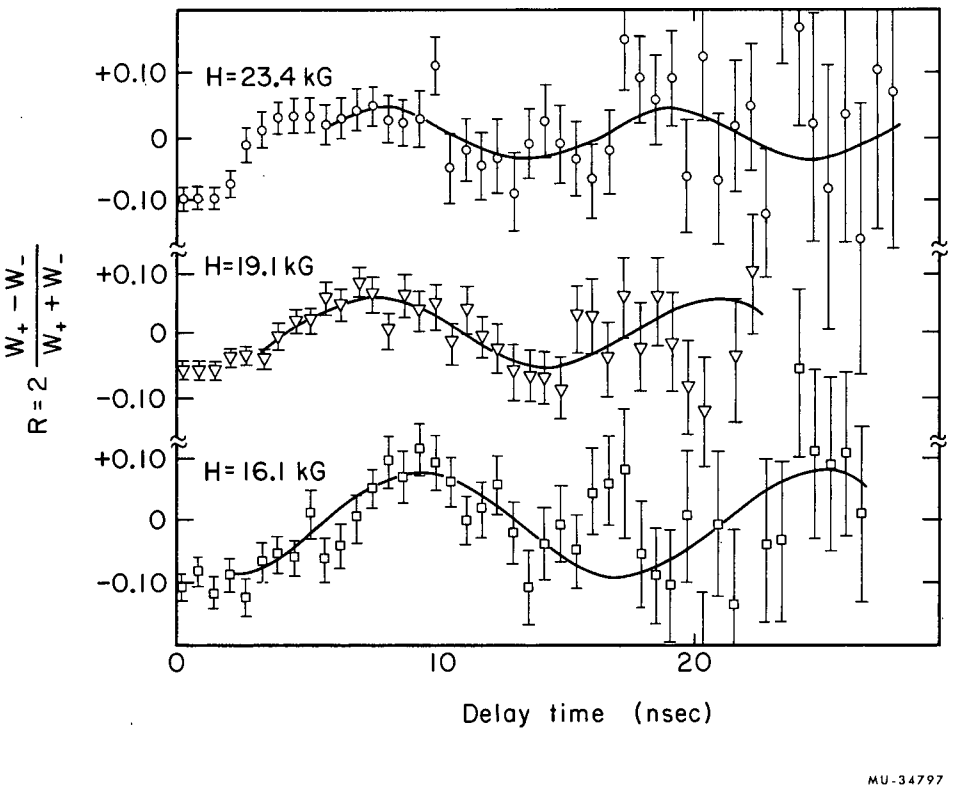

Fig. 28. Experimental anisotropy precession frequencies of 294 keV—57 keV angular correlation in Pr^{143} in acidic solution.

Table XI. Summary of differential perturbed angular correlation measurements on Pr^{143}.

Source	Field (kG)	Amplitude	Time Calibration (nsec/chan)	f($\frac{\text{cycles}}{\text{channel}}$)	gβ
Solution	19.1±0.2	5.3±0.9	0.61±0.02	0.046±0.003	2.60±0.21
Solution	19.1±0.2	5.0±2.0	0.61±0.02	0.045±0.005	2.55±0.30
Solution	16.1±0.1	8.2±1.2	0.61±0.02	0.039±0.003	2.62±0.23
Solution	23.45±0.05	3.7±1.3	0.61±0.02	0.055±0.006	2.55±0.29
Metal	12.2±0.3	9.0±3.0	0.61±0.02	0.039±0.002	3.39±0.51
Metal	12.2±0.3	8.0±3.0	0.61±0.02	0.040±0.005	3.53±0.46
Metal	9.5±0.1	9.0±1.8	1.00±0.03	0.056±0.011	3.83±0.80

c. Perturbed angular correlation—metal source

In order to obtain a guide for the assessment of the paramagnetic correction, it has been appropriate to carry out differential measurements on sources of Pr^{143} in cerium metal under fields of 12.2 kG and 9.5 kG. The latter measurement employed a small permanent magnet and required no light pipes.

A preliminary determination of the variation of anisotropy with time has been performed. The results, plotted in Fig. 29, indicated a strong time-dependent perturbation. The anisotropy decreases exponentially with a half-life of (5±1) nsec. This effect has been observed on two separate metal sources with consistent results.

While the decay of the anisotropy greatly impedes the assessment of the g-factor from R(t), three successful runs have been performed and give reasonable indication of the product $g\beta$. These are indicated in the last three rows of Table XI. Two runs with relative delay in γ_1 and γ_2 respectively are shown in Fig. 30.

Assigning relatively large errors due to the effect of the attenuation, we find for the weighted average of the measurements

$$g\beta = 3.55 \pm 0.36 \quad . \tag{9}$$

C. Discussion

1. Spin sequence

From the angular correlation anisotropy, $A_2 = 0.133 \pm 0.007$, it is impossible to label the angular momenta of the nuclear states unambiguously. While the spin of the ground state is known to be I = 7/2, neither excited state has been determined conclusively. Moreover, uncertainties in mixing ratios, particularly for the upper transition, add further confusion.

To clarify the spin assignments, we have performed a nuclear alignment experiment. The parent Ce^{143}, grown into a neodymium ethyl sulfate crystal, is suspended in a system of cryostat and dewars and adiabatically demagnetized to about 0.015°K. The apparatus and the experimental procedures

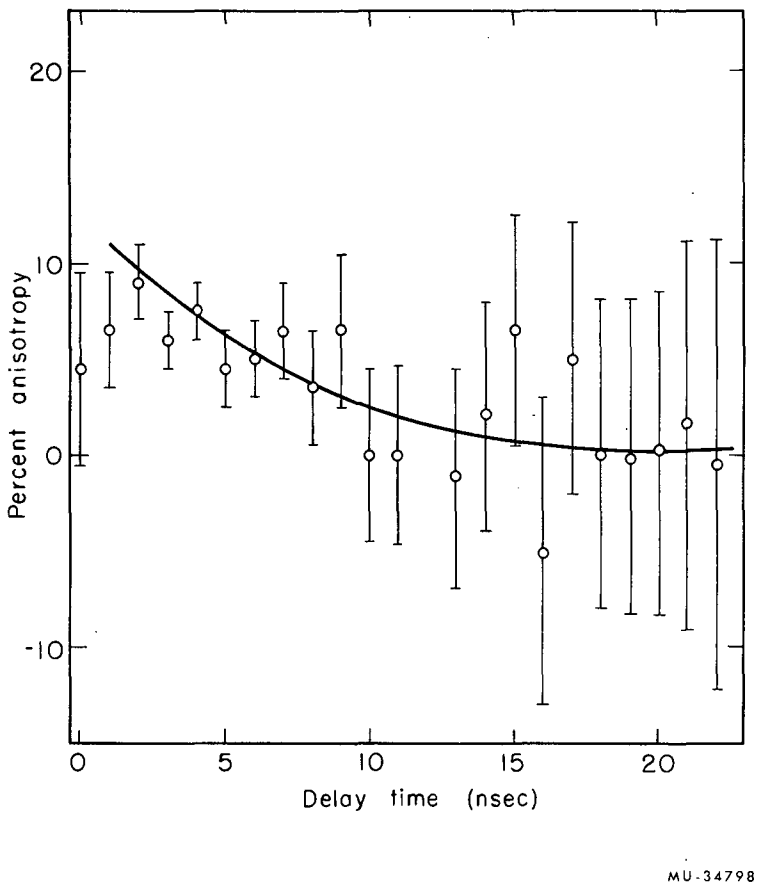

Fig. 29. Attenuation of anisotropy with time for Pr^{143} angular correlation in cerium metal.

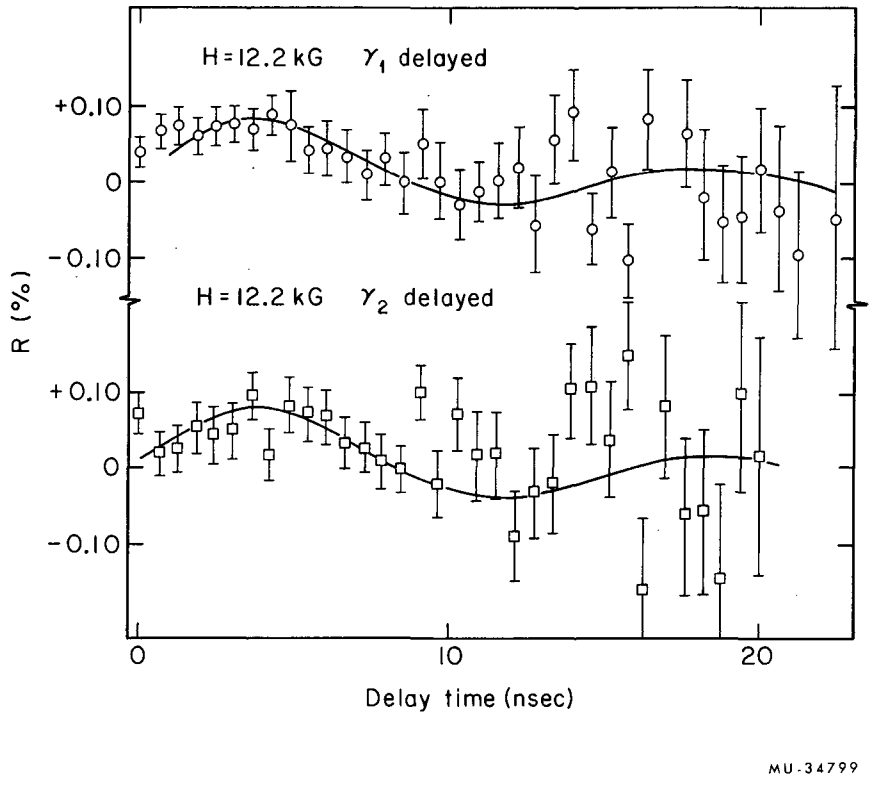

Fig. 30. Damped anisotropy in perturbed angular correlation measurements on Pr^{143} in cerium metal.

have been described in detail elsewhere.[90] At these low temperatures, the nuclear substates, split by the hyperfine field of the lowest electronic Stark level, are non-randomly populated. The resultant radiation displays an anisotropy which can be described by

$$W(\theta) = 1 + \sum_k B_k U_k F_k P_k(\cos\theta) \qquad (10)$$

where k has even values up to twice the maximum multipolarity; B_k is an alignment parameter describing the interaction of nuclear moments with effective fields as a function of temperature; U_k has the same form as that described by Eq. (II-23) and accounts for the reorientation between the aligned parent state and the gamma transition of interest; and F_k is the same constant as that which describes the second transition in an angular correlation.

In these experiments, the count taken over a period of 20 minutes from the aligned sample by a detector parallel to the crystal z-axis, is compared with a count of the same period on the non-aligned "warm" source. The difference, or the ratio of cold to warm counts, gives a direct measure of the product $B_2U_2F_2$. Studies were made of the transitions at 57 keV, 294 keV, and 351 keV using both NaI(Tl) and Ge(Li) detectors. The enhanced peak separation in the Ge(Li) counters is illustrated in Fig. 31. The cold-to-warm ratios are shown in Table XII.

We may assume, after Blin-Stoyle and Grace,[9] that the sign of B_2 is positive for NES, a crystal of axial symmetry. It can be seen, in addition, that for all the more probable β and γ transitions, U_2 is also positive. Thus the sign and anisotropy in the nuclear alignment experiments is the same as the sign of F_2.

From the magnitude of the mixing ratio in the 57 keV transition (E2 < 0.3%), we infer that F_2 (57 keV) must lie between +0.08 and +0.21. We have taken the spin of the 57 keV as 5/2. The other possibilities, 7/2 and 9/2, are improbable in view of the strong β decay branch from the 3/2- level. A stronger argument, based on the signs of F_2, show these spin assignments to be impossible.

The designation 3/2+ or 5/2+ for the 351 keV state would be consistent with angular correlation data and β decay behavior. In either case, the observed angular correlation anisotropy requires $\delta < 0$ for the 294 keV transition. This, however, implies $\delta > 0$ for nuclear alignment,

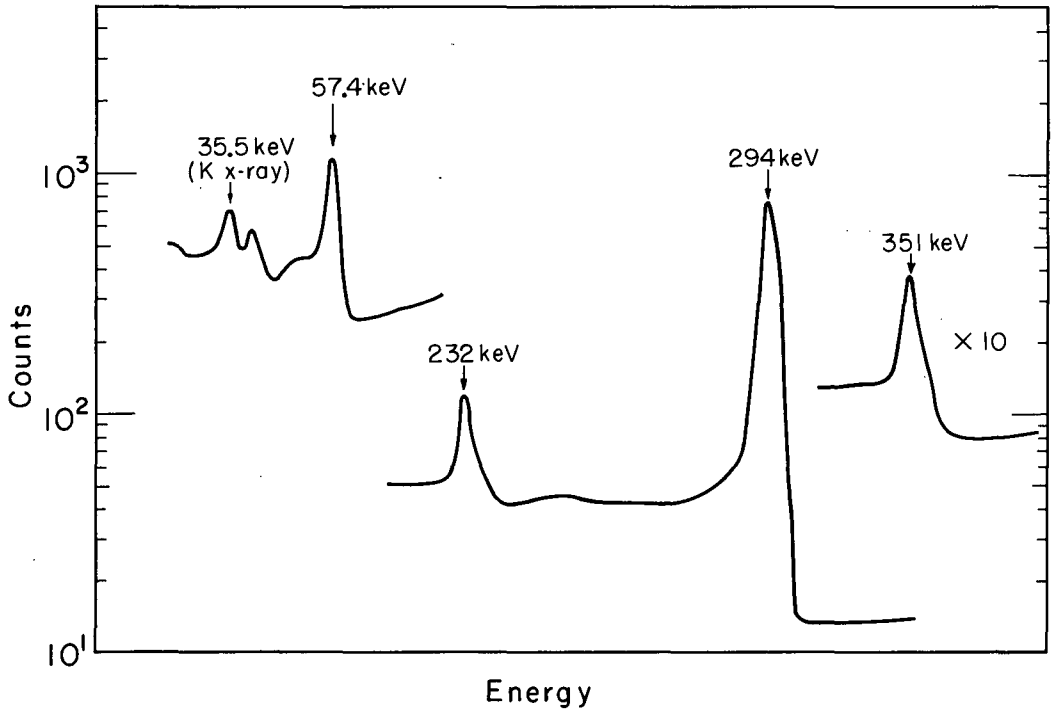

Fig. 31. Pertinent sections of 20 min spectrum in nuclear alignment of Ce^{143}, taken with Ge(Li) detector.

Table XII. Nuclear alignment results on Ce^{143} in NES at about 0.015°K. Error assignments depend upon the feasibility of background corrections.

Energy	Detector	Cold/Warm
57 keV	NaI(Tl)	1.038±0.007
	Ge(Li)	1.048±0.005
294 keV	NaI(Tl)	1.034
	Ge(Li)	1.027±0.012
351 keV	Ge(Li)	0.987±0.010

which for a $5/2 \rightarrow 5/2$ transition would give a negative F_2. A spin of 3/2+ for the 351 keV state is thus the only one consistent with the data.

The measured admixture in the 294 keV transition of $(34 \pm 16)\%$ $E2$[89] adds further proof to the 3/2 (D,Q) 5/2 (D,Q) 7/2 designation. The values of F_2 consistent with all the above conclusions are shown graphically by the shaded portions in Figs. 32-34. The applicability is explained in the figure captions.

From the angular correlation values, we see that F_2 (57 keV) must lie between 0.123 and 0.135, while a pure M1 transition has $F_2 = 0.134$. This indicates a maximum E2 admixture in the 57 keV transition of about 0.01%.

2. Time-dependent perturbation

From Eq. (II-24) and the accompanying section, we have seen that all perturbations to an angular correlation may be inserted in a term $|U^{b_1 b_2}(t)|^2$ between the interaction Hamiltonians for the two coincident transitions. This term encompasses the perturbation operator K which connects nuclear eigenfunctions $|m\rangle$ and $|m'\rangle$ of the intermediate state.

For a time-dependent, random interaction, the effect of K is averaged statistically over an ensemble of states. Abragam and Pound have shown that for a particular time-dependent perturbation upon the nucleus, which increases exponentially with electronic relaxation (i.e., represents a coupling between electrons and nucleus), the transition probability for nuclear states $m \rightarrow m'$ is given by

$$Q \propto |\langle m | K(t) | m' \rangle|^2 \tau_e \qquad (11)$$

where τ_e is a characteristic electronic relaxation time.[12] This equation applies only for electronic relaxation times very short compared with nuclear lifetimes, such that still faster electronic relaxation serves to decouple the nuclear motion and the electronic motion.

Inserting Eq. (11) into the expression for the population density in the intermediate nuclear state, Abragan and Pound show that for a time-dependent perturbation through a hyperfine coupling mechanism, the angular correlation function becomes

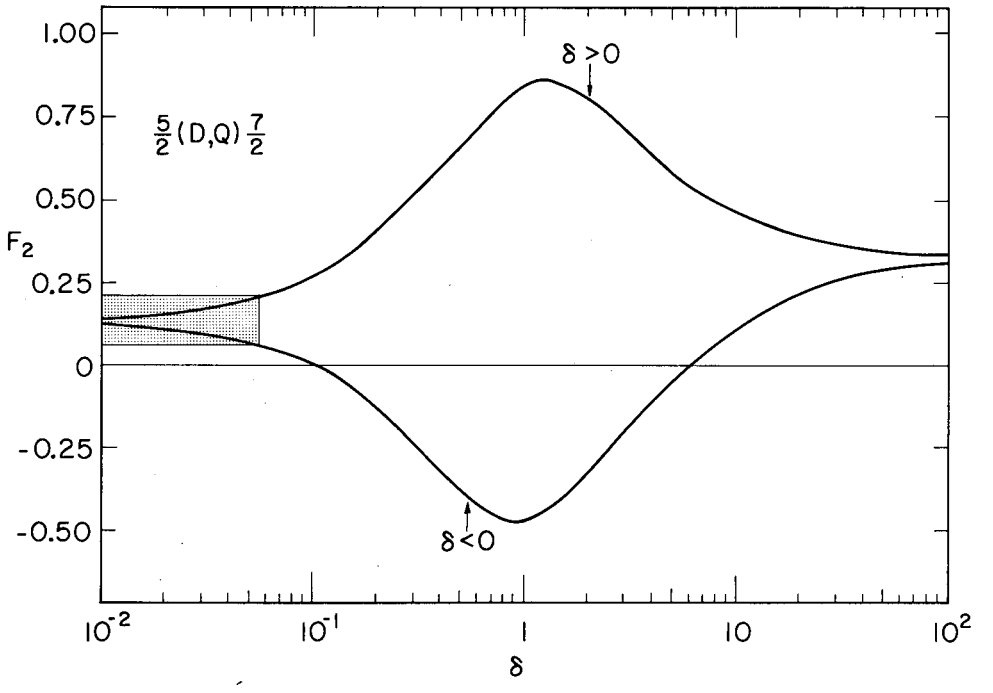

Fig. 32. F_2 as a function of mixing amplitude δ. The shaded portion represents the value of F_2 for the 57 keV transition as seen by both angular correlation and nuclear alignment.

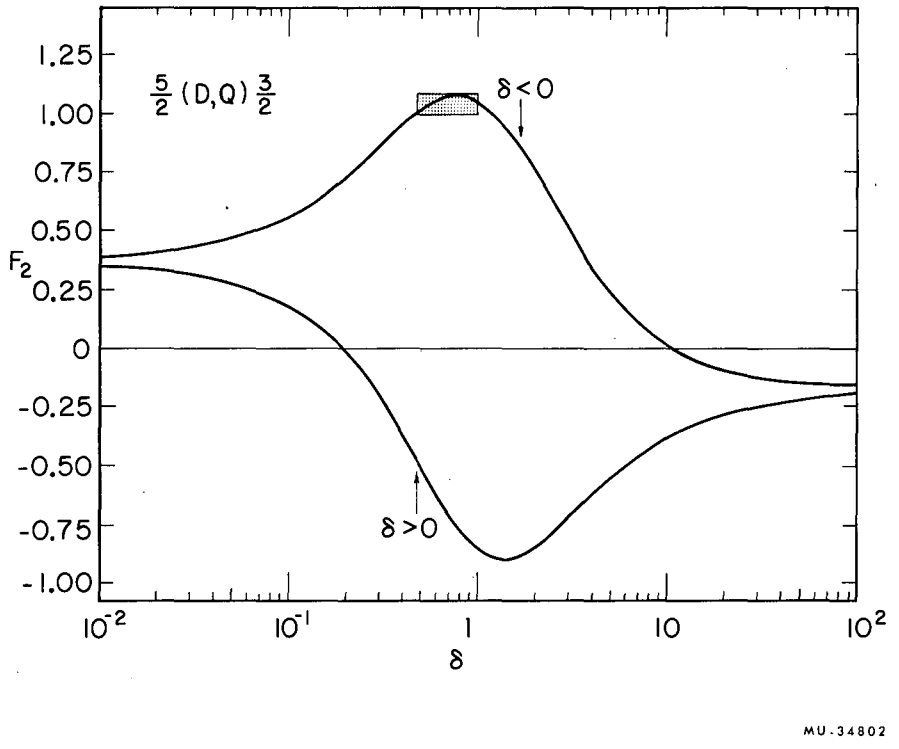

Fig. 33. F_2 as a function of mixing amplitude δ. The shaded portion represents the value of F_2 for the 294 keV transition as seen by angular correlation.

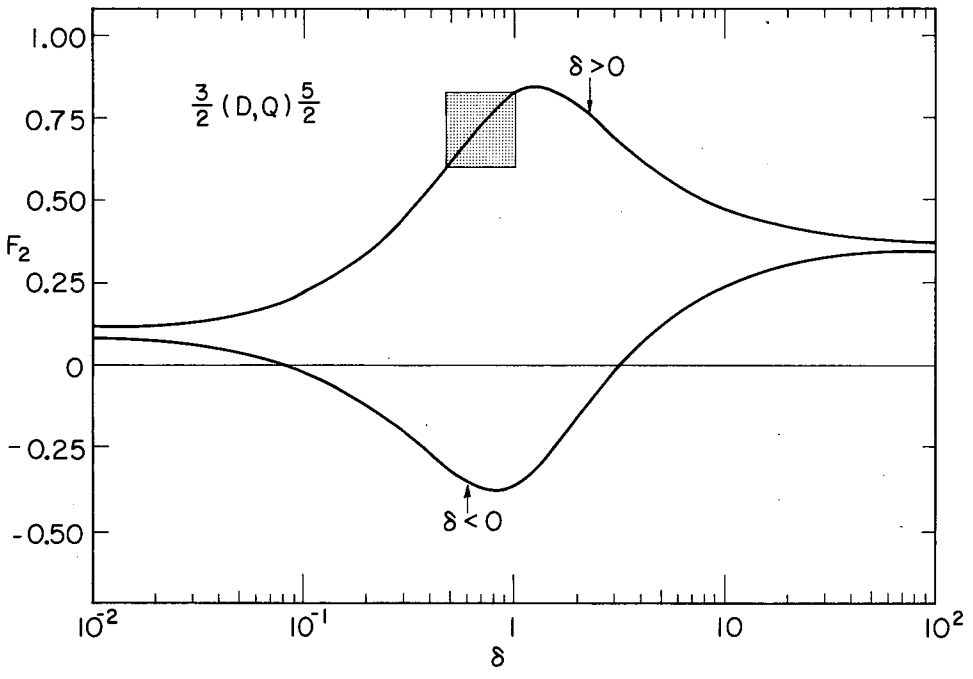

Fig. 34. F_2 as a function of mixing amplitude δ. The shaded portion represents the value of F_2 for the 294 keV transition as seen by nuclear alignment.

$$W(\theta,t) = 1 + \sum_k e^{-\lambda_k t} A_k P_k(\cos\theta)$$

$$\lambda_k = \frac{2}{3}\tau_e \omega^2 I(I+1) J(J+1) \left[1 - (2I+1) W(I\,1\,k\,I;I\,I)\right]. \quad (12)$$

The frequency ω of the nuclear rotation accounts for the strength of the hyperfine interaction.

In the case of Pr^{143} in cerium metal, we have found an anisotropy decreasing exponentially with a half-life of 5 nsec. Substitution of values in Eq. (12) shows that this corresponds to an electronic relaxation time of 1.29×10^{-11} sec.

It is worth comment that a time-dependent hyperfine effect appears in Pr^{143} and not in Ce^{140}, although it is impossible to infer any one definite reason from our single measurement. One would expect a somewhat stronger attenuation in Pr^{+3} due to the enhanced paramagnetic correction, hence stronger hyperfine coupling. However, this would not be a big enough difference to account for our results. It is therefore, possible that the spin-lattice relaxation is faster for Ce^{+3} in lanthanum metal than for Pr^{+3} in cerium metal.

As a final comment, it may be noted that the order of magnitude of the electronic relaxation time is characteristic of a spin-lattice relaxation, in contrast to the other possible mechanism in a metal, conduction electron spin-spin relaxation.[91] Overhauser has shown that, although the latter could explain nuclear relaxation, it would be several orders of magnitude slower.[92]

3. g-factor and paramagnetic correction

Because of the crucial significance of the paramagnetic correction in the evaluation of the g-factor, a careful analysis of the electronic structure of the samples investigated must be made. The critical parameter in this study is the value of $g\beta$ from the rotational frequency of Pr^{143} in cerium metal.

In view of the powerful chemical reducing capacity of the sea of conduction electrons in a metal sample, and the rapid attainment of electronic equilibrium (relaxation times on the order of 10^{-14} sec),[41] we may safely assume that all the Pr^{143} exists in the triply-ionized state.

The problem of crystal field effects may be disregarded here. Bleaney has found that Pr^{+3} in the cubic field of praseodymium metal has an electronic splitting of the $^3H_4$ electronic ground state into a singlet, two triplets, and a doublet.[78] The maximum splitting, between the ground singlet and the highest triplet, is 246°K, with the majority of the states at energies below 150°K. In the cubic lattice of cerium metal, the interatomic distance is approximately the same as in praseodymium, and one can approximate the same splitting. Thus, at the temperature of this experiment (300°K), the effect of crystal field upon $\langle J_Z \rangle$ should be negligible and we may consider the internal field as independent of this. This conclusion is borne out by room temperature susceptibility measurements on praseodymium metal.[42]

One further assumption can be made—that J=4 is a good quantum number. The spin-orbit splitting in Pr^{+3} is greater than 2900°K.

We find experimentally for the triply-ionized Pr^{143} in cerium metal that $g\beta = 3.55 \pm 0.36$. Adopting the interpolated value for $\langle r^{-3} \rangle$ and hence the paramagnetic correction $\beta = 2.00$, we find

$$g = 1.77 \pm 0.18, \qquad (13)$$

The importance of this value lies in the fact that we now have a semi-quantitative estimate of g and can use this to deduce the electronic structure of the Pr^{143} in solution.

A second and less quantitative inroad comes from a comparison of the perturbed integral runs on Ce^{+3} and Ce^{+4}. In spite of the large errors, the proximity of the experimental values indicates that the praseodymium ion is in the same oxidation state for both during the lifetime of the 57 keV nuclear level. This fact immediately eliminates the possibility of Pr^{+5} and allays worries about differing oxidation states due to differing procedures in chemical preparation.

The final analysis must come from the accurately measured differential runs on Pr^{143} in solution which give $g\beta = 2.58 \pm 0.13$. If we assume a Pr^{+3} configuration, the Bleaney paramagnetic correction is 2.00 and $g = 1.29 \pm 0.065$. This value does not overlap the value measured in the metal runs.

The paramagnetic correction expected for Pr^{+4} involves some complications, but can be predicted. It may be remembered from Sec. II that the paramagnetic correction term involves the product of a radial term, implicit in $\langle r^{-3} \rangle$, and an angular term, derived through angular momentum and symmetry considerations. The latter for Pr^{+4} is exactly the same as for Ce^{+3}, the electron configuration being $4f^1$ in both cases.

The radial term may be evaluated by induction. Bleaney has surveyed a number of cases of hyperfine interactions in doubly-ionized rare-earth ions and found the interaction constant essentially the same as for neutral atoms. Assuming the first two electrons lost in the rare earths are from the 6s shell, we may conclude that the angular properties remain the same in the 2+ ions. Consequently $\langle r^{-3} \rangle$ is unchanged. This is not surprising, as the 6s electrons lie almost entirely outside the 4f orbitals.

The loss of a third electron, from the 4f shell, alters the hyperfine interaction drastically. After correcting for the configurational differences in the 4f shell, one can calculate the ratio of $\langle r^{-3} \rangle$ for atoms and ions. Judd and Lindgren have approached this problem from a theoretical side and predicted this ratio.[30] The close agreement between their predictions and the experimental values summarized by Bleaney allows a confident estimate of the ratio. The loss of a 4f electron in Pr^{+2} ($4f^3 \rightarrow 4f^2$) increases $\langle r^{-3} \rangle$ by a factor of 1.17. The corresponding loss in Ce^{+2} ($4f^2 \rightarrow 4f^1$) multiplies $\langle r^{-3} \rangle$ by 1.20. As $\langle r^{-3} \rangle$ should change very slightly for a change of one part in 58 in nuclear charge, we shall assume an enhancement of 1.19 in going from Pr^{+3} to Pr^{+4}.

Thus, using the Bleaney value of $\langle r^{-3} \rangle = 5.06$ a.u. for Pr^{+3}, and the angular parameters for Ce^{+3}, we find the paramagnetic correction for Pr^{+4},

$$\beta = 1.49 \quad . \tag{14}$$

Division into the determined value of $g\beta$ gives

$$g = 1.73 \pm 0.09 \quad . \tag{15}$$

The excellent agreement between this value and that derived from the metal allow an unambiguous designation of the electronic state as Pr^{+4} and a confident acceptance of g.

The value of the g-factor confirms the conclusion of nuclear alignment that the 57 keV state must have spin of I = 5/2+. While the Schmidt limit for a $d_{5/2}$ state is 1.92, the other experimental values for $d_{5/2}$ states in this region average to g = 1.66, while $g_{7/2}$ levels range around g = 0.77. It is interesting to note that the g values predicted from the quasi-particle considerations of Kisslinger and Sorensen are 1.38 and 0.61 respectively,[84] both lower than empirical values.

One reservation about the entire previous argument must be aired: the complete interpretation rests upon the differential measurement of the rotational frequency in cerium metal. This measurement, due to the rapid time-dependent perturbation, is the least dependable of all the experimental work. Less than one complete cycle has been observed, and systematic errors such as drifting background could give anomalous results. However, in view of the accordance of the nuclear alignment data, and of the internal consistency of the differential runs in the metal, we feel the acceptance of the g-factor value is a reasonably good risk.

There remains a good deal of interest in the semi-stable Pr^{+4} oxidation state. This configuration has never been reported in solution although the oxide PrO_2 is stable under certain conditions. Pr^{+4} is a very strong oxidizing agent, with a predicted electromotive force potential of -3.5 V and a free energy of reaction of -56 kcal/mole (compared to -12 kcal/mole for $Ce^{+4} \rightarrow Ce^{+3}$).[75] The rate-determining step in the oxidation of water has been cited as the formation of atomic oxygen. Our data show that the reaction requires at least longer than 30×10^{-9} sec. This contrasts sharply with the reduction of Pr^{+5}, which must proceed faster than nanoseconds.

Acknowledgements

For moral, intellectual, and practical support, I am indebted to the following:

Dr. David A. Shirley, who conceived and directed this research and whose tact, patience, and timely criticism have pushed a reluctant graduate student to the brink of scientific maturity;

Dr. Eckart Matthias, who built most of the electronic apparatus, and who through his quiet persistence and devotion to science provided an inspiration by example;

My parents, who suffered through crises and shared gratifications with me, and whose faith and understanding made this work possible;

Mr. Michiyuki Nakamura and Mr. George Killian, whose electronic support groups provided technical assistance with promptness and enthusiasm;

Mr. Gardner G. Young, whose advice and expertise in mechanical matters became an indispensible facet of the experimental work;

Dr. Nicholas J. Stone and Mr. Richard B. Frankel, who collaborated on the nuclear alignment experiments with their customary skill and vigor;

Dr. Gene A. Westenbarger, Dr. H.H. Wickman, Mr. Johan Blok, and Mrs. Marjorie O. Faltens, fellow graduate students throughout most of this work, whose smiling faces and cameraderie contributed very necessary moral support;

Mrs. Gertrude Bolz, a health chemist with patience and affability, who kept the laboratory safe from people like me;

Mr. Steve Rosenblum, Mr. Jim Huntzicker, Mr. Warren Easley, and many other good friends, whose mere existence made these years a pleasureable and meaningful period.

This work was done under the auspices of the United States Atomic Energy Commission.

References

1. D.R. Hamilton, Phys. Rev. 58, 122(1940).

2. H. Frauenfelder, Angular Correlation, in Beta and Gamma Ray Spectroscopy, ed. by Kai Siegbahn(Interscience, New York, 1955), p. 531.

3. F. Coester, Gamma-Gamma Angular Correlations, Argonne National Laboratory Report ANL- 5316, September 1954.

4. Brian R. Judd, Operator Techniques in Atomic Spectroscopy(McGraw-Hill Book Co., Inc., New York, 1963), Chap. 4.

5. L.C. Biedenharn and M.E. Rose, Rev. Mod. Phys. 25, 729(1953).

6. M. Tinkham, Advanced Quantum Mechanics of Atoms, Molecules, and Solids,(Univ. of California, Berkeley, 1960).

7. A. Simon, J.H. Vander Sluis, and L.C. Biedenharn, Table of Racah Coefficients, Oak Ridge National Laboratory Report ORNL-1679 special, April 1954.

8. M. Ferentz and N. Rosenzweig, Table of F Coefficients, Argonne National Laboratory Report ANL-5324, 1955.

9. R.J. Blin-Stoyle and M.A. Grace, Oriented Nuclei, in Handbuch der Physik, ed. by S. Flugge(Springer-Verlag, Berlin, 1957), p. 555.

10. J.A. Spiers, Directional Effects in Radioactivity, National Research Council of Canada Limited, Chalk River, April 1949.

11. R.M. Steffen and H. Frauenfelder, Influence of Extranuclear Fields, in Perturbed Angular Correlations, ed. by E. Karlsson, E. Matthias, K. Siegbahn(North-Holland, Amsterdam, 1964), p.1.

12. A. Abragam and R.V. Pound, Phys. Rev. 92, 943(1953).

13. K. Alder, E. Matthias, W. Schneider, and R.M.Steffen, Phys. Rev. 129, 1199(1963).

14. Maria G. Mayer and Hans D. Jensen, Elementary Theory of Nuclear Shell Structure(John Wiley and Sons, Inc., New York, 1960).

15. H. Kopferman, Nuclear Moments (Academic Press, Inc., New York, 1958).

16. Aage Bohr, Dan. Mat. Fys. Medd. 26, no. 14(1952).

17. Aage Bohr and Ben R. Mottelson, Dan. Mat. Fys. Medd. 27, no. 16(1953).

18. Sven Gosta Nilsson, Mat. Fys. Medd. Dan. Vid. Selsk. 29, no. 16(1955).

19. J. Bardeen, L. Cooper, and J. Schrieffer, Phys. Rev. 108, 1175 (1957).

20. Michael Baranger, Theory of Finite Nuclei, in Cargese Lectures in Theoretical Physics, ed. by Maurice Levy(W.A. Benjamin, Inc., New York, 1963).

21. E. Bodenstedt and J.D.Rogers, Magnetic Moments of Nuclear Excited States, in Perturbed Angular Correlations, ed. by E. Karlsson, E. Matthias, K. Siegbahn(North-Holland, Amsterdam, 1964), p.93.

22. S.G. Nilsson and O. Prior, Mat. Fys. Medd. Dan. Vid. Selsk. 32, no. 16(1960).

23. L.S. Kisslinger and R.A. Sorensen, Mat. Fys. Medd. Dan. Vid. Selsk. 32, no. 9(1960).

24. H. Noya, A. Arima, and H. Horie, Progr. Theoret. Phys. (Kyoto) (Suppl.) 8, 33(1959).

25. E. Bodenstedt, Fortschr. Physik 10, 321(1962).

26. C. Gunther and I. Lindgren, Paramagnetic Effects, in Perturbed Angular Correlations, ed. by E. Karlsson, E. Matthias, K. Siegbahn(North-Holland, Amsterdam, 1964), p. 357.

27. R.J. Elliot and K.W.H. Stevens, Proc. Roy. Soc. A 218, 553(1953).

28. J.H. Van Vleck, Theory of Electric and Magnetic Susceptibilities (Clarendon Press, Oxford, 1932).

29. G. Goldring and R.P. Scharenberg, Phys. Rev. 110, 701(1958).

30. B.R. Judd and I. Lindgren, Phys. Rev. 122, 1802(1961).

31. B. Bleaney (to be published).

32. B. Bleaney, Proc. Phys. Soc. A 68, 937(1955).

33. E.C. Ridley, Proc. Cambridge Phil. Soc. 56, 41(1960).

34. A.Y. Cabezas and I. Lindgren, Phys. Rev. 120, 920(1960).

35. I. Lindgren, Nucl. Phys. 32, 151(1962).

36. A.J. Freeman and R.E. Watson, Phys. Rev. 127, 2058(1962).

37. P.G.H. Sandars and G.K. Woodgate, Proc. Roy. Soc. A 257, 269 (1960).

38. F.M. Pichanick, P.G.H. Sandars, and G.K. Woodgate, Proc. Roy. Soc. A 257, 277(1960).

39. J.B. Baker and F.I.B. Williams, Proc. Roy. Soc. A 267, 283(1962).

40. A. Bohr and V.F. Weisskopf, Phys. Rev. 77, 94(1950).

41. Charles Kittel, Introduction to Solid State Physics, Chap. 9, (John Wiley and Sons, Inc., New York, 1962).

42. Sigurds Arajs and R.V. Colvin, Paramagnetism of Polycrystalline Rare Earth Metals, in Rare Earth Research, ed. by Eugene V. Kleber, (MacMillan Co., New York, 1961).

43. E. Bodenstedt, H.J. Korner, C. Gunther, and J. Radeloff, Nucl. Phys. 22, 145(1961).

44. A.Z. Hrynkiewicz, Nucl. Inst. and Methods 16, 317(1962).

45. Donald L. Wieber, A Fast, Wide-Range Time-to-height Conversion System, University of California Radiation Laboratory Report UCRL-10425, September, 1962.

46. M.E. Rose, Phys. Rev. 91, 610(1953).

47. M.J.L. Yates, Finite Solid Angle Corrections, in Perturbed Angular Correlations, ed. by E. Karlsson, E. Matthias, K. Siegbahn (North-Holland, Amsterdam, 1964), p.453.

48. Gertrude Scharff-Goldhaber and J. Weneser, Phys. Rev. 98, 212 (1955).

49. J.P. Elliot, Collective Motion in Nuclei, University of Rochester Report NYO-2271, September 1958.

50. V.N. Lutsenko, Nucl. Phys. 47, 42(1963).

51. S. Ofer and A. Schwarzschild, Phys. Rev. 116, 725(1959).

52. B.S. Dzelepov, Yu. V. Khol'nov, and V.P. Prikhodtseva, Nucl. Phys. 9, 665(1958).

53. W.M. Currie, Nucl. Phys. 32, 574(1962).

54. J.M. Cork, A.E. Stoddart, J.M. LeBlanc, C.E. Branyan, D.W. Martin, and W.J. Childs, Phys. Rev. 83, 856(1951).

55. C.L. Peacock, J.F. Quinn, and A.W. Oser, Jr., Phys. Rev. 94, 372(1954).

56. G.R. Bishop, Richard Wilson, and H. Halban, Phys. Rev. 77, 416 (1950).

57. Herbert H. Bolotin, Charles H. Pruett, Paul L. Roggenkamp, and Roger G. Wilkinson, Phys. Rev. 99, 62(1955).

58. V.P. Prikhodtseva and Yu. V. Khol'nov, Izvest. Akad. Nauk. SSSR, Ser. Fiz., 22, 176(1958).

59. B.S. Dzhelepov, B.A. Emel'yanov, K.P. Kupriyanova, and Yu. N. Podkopaev, JETP 38, 282(1960).

60. P.G. Hansen and K. Wilsky, Nucl. Phys.30, 405(1962).

61. L. Simons, K.E. Nysten, P. Holmberg, H. Jungner, A. Anttila, S. Bergström, and E. Hagebø, Acta Polytech. Scand. Phys., Nucl. Ser., no. 22, 1(1963).

62. M. Dorikens, J. Demuynck, L. Dorikens-Vanpraet, and O. Segaert, J. Phys. (Paris) 24, 866(1963).

63. G.R. Bishop and J.P. Perez Y. Jorba, Phys. Rev. 98, 89(1955).

64. W.H. Kelly and M.P. Wiedenbeck, Phys. Rev. 102, 1130(1956).

65. L. Dorikens-Vanpraet, O. Segaert, M. Dorikens, and J. Demuynck, Proc. Phys. Soc. 82, 488(1963).

66. N. Kaplan, S. Ofer, and B. Rosner, Phys. Lett. 3, 291(1963).

67. M. Schmorak, H. Wilson, P. Gatti, and L. Grodzins, Phys. Rev. 134, B718(1964).

68. L.M. Langer and D.R. Smith, Bull. Am. Phys. Soc. 5, 254(1960).

69. H.J. Körner, E. Gerdau, C. Gunther, K. Auerbach, K. Mielken, G. Strube, and E. Bodenstedt, Z. Physik 173, 203(1963).

70. Mannque Rho, On the Quasi-Particle Reactions in Spherical Nuclei (Ph.D. Thesis), University of California Radiation Laboratory Report UCRL-11080, October, 1963.

71. C. Stapleton, C. Jeffries, and D.A. Shirley, Phys. Rev. 124, 1455(1961).

72. J.M. Baker and B. Bleaney, Proc. Roy. Soc. A 245, 156(1958).

73. E. Bodenstedt, H.J. Körner, F. Frisius, D. Hovestadt, and E. Gerdau, Z. Physik 160, 33(1960).

74. Therald Moeller, The Chemistry of the Lanthanides, (Reinhold Publishing Co., New York, 1963).

75. B.B. Cunningham, Comparative Chemistry of the Lanthanide and Actinide Elements, in Proceedings of the International Congress of Pure and Applied Chemistry, (Butterworths, London, 1961).

76. Karl A. Gschneider, Jr., Crystallography of Rare Earth Metals, in The Rare Earths, ed. by F.H. Spedding and A.H. Daane, (Wiley and Sons, New York, 1961), Chap. 14.

77. R.J. Elliot and K.W.H. Stevens, Proc. Roy. Soc. A 215, 437(1952).

78. B. Bleaney (to be published).

79. Hermann Eicher, Z. Physik 169, 178(1962).

80. J.A. White, H.J. Williams, J.H. Wernick and R.C. Sherwood, Phys. Rev. 131, 1039(1963).

81. T. Murao and T. Matsubara, Progr. Theoret. Phys. (Kyoto) 18, 215(1957).

82. D.W. Martin, M.K. Brice, J.M. Cork, and S.B. Burson, Phys. Rev. 101, 182(1956).

83. G.N. Rao and H.S. Hans, Nucl. Phys. 41, 511(1963).

84. L.S. Kisslinger and R.A. Sorensen, Rev. Mod. Phys. 35, 853(1963).

85. I. Lindgren, Table of Nuclear Spins and Moments, in Perturbed Angular Correlations, ed. by E. Karlsson, E. Matthias, K. Siegbahn (North-Holland, Amsterdam, 1964), Appendix 1.

86. B. Budick, W.M. Doyle, R. Marrus, and W.A. Nierenberg, Bull. Am. Phys. Soc. 7, 417(1962).

87. I. Maleh, private communication.

88. E. Bozek, A.Z. Hrynkiewicz, S. Ogaza, M. Rybicka, and J. Styczen, Phys. Lett. 6, 89(1963).

89. R.L. Graham, J.M. Hollander, and P. Kleinheinz, Properties of the 57- and 351-keV Excited States in $_{59}Pr^{143}$, University of California Radiation Laboratory Report UCRL-10792, June, 1963.

90. James N. Haag, Nuclear Alignment Experiments on Cerium Radioisotopes (Ph.D. Thesis), University of California Radiation Laboratory Report UCRL-9872, September, 1961.

91. Carson D. Jeffries, Dynamic Nuclear Orientation (Interscience, New York, 1963), Chap. III.

92. A.W. Overhauser, Phys. Rev. 89, 689(1953).